RHEA-2011

Robotics and Associated High-technologies and Equipment for Agriculture

Edited by:

Pablo Gonzalez-de-Santos and Gilles Rabatel

PROCEEDINGS OF THE FIRST INTERNATIONAL WORKSHOP ON

ROBOTICS AND ASSOCIATED HIGH TECHNOLOGIES AND EQUIPMENT FOR AGRICULTURE

(RHEA-2011)

Montpellier, France

September 9, 2011

Edited by

Pablo Gonzalez-de-Santos and Gilles Rabatel

The research leading to these results has received funding from the European Union's Seventh Framework Programme [FP7/2007-2013] under Grant Agreement nº 245986

ISBN: 978-84-615-6184-1

Printed by *Producción Gráfica Multimedia*, PGM

Rafael Alberti 14; 28400 Madrid, Spain

Proceedings are available at: http://www.rhea-project.eu

EDITORS

Pablo Gonzalez-de-Santos (*CSIC-Centre for Automation and Robotics*)

Gilles Rabatel (*Cemagref*)

CHAIR COMMITTEE

Pilar Barreiro (*Technical University of Madrid*)

Angela Ribeiro (*CSIC-Centre for Automation and Robotics*)

Maria Guijarro (*Complutense University of Madrid*)

Nathalie Gorretta (*Cemagref*)

The RHEA consortium is formed by:

	**Agencia Estatal Consejo Superior de Investigaciones Científicas (CSIC)** (Coordinator) Spain
(CSIC-CAR **(CSIC-ICA)** **CSIC-IAS)**	*Centro de Automatica y Robotica* *Instituto de Ciencias Agrarias* *Instituto de Agricultura Sostenible*
	**CogVis GmbH (CV)** Austria
	**Forschungszentrum Telekommunikation Wien Ltd. (FTW)** Austria
	**Cyberbotics Ltd (CY)** Switzerland
	**Università di Pisa (UP)** Italy
	**Universidad Complutense de Madrid (UCM)** Spain
	**Tropical (TRO)** Greece
	**Soluciones Agrícolas de Precisión S.L. (SAP)** Spain
	**Universidad Politécnica de Madrid (UPM)** Spain
UPM-EIA **UPM-EII**	ETS Ingenieros Agrónomos ETS Ingenieros Industriales
	**AirRobot GmbH & Co. KG (AR)** Germany
	**Università degli Studi di Firenze (UF)** Italy
	**Centre National du Machinisme Agricole, du Génie Rural, des Eaux et des Forêts -CEMAGREF (CE)** France
	**Case New Holland Belgium N.V (CNH)**
CNH-B **CNH-F**	*Case New Holland Belgium N.V. Belgium* *Case New Holland Belgium S.A. France*
	**Bluebotics S.A. (BL)** Switzerland
	**CM Srl (CM)** Italy

FOREWORD

These proceedings are the result of the work developed by the RHEA consortium throughout the first year of the RHEA project (Robot fleets for highly effective agriculture and forestry management-FP7-NMP 245986). RHEA comprises a number of research centres, universities, and companies funded by the European Commission through the Seventh Framework Programme to develop robotic fleets for weed control and pesticide management in agriculture and forestry.

In the planning stages of the workshop, researchers and engineers were invited to present ideas, research results, works in progress and system demonstrations related to robotics, perception and actuation for agricultural tasks. Associated technologies that allow these different techniques to be merged, such as communication, localisation and human-system interfaces, were also addressed. The objective of this workshop is to facilitate the dissemination of project results, but it also provides a forum for building community and motivating discussion, new insight and experimentation.

This workshop was held in the pleasant city of Montpellier, France, on September 9, 2011. It consisted of three sessions: (I) Weed Management, (II) Perception and analysis and (III) Specific Techniques for the RHEA Fleet. The editors appreciate the contributions of the speakers, authors and attendees to this first RHEA workshop, which can be considered a first step towards two International Conferences that will be arranged by the consortium in the coming years.

Pablo Gonzalez-de-Santos and Gilles Rabatel

Editors

CONTENTS

Weed management

A Five-Step Approach for Planning a Robotic Site-Specific Weed Management Program for Winter Wheat
C. Fernández-Quintanilla, J. Dorado, C. San Martín, J. Conesa-Muñoz and A. Ribeiro 3

Effect of thermal and mechanical weed control on garlic
C. Frasconi, M. Fontanelli, M. Raffaelli, L. Martelloni and A. Peruzzi, 13

Effect of flaming at different LPG doses on maize plants
M. Fontanelli, C. Frasconi, M. Raffaelli, L. Martelloni and A. Peruzzi, 23

Perception and analysis

Hyperspectral imagery to discriminate weeds in wheat
G. Rabatel, F. Ougache, N. Gorretta and M. Ecarnot 35

Strategies for video sequence stabilization
A. Ribeiro, N. Sainz-Costa, G. Pajares and M. Guijarro, 47

How the spatial resolution can affect the quality of mosaics and assessment of optimum number of tie points necessary to obtain good quality images
D. Gómez-Candón, S. Labbé, M. Jurado-Expósito, J. M. Peña-Barragán, G. Rabatel and F. López-Granados 61

Camera System geometry for site specific treatment in precision agriculture
M. Montalvo, J. M. Guerrero, M. Guijarro, J. Romeo, P. J. Herrera, A. Ribeiro and G. Pajares 73

Techniques for Area Discretization and Coverage in Aerial Photography for Precision Agriculture employing mini quad-rotors
J. Valente, D. Sanz, J. del Cerro, C. Rossi, M. Garzón, J. D. Hernández, and A. Barrientos 85

Specific Techniques for the RHEA Fleet

Analysis of Engine Thermal Effect on Electronic Control units for "Robot Fleets for Highly effective Agriculture and Forestry Management" (RHEA)
M. Garrido, H. T. Jiménez-Ariza, M. A. Muñoz, A. Moya, C. Valero and P. Barreiro 101

Path-planning of a Robot Fleet Working in Arable Crops. First experiments and results
A. Ribeiro and J. Conesa-Muñoz 117

Simulation of communication within the RHEA robotic fleet
M. Roca and S. Tomic,
(Forschungszentrum Telekommunikation Wien - FTW) 129

Safety functional requirements for "Robot Fleets for Highly effective Agriculture and Forestry Management" (RHEA)
P. Barreiro, M. Garrido, A. Moya, B. Debilde, P. Balmer, J. Carballido, C. Valero, N. Tomatis and B. Missotten 141

Application of mechanical and thermal weed control in maize as part of the RHEA project
A. Peruzzi, M. Raffaelli, M. Fontanelli, C. Frasconi and L. Martelloni, (Universita di Pisa) 159

Wireless QoS-enabled Multi-Technology Communication for the RHEA Robotic Fleet
T. Hinterhofer and S. Tomic
(Forschungszentrum Telekommunikation Wien - FTW) 173

Vehicle Guidance on a Single-Board Computer
M. Hödlmoser, C. Bober, M. Kampel and M. Brandstötter 187


Weed Management

A Five-Step Approach for Planning a Robotic Site-Specific Weed Management Program for Winter Wheat

Cesar Fernández-Quintanilla*, Jose Dorado*, Carolina San Martín*,

Jesus Conesa-Muñoz and Angela Ribeiro****

**Institute for Agricultural Sciences (CSIC), C/ Serrano 115B, 28006 Madrid, Spain*

(e-mail: cesar@ica.csic.es)

***Centre for Automation and Robotics (UPM-CSIC), Crtra. Campo Real Km 0,2 28500 Arganda del Rey, Madrid, Spain*

(e-mail: angela.ribeiro@csic.es)

Abstract: A Five-Step procedure is proposed to be used in weed control programs based on the use of a robot fleet. The five steps are: 1) field inspection, 2) long-term decisions, 3) current year decisions, 4) unit distribution & path planning, and 5) online decisions. Monitoring weed populations at various times could be achieved using unmanned aerial vehicles (UAV) equipped with cameras and GPS. A long-term decision module could be used to optimize the choice of crop and herbicide rotations as well as the tillage system. A computerized system should quickly query databases containing information about the weeds present in each field and the herbicides available to control them, performing calculations to determine the cost effectiveness of each option. The system should generate a georeferenced prescription map indicating the sites were each herbicide should be sprayed. This map should provide the information required to decide the optimal distribution of the spraying units of the fleet and their corresponding navigation plans. Final spraying decisions should be based on both, prescription maps and online information coming from sensors located in the sprayer.

1. Introduction

Weed control can be approached either on a hit or miss basis or as a carefully planned and coordinated program. The second alternative is most likely to yield success. A well planned program consists of a number of appropriate operations coordinated in a sequence. Various types of weed management programs have been devised to fit different types of situations (Clarke, 2002; Newman, 2002; Sheley et al., 2010).

A Five-Step Approach for Planning a Robotic Site-Specific Weed Management Program for Winter Wheat

Site-specific weed management is defined as the use of equipment embedded with technologies that detect weeds growing in a crop and, taking into account predefined factors such as economics, take action to maximize the chances of successfully controlling them (Christensen et al., 2009). Although several weed sensing systems and precision implements have been developed over the last two decades, several barriers still prevent the commercial implementation of these technologies. A reliable, high resolution weed detection system and a decision support system capable to integrate site-specific information on weed distribution, weed species composition and density and the effect on crop yield are decisive for an effective site-specific management (Christensen et al., 2009).

Robotic weed control systems hold promise toward the automation of these operations and provide a means of reducing herbicide use. Although a few robotic weed control systems have demonstrated the potential of this technology in the field (Slaughter et al., 2008), additional research is needed to fully realize this potential.

In this work, a Five-Step procedure has been proposed to be used in weed control programs based on the use of a robot fleet. The five steps are: 1) field inspection, 2) long-term decisions, 3) current year decisions, 4) unit distribution & path planning, 5) online decisions. The outline structure of the system is shown in Fig. 1. Although the same structure can be used for a variety of crop situations, weed control tactics and local conditions, the system described in this paper has been developed for a concrete scenario: site-specific application of herbicides in winter wheat crops in Central Spain.

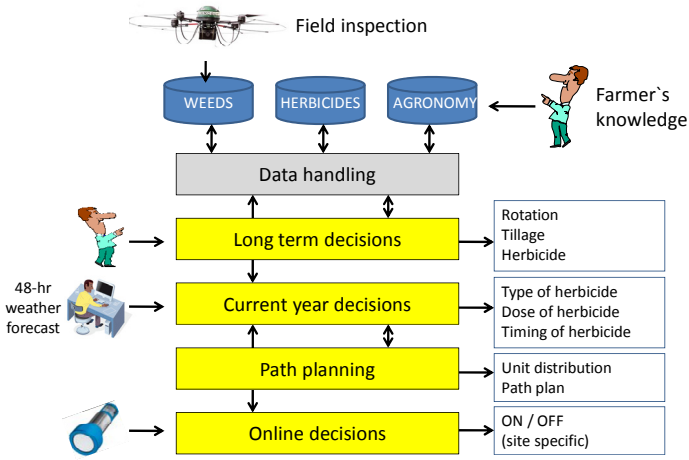

Fig. 1. System architecture of RHEA Mission Planner for site-specific application of herbicides in wheat

2. Step 1: Field inspection

Information on weed spatial distribution and abundance will be generated from aerial images obtained at different times prior to herbicide spraying and from information obtained from ground vehicles at spraying time. Aerial inspection of the fields in spring, when some broadleaved weeds are in full bloom (and can be easily discriminated from the crop) provide an excellent opportunity to discriminate and map infestations of selected weed species. Numerous studies have shown that detection of late-season weed infestation has considerable possibilities when the weeds exceed the crop canopy and the spectral differences between crops and weeds are maximum (López-Granados, 2011). Detection of bright coloured red poppies (*Papaver rhoeas*) on the green background provided by the crop may be a paradigmatic example of this situation. Monitoring weed populations at various times will be achieved using unmanned aerial vehicles (UAV). These vehicles provide high spectral, spatial and temporal resolutions with a relatively low cost (López-Granados, 2011). Additional georeferenced data on weed infestations will be obtained at spraying time by the cameras or sensors located on the sprayers (Andújar et al., 2011; Burgos-Artizzu et al., 2011).

3. Step 2: Long-term decisions

Farmers usually consider two different time-scales for decision making: long term (with a 3-5 year horizon) and current year. Consequently, a comprehensive system should include a long-term planning tool allowing users to consider various cultural practices (rotations, tillage systems) conducted over several years and a within season planning tool to investigate a range of weed control options in a single season (Parsons et al., 2009).

The objective of the our long-term decision module is to optimize the choice of crop and herbicide rotations as well as the tillage system throughout a rotation (up to 5 years) defined by the user, trying to find the best long-term strategy. The decision process could be made using a finite horizon stochastic dynamic program, trying to identify the policy that maximizes the long term expected discounted return. Other option could be using a set of decision rules coupled with a rule editor and an inference engine. In order to take these decisions, different types of data are required.

Historic maps, constructed using the weed distribution data obtained in the previous step, provide one major element for this process. In addition, empirical knowledge of the farmer, gathered through many years of working the field, is also a valuable data source that should be exploited, particularly when digital maps with historical records are not available. All this information is stored in a `Weed spatial´ database.

Biological data on the major weeds that are present in the field are required to assess the actual risks posed by those plants and the opportunities and possibilities

to manage them using different control tactics. Information on the life cycle, tendency to aggregate in patches, competitiveness with the crop, longevity of the seeds and possible beneficial effects to wildlife of all the major weed species present in winter wheat in Spain has been stored in a `Weed generic´ database (Fig. 2).

	Common names	Present?	Patchiness	Competitiveness	Longevity	Beneficial
BROADLEAVED						
Galium aparine	Cleavers		Medium	High	Low	No
Papaver rhoeas	Poppy		Low	Medium	Very high	Yes
Sinapis arvensis	Wild mustard	✔	Medium	High	Medium	Yes
Veronica hedaerefolia	Speedwell	✔	Low	Low	Medium	No
GRASSES						
Avena sterilis	Wild oat	✔	High	High	Medium	No
Lolium rigidum	Ryegrass	✔	Medium	Medium	Low	No
Bromus diandrus	Rigput brome		High	High	Low	No
Phalaris brachistachis	Canarygrass		High	Medium	Medium	Yes

Fig. 2. Example of a generic database with some of the major biological characteristics of selected weed species present in winter wheat crops in Spain.

In the case of herbicides, a `Herbicide spatial´ database will be constructed using the prescription and spraying maps generated in previous years (in case the system is used over a series of years) as well as with information coming directly from the user (e.g. control failures in some zones of the field). A comprehensive `Herbicide generic´ data base with all the commercial herbicides available in Spain for winter wheat has been constructed. This database contains information on their optimal timing, weed selectivity, risk of resistance, toxicity, environmental effects, cost, etc. (Fig. 3).

1. Optimal growth stage:

	1 leaf	2 leaves	3 leaves	Early tillering	Medium tillering	Late tillering	Jointing
Tribenuron							
Dicamba							
Fluroxipir							
Diclofop							
Fenaxaprop							
Clodinafop							

2. Weed selectivity:

	Broadleaved weeds				Grasses		
	Galium	*Papaver*	*Sinapis*	*Veronica*	*Avena*	*Lolium*	*Phalaris*
Tribenuron							
Dicamba							
Fluroxipir							
Diclofop							
Fenaxaprop							
Clodinafop							

3. Other data:

	Commercial product	Dose /ha	Cost (€ / ha)	Toxicity	Wildlife risk	Resistance group
Tribenuron	GRANSTAR	15-25 gr	20	Xi	B	B
Dicamba	BANVEL	0.3-0.5 l	10	Xi	B	O
Fluroxipir	STARANE	0.75-1 l	25	Xi	-	O
Diclofop	COLT	2.5 l	25	Xn	B	A
Fenaxaprop	PUMA	1.0-1.25 l	38	Xn	A	A
Clodinafop	TOPIK	0.17-0.35 g	40	Xn	A	A

Fig. 3. Example of a generic database of selected herbicides for winter wheat

Finally, the `Agronomy´ database will provide information on field size, boundaries and obstacles, cropping history, drilling and harvest dates, expected yields, expected crop value, basic costs for operations such as soil tillage, fertilizing and spraying as well as values for the variable costs associated with each crop. Although default values are provided by the system in some cases, in other cases they should be filled by the user.

4. Step 3: Current year decisions

Weed management in conventional wheat production relies heavily on herbicide use. Current year decision-making for herbicide use is a complex task requiring the integration of information on weed biology, expected crop yields and potential yield losses caused by different weeds, herbicide options, timing and efficacy of each herbicide, economic profitability of the treatment and environmental risks (Fig. 4). Agricultural growers and consultants can manage the integration of these complex factors by using decision support systems (DSS) (Parsons et al., 2009).

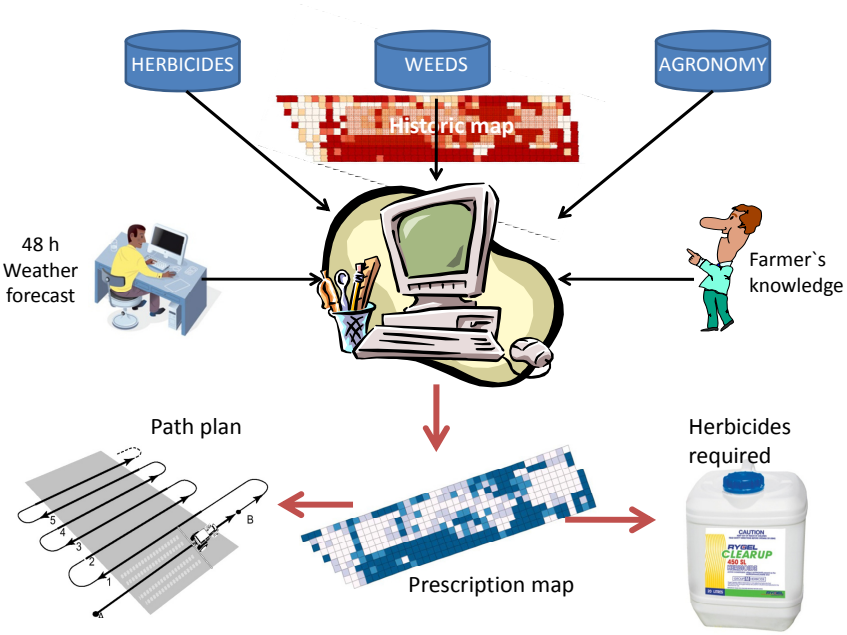

Fig. 4. Outline structure of the major inputs and outputs involved in current year decisions

The objective of the current year decision module is to suggest a range of different herbicides that result in good profits for the current season. The economic margin used considers both, the value of the wheat grain losses avoided by each treatment and the cost of that treatment. All the parameter values may be changed by the user. Optimization algorithms are used to assess each possible decision variable.

Computer programs will be designed to facilitate this decision-making process. A computerized system should quickly query databases containing information about many different herbicide products, perform calculations to determine the cost effectiveness of each of them, and store detailed field records. The system will generate a georeferenced prescription map indicating the sites were each herbicide should be sprayed (Fig. 4). In addition, this map will provide the information required to adjust herbicide acquisition and loading the ground units to actual needs, to decide the optimal distribution of the spraying units of the fleet and their corresponding navigation plans.

The final decision on field spraying depends heavily on weather conditions. Consequently, the system includes a set of decision rules based on the expected wind, temperatures and rainfall at treatment time and in the following 24 h (Fig. 4).

5. Step 4: Unit distribution & path planning

Numerous planning methods for obtaining the routes that allow an efficient operation of agricultural vehicles have been proposed (Stoll, 2003; Jin and Tang, 2010; Taix et al., 2006). These methods take into account, for only one vehicle, different factors: the strategy of operation, the surrounding areas, the geometry of the field, field-specific data (size, slope, obstacles in the field), specific restriction on the machinery (p.e. turning radius), or the operation direction. The change of the direction in the headlands is an important issue because of the long time needed for this operation. Stoll (2003) has calculated the turning paths keeping in mind the effective width, the minimum turning radius, the driving speed and the turning acceleration of the vehicle. It also includes additional time to consider the change of the direction in the turning.

Path planning taking into account the previous factors is a very complex process that requires rather sophisticated tools in order to search the optimal solution. The problem becomes even more complex when a fleet of robots is used to perform the herbicide treatment. The problem can be enunciated as follows (Conesa-Muñoz and Ribeiro, 2011): Given a set of robots with certain features (i.e., herbicide loading capacity, motion characteristics, width of the spraying boom), a field with specific dimensions, a crop growing in rows and a map of the weed patches, the aim is to find the subset of robots and associated paths that ensure the whole cover of the weed with the minimum cost (Fig. 5). The solution of this problem can be faced with a genetic algorithm approach where the fitness function considers several of the factors above explained (Conesa-Muñoz and Ribeiro, 2011).

6 Step 5: Online decisions

Although the prescription map provides basic information of the field areas that should be sprayed, this information needs to be contrasted with that obtained at spraying time with cameras or sensors that detect weed presence and discriminate different weed types. Once the detected weed patch has been considered as a suitable target for spraying, a fast-response controller will regulate discharge of the different herbicides in each individual nozzle (Fig. 6). Decision making could be made using a set of decision rules similar to those used in the long-term decision module.

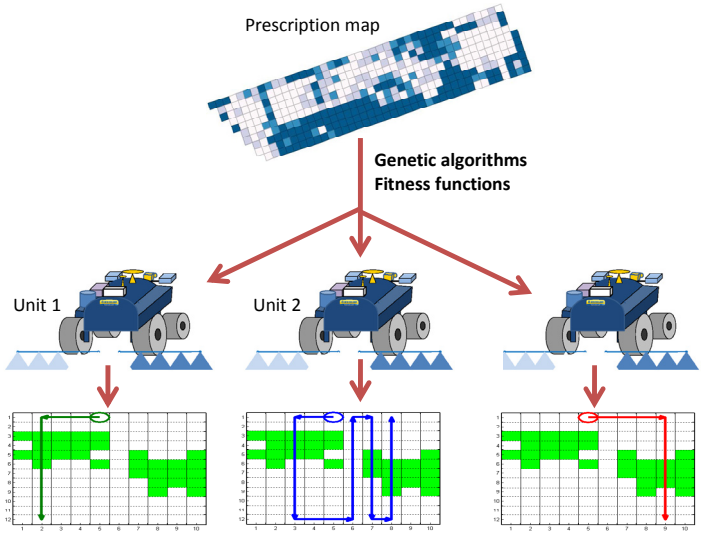

Fig. 5. Distribution of three ground units to conduct a spraying operation following a predefined prescription map. Path plan for each individual unit marked with a different colour. Green cells indicate the presence of weeds. Circles indicate the starting position

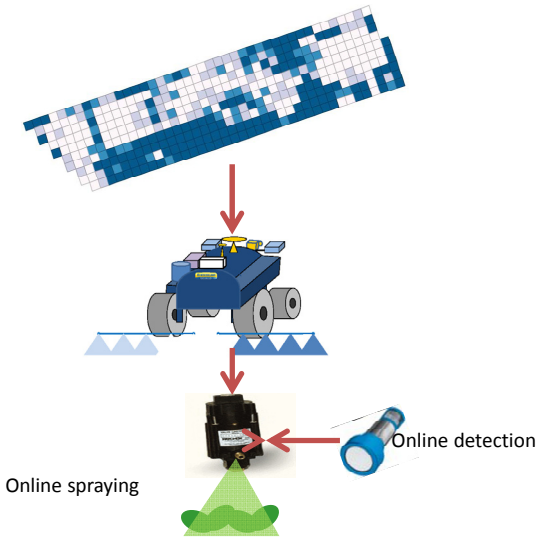

Fig. 6. Online detection and spraying by a fast-response controller

Acknowledgement

The research leading to these results has received funding from the European Union's Seventh Framework Programme [FP7/2007-2013] under Grant Agreement nº 245986.

References

Andújar, D., A. Ribeiro, C. Fernández-Quintanilla and J. Dorado (2011). Accuracy and feasibility of optoelectronic sensors for weed mapping in row crops. *Sensors* 11, 2304-2318.

Burgos-Artizzu, X.P., A. Ribeiro, M. Guijarro and G. Pajares (2011). Real-time image processing for crop/weed discrimination in maize fields. *Computers and Electronic in Agriculture*, 75, 337-346.

Christensen, S., H.T. Sogaard, P. Kudsk, M. Norremark, I. Lund and E.S. Nadimi (2009). Site-specific weed control technologies. *Weed Research*, 49, 233-241.

Clarke, J. (2002). Weed management strategies for winter cereals. In: *Weed Management Handbook* (R.E.L. Naylor, Ed.), pp. 354-358. Blackwell Science Ltd. for British Crop Protection Council, Oxford, UK.

Conesa-Muñoz, J. and A. Ribeiro (2011). An evolutionary approach to obtain the optimal distribution of a robot fleet for weed control in arable crops. In: *EFITA/WCCA '11: 8th European Federation for Information Technology in Agriculture, Food and the Environment Congress/Word Congress on Computers in Agriculture* (E. Gelb and K. Charvát, Eds.), pp. 141-155. Czech Centre for Science and Society, Prague, Czech Republic.

Jin, J. and L. Tang (2010). Optimal coverage path planning for arable farming on 2D surfaces. *Transactions of the ASABE*, 53, 283-295.

López-Granados, F. (2011). Weed detection for site-specific weed management: mapping and real-time approaches. *Weed Research* 51, 1-11.

Newman, J.R. (2002). Management of aquatic weeds. In: *Weed Management Handbook* (R.E.L. Naylor, Ed.). Pp. 399-414. Blackwell Science Ltd. for British Crop Protection Council, Oxford, UK.

Parsons, D.J., L.R. Benjamin, J. Clarke, D. Ginsburg, A. Mayes, A.E. Milne and D.J. Wilkinson (2009). Weed Manager-A model-based decision support system for weed management in arable crops. *Computers and Electronics in Agriculture*, 65, 155-167.

Sheley, R.L., J.J. James, B.S. Smith and E.A. Vasquez (2010). Applying ecologically based invasive-plant management. *Rangeland Ecology and Management*, 63, 605-613.

Slaughter, D.C., D.K. Giles and D. Downey (2008). Autonomous robotic weed control systems: A review. *Computers and Electronics in Agriculture*, 61, 63-78.

Stoll, A. (2003). Automatic operation planning for GPS-guided machinery. In: *Precision Agriculture '03* (J.V. Stafford and A. Werner, Eds.), pp. 657-664. Wageningen Academic Publishers, Wageningen, The Netherlands.

Taïx, M., P. Souères, H. Frayssinet and L. Cordesses (2006). Path planning for complete coverage with agricultural machines field and service robotics. In: *Field and Service Robotics* (S. Yuta, H. Asama and S. Thrun, Eds.), pp. 549-558. Springer Tracts in Advanced Robotics, Vol. 24. Berlin, Germany.

Effect of thermal and mechanical weed control on garlic

Christian Frasconi, Marco Fontanelli, Michele Raffaelli, Luisa Martelloni and Andrea Peruzzi

CIRAA "E. Avanzi", University of Pisa, Via Vecchia di Marina 6, 56010 S. Piero a Grado PI, Italy

(e-mail: cfrasconi@agr.unipi.it)

Abstract: Vessalico is a small village close to Imperia (Liguria, Italy), where garlic is a typical crop. The garlic of Vessalico is one of the most traditional and top quality foods in Italy. A study was carried out on the possibility of introducing a mechanization chain to solve the main agronomic problems of garlic cultivation in this area, such as planting, weed control and harvesting, which would thus improve garlic yield and quality. Ordinary organic garlic crop management was compared with an innovative system in which physical weed control was carried out using a rolling harrow, two flame weeding machines and a precision hoe. The innovative treatments increased the whole plant and bulb dry weight by approximately 38% and 78% respectively, and reduced weed biomass at harvest by up to 77%.

1. Introduction

Vessalico is a village (Latitude 44°3 N, Longitude 7°58' E) in the district of Imperia, Liguria, NW Italy. The farms in this area are very small, and crops are grown in small terraced plots. As a result, operative machines must be easy to handle and not cumbersome. Garlic is the main crop in this area, it is sold as a dried or processed high quality product, and is famous worldwide. Furthermore all the garlic cultivation in the area is organic, which provides added value to the crop. The division of Agriculture Engineering and Farm Mechanization Department of Agronomy and Agro-Ecosystem Management and the Centro Interdipartimentale di Ricerche Agro-Ambientali "Enrico Avanzi" of the University of Pisa, in collaboration with the Agriculture and Civil Defence department of Liguria and the "A Resta" Cooperative of farmers carried out a study on the possibility of introducing a mechanization chain to solve the main agronomic problems involved in the cultivation of garlic in this area, such as planting, weed control and harvesting, which would thus improve garlic yield and quality (Peruzzi et al. 2007).

2. Materials and methods

The study was carried out in 2006-2007 in Vessalico (Imperia, Italy). The traditional organic garlic farming system was compared with an innovative system.

2.1 The traditional farming system

The farmers of Vessalico usually plant bulbs using a “one row” potato planter (Fig. 1), modified for garlic. This equipment reduces working time compared to hand sowing, however it places the bulbs very deep in the soil, making it difficult for the plants to emerge.

Fig. 1. Modified single row potato planter used in the traditional farm system of Vessalico for planting garlic

The usual inter-row space is 50 cm. Weed control is carried out with a self-propelled cultivator (Fig. 2) between the rows, and by hand in the row. This technique is very expensive and can damage the garlic root system if the treatment is performed in a late phenological crop stage.

Fig. 2. Self-propelled cultivator used for inter-row weed control in the traditional farm system of Vessalico

2.2 The innovative farming system

In the innovative system, three different machines, each 1.4 m wide, were used for physical weed control: a rolling harrow, two flamers and a precision hoe.

2.3 Rolling harrow

The rolling harrow is equipped with specific tools (Fig. 3: spike discs placed at the front, and cage rolls mounted in the rear. The front and rear tools are connected by an overdrive with a ratio equal to 2. The disc and the rolls can be placed differently on the axles: in close arrangement, in order to create a very shallow tillage (3-4 cm) of the whole treated area (for seedbed preparation and non-selective weed control after false seed bed) and in a spaced arrangement, in order to create efficient selective post emergence weed control (for precision inter-row weeding) (Peruzzi, 2005 and 2006).

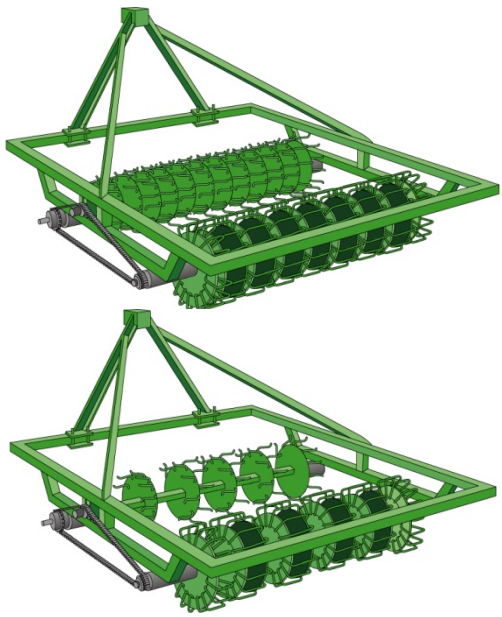

Fig. 3. The rolling harrow: close arrangement for full surface treatment (top); spaced arrangement for inter row treatment (down)

2.4 Flaming machines

The mounted flamer (Fig. 4) is an open flame machine equipped with three LPG 50 cm wide rod burners. The machine has a “thermal exchanger”, which consists in a hopper containing water heated by the exhaust gas of the tractor engine. Each burner is placed on a wheeled articulated parallelogram in order to maintain the correct distance from the soil surface. In the experimental field trials, the machine

was used for crop emergence treatment with a driving speed of about 3 km h^{-1} and different LPG pressures. During the trials, a hand flamer, equipped with a 15 cm wide rod burner was also used by a walking operator at a LPG pressure of 0.2 MPa and average speed of 2 km h^{-1}.

Fig. 4. Mounted flaming machines used during the study in Vessalico

2.5 Precision hoe

The precision hoe is equipped with a hand guidance system and six working units connected to the frame by articulated parallelograms (Fig. 5). Each unit has a 9 cm wide horizontal blade and two sets of tools (spring tines suitable as vibrating tines and a torsion weeder) in order to perform both inter and intra row weed control (Fig. 6).

2.6 The experimental trial

Our weed control strategy consisted in creating a false seedbed with a rolling harrow, followed by flaming after crop emergence. This is because garlic can tolerate exposure to thermal radiation for a few tenths of second. Flaming or precision hoeing were used for further weed control . Harvesting was carried out manually for both systems. This is because the garlic plants are dried with whole leaves, in order to twist them into the traditional strings. During the experimental trials, physical weed control treatments were carried out separately. Firstly, a false seed bed was created with the rolling harrow on each experimental plot. Subsequently, garlic was sown manually in three rows spaced 20 cm apart. At early post emergence, flame weeding was carried out at different working pressures (0.2; 0.3; 0.4; 0.5 MPa) using a 3 km h^{-1} driving speed. At the four leaf stage, three different secondary treatments for each working pressure were performed:

precision hoeing with vibrating tines + torsion weeder, precision hoeing + torsion weeder and manual flaming carried out with a device carried on the operator's back and operating at a speed of about 2 km h^{-1} and a working pressure of 0.2 MPa. On some experimental plots, no secondary treatment was performed. Weed inter-row and intra-row densities were determined on the basis of a 25×30 cm sampling area. At harvest, crop production and weed biomass were determined. The experimental design was a strip plot with three replicates. Data were analysed by ANOVA. Treatment means were separated using Fisher's least square difference at $P< 0.05$ (Gomez and Gomez 1984)

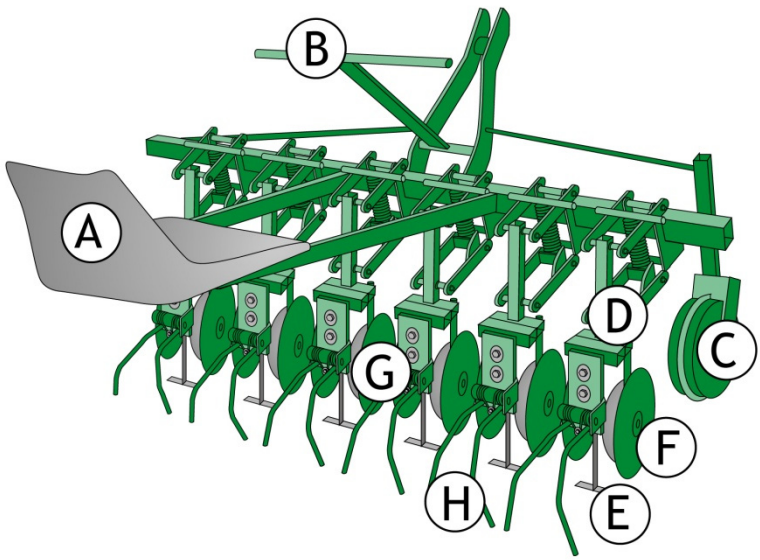

Fig. 5. The six-element precision hoe: A) seat for the operator; B) hand guidance system; C) directional wheel; D) articulated parallelogram; E) horizontal blade; F) lateral disc; G) wheel of the articulated parallelogram; H) spring tines

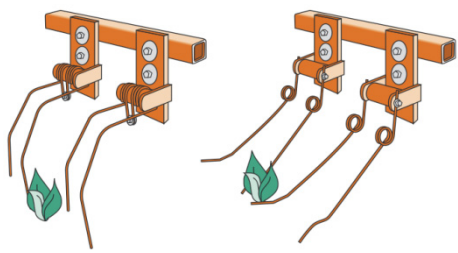

Fig. 6. The precision hoe spring tools: vibrating tines (left); torsion weeder (right)

3. Results

Data collected 29 days after the first thermal treatment showed that the most efficient working pressure in controlling inter-row weeds was 0.3 MPa (Fig. 7). Weed density recorded 35 days after the secondary treatment revealed significant differences between the treated and untreated plots, but no significant differences were observed between the different secondary performed operations (Fig. 8). The weed flora percentage reduction ranged from 24% to 57%.

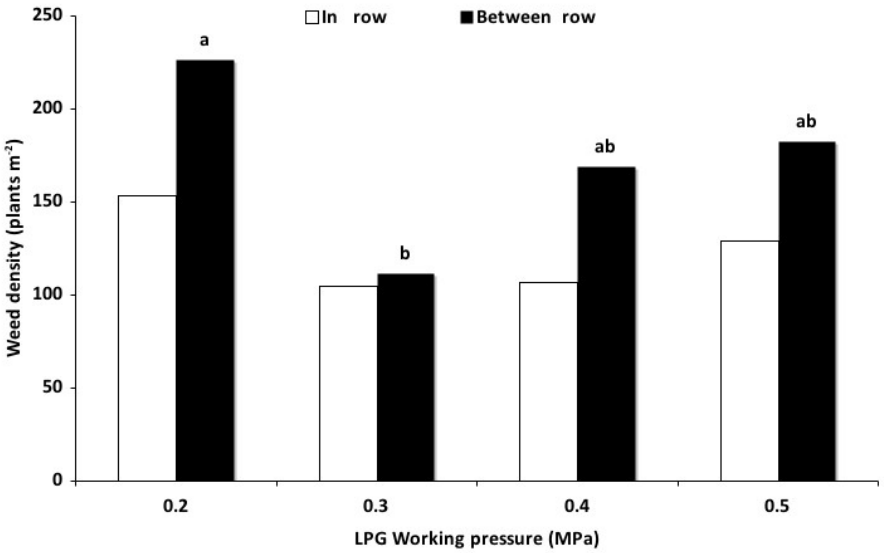

Fig. 7. Effects of the different flame weeding working pressures on weed density 29 days after the treatment. Different letters within bar of the same color indicate statistically significant differences (LSD $P \leq 0.05$)

Significantly higher total dry weights and bulb dry weights were observed using a working pressure of 0.2 MPa (fig. 9). No significant differences were observed between the secondary treatments. Comparing results obtained in the experimental plots flamed at a working pressure of 0.2 MPa, with those obtained in plots managed traditionally, a significantly higher yield in terms of total and bulb dry weight (Fig. 10), and a significant lower value of weed dry biomass at harvest were observed (Fig. 11).

4. Discussion

Weed control is the main agronomic problem of garlic in this area. Flame weeding seems to result in good weed control. The working pressure of 0.3 MPa

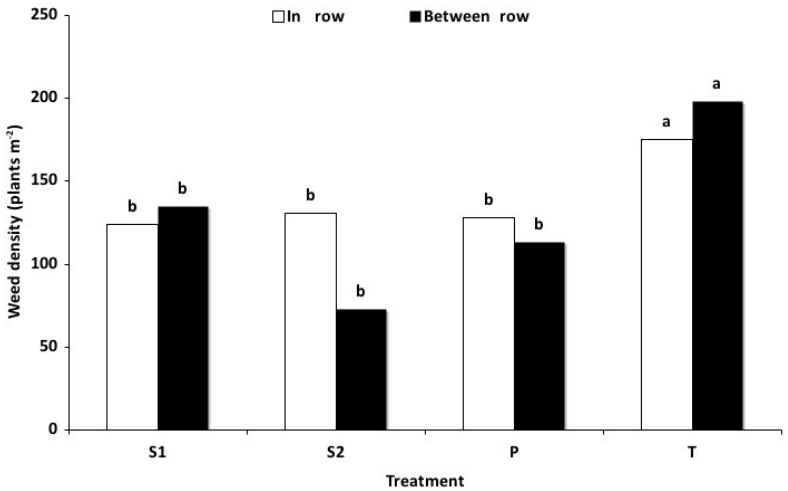

Fig. 8. Effect of the different secondary treatments on weed density : S1) Precision hoeing with torsion weeder; S2) Precision hoeing with vibrating tines and torsion weeder; P) Flame weeding; T) No treatment. Different letters within bar of the same color indicate statistically significant differences (LSD P≤ 0.05)

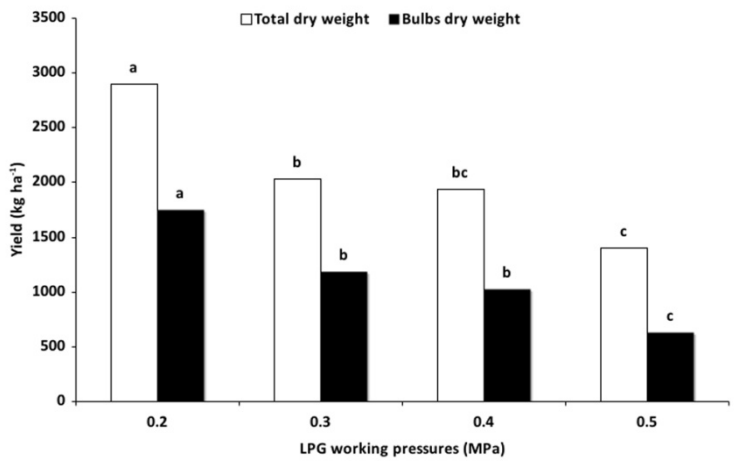

Fig. 9. Effects of the different flame weeding working pressures on garlic yield days after the treatment. Different letters within bar of the same color indicate statistically significant differences (LSD P≤ 0.05)

Effect of flaming with different LPG doses on maize plants

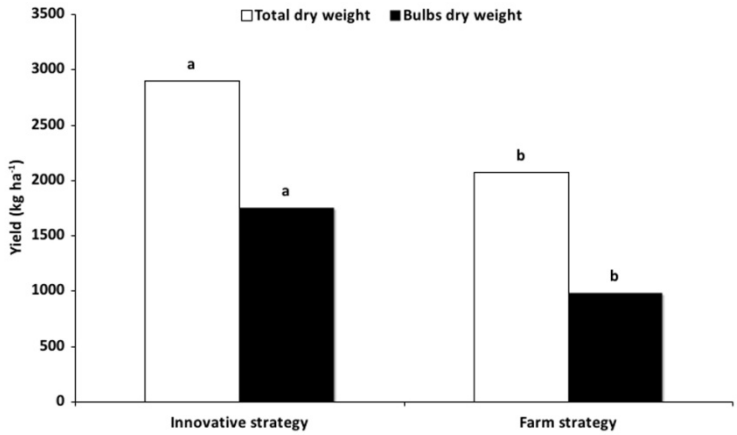

Fig. 10. Data of estimated garlic yield of our weed control strategy and the traditional system adopted by the farm. Different letters within bar of the same color indicate statistically significant differences (LSD P≤ 0.05)

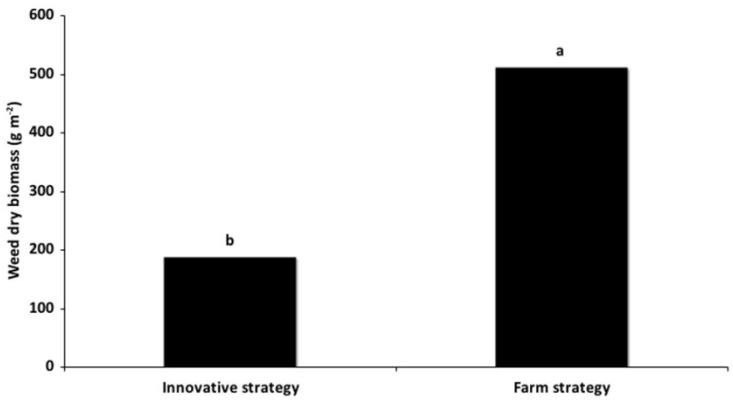

Fig. 11. Data of estimated garlic yield of the innovative weed control strategy and the traditional system adopted by the farm. Different letters within bar of the same color indicate statistically significant differences (LSD P≤ 0.05)

ensured the best weed control results in terms of plant density. The working pressure of 0.2 MPa gave the highest yield and good control of the weed flora, compared with traditional weeding.

These results can be simply explained by considering that the use of increasing pressure (without any change in speed) resulted in a increase in heat transmission both to the weeds and crops. This higher pressure resulted in a higher degree of weed control, but lead to a decrease in garlic yield, while a pressure of 0.2 MPa seemed to represent the best compromise.

5. Conclusions

The introduction of a mechanization chain in organic garlic in Vessalico seems feasible, using machines already available on the market with modifications where necessary. Regarding weed control, the experimental trials carried out using the equipment designed at the University of Pisa showed interesting results that could lead to a more precise definition of the best strategy for these environments.

Acknowledgement

The research leading to these results has received funding from the European Union's Seventh Framework Programme [FP7/2007-2013] under Grant Agreement nº 245986.

References

Gomez K.A., Gomez A.A. (1984) *Statistical procedures for agricultural research II edition*. Eds John Wiley & Sons U.S.A.

Peruzzi A. (2005): *La gestione fisica delle infestanti su carota biologica e su altre colture tipiche dell'altopiano del Fucino*. Stamperia Editoriale Pisana Agnano Pisano (PI).

Peruzzi A. (2006): *Il controllo fisico delle infestanti su spinacio in coltivazione biologica ed integrata nella Bassa Valle del Serchio*. Stamperia Editoriale Pisana Agnano Pisano (PI).

Peruzzi A., Raffaelli M., Ginanni M., Fontanelli M., Lulli L., Frasconi C. (2007): *La Meccanizzazione dell'Aglio di Vessalico*. Proceedings of Convegno Nazionale III V e VI Sezione AIIA Pisa-Volterra 5-7 settembre 2007 "Tecnologie innovative nelle filiere: orticola, vitivinicola e olivicolo-olearia." p. 120-123.

Effect of flaming with different LPG doses on maize plants

Marco Fontanelli, Christian Frasconi, Luisa Martelloni, Michele Raffaelli and Andrea Peruzzi

**Centro Interdipartimentale di Ricerche Agro-Ambientali "Enrico Avanzi", via Vecchia di Marina 6, 56122, San Piero a Grado, Pisa, Italy*

(e-mail: mfontanelli@agr.unipi.it).

Abstract: Despite now being considered as a very innovative technique, the use of flaming for weed control is an old tradition. It was very common in the USA until the 1960s, when herbicides were still not very popular. After several decades, interest has been renewed in the USA, Canada and Europe, because of increasing environmental and health concerns. Flaming can be used to control weeds before crop planting/emergence (non-selective) and after crop emergence (selective).
In this context, a specific machine for mechanical-thermal weed control in maize is being developed within the European Project RHEA. This machine will provide selective thermal in-row weed control and mechanical between-row weed removal.
This paper focuses on thermal weed control and reviews some of the studies that describe the tolerance of maize to flaming. The yield loss is generally very low and the treatment does not greatly affect the production, especially with doses lower than or equal to 50 kg ha^{-1}. The maximum threshold is generally not higher than 15-20% of yield loss and is usually reached just with doses higher than 100 kg ha^{-1}.

1. Introduction

Public concern regarding agrochemical issues is constantly increasing (Ascard et al. 2007). This is probably one of the most important reasons for the great diffusion of alternative/integrated/organic farming systems in Europe and North America (IFOAM et al. 2009, Ulloa, Datta and Knezevic 2010b, van der Weide et al. 2008). The European organic food market grew from about twelve thousand million euros in 2005 to eighteen thousand million in 2008 (IFOAM et al. 2009). There was a considerable increase in organic areas in Europe between 2005 and 2008, with cereals and fodders as the main crops (Eurostat, Press and Office 2010). In addition severe EU Directives and Regulations are having a big impact on farmers' choices for an environmental-friendly/sustainable agriculture. There has recently been a substantial reduction in the number of the active ingredients available (the ones considered potentially dangerous by the EU Commission), and probably many other products are about to be banned by the EU (EU/Directive 1991, DIRECTIVE 2009, REGULATION 2009). Farmers are encouraged to use "integrated pest management

means" and "sustainable, biological, physical and non-chemical methods must be preferred to chemical methods if they provide satisfactory pest control" (DIRECTIVE 2009).

Weed control has always been a major problem in agriculture and probably is the biggest in organic farming systems (Bàrberi, 2002). The only solution for organic farmers is to use mechanical and thermal means. Mechanical weed control consists in using soil tillage, and cutting and extracting/pulling weeds (Cloutier et al., 2007). Thermal weed control involves different kinds of radiation (i.e. fire, flaming, hot water, steam) in order to cause thermal injury to the weeds (Ascard et al. 2007). Therefore a "holistic" approach is generally the most advisable way to provide an efficient non-chemical weed management. The integration of preventive, cultural and direct means is often the only solution for satisfying and remunerative crop production (Bàrberi, 2002, Bond and Grundy, 2001). A hot topic in weed science and agricultural engineering is the study of mechanical and thermal means for non-chemical weed management, along with research into new types of machines for non-chemical weed control (Cloutier et al., 2007, Ascard and van der Weide, 2011).

This paper focuses on flame weeding, which is the most widely used thermal control method (Ascard et al., 2007), and its application to maize, as a selective post-emergence treatment (Ulloa et al., 2011). A review of some of the studies carried out to investigate the maize response to heat is presented, since an innovative autonomous machine will be built within the RHEA project for mechanical-thermal weed control in maize. This machine will provide mechanical weed control between the rows and selective thermal weed control in the row. For further information please see the specific work in the proceedings of this workshop.

2. Flaming: the general and "historical" background

Flaming consists of the use of an open flame to control weeds. This method does not leave any residue either in the soil, the water or the crop, and it is acceptable practice in organic agriculture (Ascard et al., 2007).

The principle is based on heating up the cells of the plant, which causes the denaturation and aggregation of cellular proteins and protoplast expansion and rupture. The final result is the desiccation of the upper part of the plant, but the roots are not injured. Depending on the stage and the type of plant, several treatments may be required as shoots may regenerate (Ascard et al., 2007, Vanhala et al., 2004).

Large-scale flaming was used between 1940-1960 mainly for selective post emergence applications (Ascard et al., 2007). The first flame weeder was developed in the USA in 1852, and numerous machines were patented thereafter. Initially the

main purpose of these machines was to destroy insects. Afterwards flaming was mainly used for weeds. In Australia flaming was used in the early 1930s for weed control in sugar cane without injuring the crop. In 1935 it was used for the first time in cotton fields. In 1941 flaming was successfully applied in Louisiana on sugar cane, and 10 flaming machines were constructed and used in 1943 (de Rooy, 1992).

In 1945 LPG (liquefied petroleum gas, mainly propane and butane) equipment was introduced for farm use ,and replaced liquid fuels such as kerosene and oils (de Rooy, 1992, Ascard et al., 2007). With the introduction of LPG, a completely different technology was developed. It was a tough task for agricultural engineering research (de Rooy, 1992). Flaming was then widely used in the USA until the mid 1960s in cotton, maize soybeans, lucerne, potatoes, onions, grapes, blueberries and strawberries (Ascard et al., 2007). Because of the increase in the cost of petrol and the development of the agrochemical industry, flaming became less popular in the USA in the 1970s (Ascard et al., 2007).

Interest in this technique in USA and Canada has been renewed because of public concern regarding agrochemicals (Ascard et al., 2007, Bruening et al., 2009, Domingues et al., 2008, Knezevic et al., 2009a, Knezevic, Datta and Ulloa 2009b, Knezevic et al., 2009c, Knezevic and Ulloa 2007, Teixeira et al., 2008). In Europe flaming was not popular in the 1960s. Subsequently it became more widely used for organic farming systems and was first adopted in Germany and Switzerland (Ascard et al. 2007). Flaming is still quite common in Europe for organic farming systems, especially in seeded horticultural crops, and research into physical and cultural weed control is currently being carried out (Ascard, 1990, Ascard and van der Weide 2011, Vanhala et al., 2004, Peruzzi et al., 2007, Raffaelli et al., 2010, Raffaelli et al., 2011).

There are two main groups of LPG burners for weed control: the liquid or self vapourizing type, and the vapour type (Ascard et al., 2007, de Rooy, 1992). In the first type, the LPG is liquid from the tank to the burner and is vapourized into gas when it reaches the burner. In the second group, LPG is already in the gas phase when drawn from the tank (de Rooy, 1992). This second group generally requires a heat exchange system to avoid the tank freezing because of the high energy requirement of the LPG passing from the liquid to the gas phase (Peruzzi et al., 2007, Raffaelli et al., 2010, Raffaelli et al., 2011).

The shape of the burner and the flame can be flat or tubular. Burners can be open or covered by a specific hood. This second option is generally used for non-selective flaming before crop emergence, for weed control in urban areas and for haulm destruction (Ascard et al., 2007). The burner should be set appropriately in order to avoid flame deflection. Generally the angle of the burner should be around 45°, with a ground clearance of about 10 cm (Ascard et al., 2007). One of the most common is the Hoffmann burner, which was developed in Germany. It is shaped like a rod and provides a stable and controllable flame (Ascard et al., 2007, de

Effect of flaming with different LPG doses on maize plants

Rooy, 1992). For a common open flamer, LPG consumption, usually varies from 20 to 50 kg ha^{-1} (Ascard et al., 2007, Peruzzi et al., 2007, Raffaelli et al., 2010, Raffaelli et al., 2011).

3. Flaming: when and where it can be used

Flaming can be applied:

Before crop planting/emergence on the whole surface (non-selective broadcast flaming). This method obviously does not require a heat tolerant crop.

After crop emergence:

Non-selective flaming between rows (does not require a heat tolerant crop)

Selective flaming. These methods require heat tolerant crops:

Broadcast flaming (the whole surface area where the crop is located is flamed)

Burners are placed in the rows

Burners are directed at the collar of the crop ("cross flaming") (Fig. 1)

Non selective flaming before crop planting/emergence is very common in organic farming with the false seedbed technique, which provides preventive weed control through seedbank depletion. Weed emergence is stimulated by a delayed seedbed preparation and the last phase before crop emergence is carried out by flaming. This does not disturb the soil and the emerging crop and does not stimulate further weed emergence. This technique is very common in low competitive vegetable production (i.e. carrot) and is combined with post-emergence mechanical weed control (Peruzzi et al., 2007, Raffaelli et al., 2010, Raffaelli et al., 2011, Ascard and van der Weide, 2011).

Non-selective flaming after crop emergence between rows was developed in the 1960s in the USA for weed and insect control in many crops, and for potato haulm desiccation (Ascard et al., 2007). However this application is not common as a cultivator/hoe provides less energy-consuming weed control between rows.

Selective broadcast flaming provides weed control on the whole surface where the crop is located. Heat tolerant crops are required such as maize and onions (Ascard et al., 2007). Several successful trials were carried out at the University of Nebraska, in order to investigate the responses of maize, sweet maize, popcorn, soybean, sorghum, and wheat to broadcast flaming (Ulloa et al., 2011, 2010a, 2010b, 2010c).

Intra-row weed control is challenging for organic farming systems because it is often very labour intensive, especially in vegetable crops (Fogelberg, 2007, van der Weide, et al. 2008). This is why in-row flaming *plus* between row cultivation is a good option in order to reduce LPG consumption and crop injury compared to

broadcast flaming (Peruzzi et. al., 2000, Knezevic et al., 2011). LPG consumption is lower as the treatment is performed in bands. Crop injury can be reduced by choosing a "cross" adjustment of the burners. Two burners are placed on each row, perpendicular to the driving direction and directed at the lower part of the stem, which is more resistant than the higher part (Ascard et al., 2007). This option was chosen for the RHEA project.

4. Is maize really resistant to flaming?

The effect of flame weeding on maize has been widely studied since the 1940s (de Rooy, 1992):

"Flame weeding is a matter of differential burning. Just enough heat should be applied to kill the weeds, but not enough to kill the crop plants. Some crop plants, such as corn, have more resistance to flame than do the common weeds; therefore, corn is flamed successfully (Wright, 1947 cited in de Rooy 1992)."

Research on flaming in maize were carried out in the USA in the 1960s. In 1969 flaming was tested for the first time before crop emergence with the "delayed seeding technique" (de Rooy, 1992). Specific experiments on selective flaming were carried out in maize when the crop was about 30 cm tall. The results showed that flaming should be used in combination with other methods such as mechanical hoeing or cultivation.

Guidelines provided by Hoffman specify that maize should be flamed up to 25 cm tall (de Rooy, 1992). His burner was improved by Lincoln University in New Zealand in the 1990s (de Rooy, 1992).

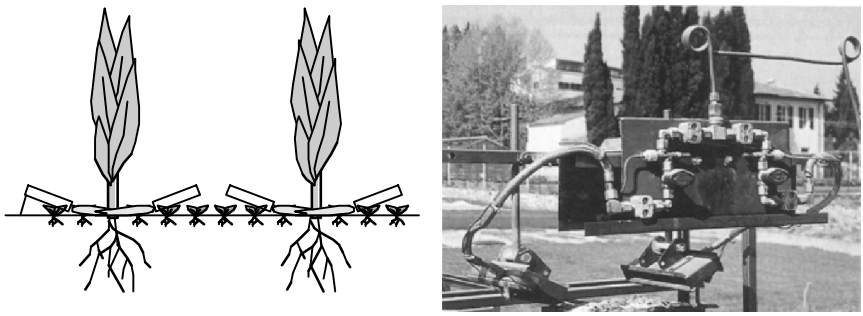

Fig. 1. Cross flaming, and the test bench developed by the University of Pisa (Peruzzi et al., 2000)

Laboratory and field trials carried out in Canada showed that maize can tolerate two different treatments at the 2-3 leaf and 6-7 leaf stages without a significant reduction in yield. An intermediate treatment at the 4-5 leaf stage was not advisable as it resulted in a considerable reduction in yield (Leroux et al., 2001).

Effect of flaming with different LPG doses on maize plants

Table 1. The effect of LPG dose on maize dry grain as affected by the growth stage of flaming (Peruzzi et al., 2000). Different letters indicate significant differences at $P < 0.05$ (Duncan's Multiple Range Test)

LPG Consumption (kg/ha) Stage	Maize dry grain per plant (g)		
	1-2 leaves	4 leaves	8 leaves
7,24	103.8 abc	108.9 abcd	111.7 a
9,31	98.1 abc	125.9 abc	117.3 a
11,96	96.8 abc	107.9 abcd	103.8 ab
13,04	112.1 abc	129.3 abc	120.4 a
15,37	95.6 abc	117.1 abc	122.8 a
17,02	123.3 abc	109.1 abcd	116.4 a
21,70	122.2 abc	113.0 abcd	114.4 a
21,89	124.0 ab	108.6 abcd	110.1 ab
22,22	93.4 bc	99.7 cd	100.4 ab
25,52	95.1 bc	132.6 a	129.9 a
28,57	88.5 c	102.4 abcd	102.3 ab
30,64	100.4 abc	111.8 abcd	108.5 ab
35,80	120.0 abc	106.8 abcd	116.5 a
40,00	88.6 c	104.8 abcd	81.9 b
51,07	95.7 abc	110.3 abcd	103.1 ab
65,20	130.2 a	130.3 ab	117.3 a
66,67	88.8 c	100.8 bcd	82.7 b
107,60	130.3 a	132.7 a	115.4 a
153,20	96.3 abc	116.0 abcd	106.9 ab
200,00	89.9 bc	85.8 d	82.1 b
Control	110.4 abc	110.4 abcd	110.4 ab

At the University of Pisa, we carried out laboratory experiments on selective "cross flaming" in maize using a 25 wide rod open flame burner (Fig. 1). Different combinations of LPG pressures and working speeds were tested, resulting in a different LPG consumption ha^{-1} (total amount of LPG per ha, whose dosage did not correspond to the actual dose on the row-band) from 7 to 200 kg ha^{-1} (Tab. 1). No statistically significant yield reductions were observed with any of the tested doses and at any growth stage (Peruzzi et al., 2000). For example, the yield loss observed with an LPG consumption of about 50 kg ha^{-1} was just 7%. The average yield loss obtained using the highest LPG consumption ha^{-1} (200 kg) was about 20%.

Recent studies carried out by the University of Nebraska (USA) on broadcast flaming in maize partially contradict the results previously reported by Leroux and colleagues (2001), as V5 stage had in this case the least yield loss followed by V7 and V2 (maximum yield losses of 3%, 11% and 17% obtained with the highest propane dose 85 kg ha^{-1} respectively). A yield reduction of about 12%, 8% and 3% were observed at V2, V7 and V5 stages respectively, with a propane dose from 45 up to 55 kg ha^{-1} (Ulloa et al., 2011). Further experiments have been carried out by the same research group in order to test a combined flaming-cultivation treatment in maize. Results of just the first year showed that this kind of treatment should be preferably performed twice, at V3 and V6 stages (Knezevic et al., 2011).

5. Conclusions

The RHEA project will lead to the development of a new machine for combined thermal-mechanical weed control treatments in maize. Flaming will be performed selectively in rows. The flames will be targeted at the base of the crop. The actual in-row doses will vary from about 45 kg ha^{-1} to about 55 kg ha^{-1}, which corresponds to a maximum LPG consumption of less than 20 kg ha^{-1}, if the treatment is performed on all the surface.

Based on the results from recent research on maize, the mechanical-thermal treatment could be repeated twice with the recommended doses, without significantly affecting the maize yield. As the flaming dose is strictly related to the type of burner, the effects of flaming on maize and weeds using the new burners will be investigated at the University of Pisa specifically for the RHEA project.

Acknowledgement

The research leading to these results has received funding from the European Union's Seventh Framework Programme [FP7/2007-2013] under Grant Agreement nº 245986.

References

Ascard, J. (1990). Thermal weed control with flaming in onions. Proceedings 3rd International Conference IFOAM, Non-Chemical Weed Control, 34, 175-188.

Effect of flaming with different LPG doses on maize plants

Ascard, J., P. E. Hatcher, B. Melander and M. K. Upadhyaya (2007). Thermal weed control. Non-chemical Weed Management, 155-175.

Ascard, J. and R. Y. van der Weide. (2011). Thermal weed control with the focus on flame weeding. In Physical weed control: Progress and challenges, eds. D. C. Cloutier & M. L. Leblanc, 71-90. Pinawa, Manitoba, Canada R0E 1L0: Canadian Weed Science Society - Société canadienne de malherbologie.

Bàrberi, P. (2002). Weed management in organic agriculture: are we addressing the right issues? Weed research, 42, 176-193.

Bond, W. and A. C. Grundy (2001). Non-chemical weed management in organic farming systems. Weed Research, 41, 383-405.

Bruening, C. A., G. Gogos, S. M. Ulloa and S. Z. Knezevic (2009). Performance advantages of flaming hood. Proc. North Central Weed Sci. Soc, 64, 30.

Cloutier, D. C., R. Y. van der Weide, A. Peruzzi and M. L. Leblanc. (2007). Mechanical weed management. In Non-chemical weed management, eds. M. K. Upadhyaya & R. E. Blackshaw, 111-134. Oxon, UK.

de Rooy, S. C. (1992). Improved efficiencies in flame weeding. In Department of Natural Resources Engineering, 87. Canterbury, New Zeland: Lincoln University.

DIRECTIVE, 2009/128/EC, OF, THE, EUROPEAN, PARLIAMENT, AND, OF, THE, COUNCIL, of, 21 and October. (2009). establishing a framework for Community action to achieve the sustainable use of pesticides. Web Page: http://eur-lex.europa.eu.

Domingues, A. C., S. M. Ulloa, A. Datta and S. Z. Knezevic (2008). Weed response to broadcast flaming. RURALS.

Eurostat, Press and Office (2010). Organic area up by 21% in the EU between 2005 and 2008. eurostat newsrelease., 30/2010. Web Page: http://ec.europa.eu/eurostat.

Fogelberg, F. (2007). Reduction of manual weeding labour in vegetable crops – what can we expect from torsion weeding and weed harrowing? In 7th EWRS Workshop on Physical and Cultural Weed Control, 113-116. Salem, Germany.

IFOAM, EU, Group and FiBL (2009). Organic Farming in Europe– A Brief Overview. Web page: www.fibl.org.

Knezevic, S., A. Datta, S. Stepanovic, C. Bruening, B. Neilson and G. Gogos. (2011). Weed control with flaming and cultivation in maize. In 9th EWRS Workshop on Physical and Cultural Weed Control, 79. Samsun, Turkey, 28 – 30 March.

Knezevic, S. Z., C. M. Costa, S. M. Ulloa and A. Datta (2009a). Response of corn (Zea mays L.) types to broadcast flaming. Proceedings of the 8th European Weed Research Society Workshop on Physical and Cultural Weed Control, 92-97.

Knezevic, S. Z., A. Datta and S. M. Ulloa (2009b). Tolerance of selected weed species to broadcast flaming at different growth stages. Proceedings of the 8th European Weed Research Society Workshop on Physical and Cultural Weed Control, 98-103.

Knezevic, S. Z., J. F. Neto, S. M. Ulloa and A. Datta. (2009c). Winther wheat (Triticum aestivum L.) tolerance to broadcast flaming. In 8th EWRS Workshop on Physical and Cultural Weed Control, 104-110. Zaragoza, Spain.

Knezevic, S. Z. and S. M. Ulloa (2007). Flaming: potential new tool for weed control in organically grown agronomic crops. J. Agric. Sci., 52, 95-104.

Leroux, G. D., J. Douheret and M. Lanouette (2001). Flame weeding in corn. Physical Control Methods in Plant Protection, 47-60.

Peruzzi, A., M. Ginanni, M. Fontanelli, M. Raffaelli and P. Bàrberi (2007). Innovative strategies for on-farm weed management in organic carrot. Renewable Agriculture and Food Systems, 22, 246-259.

Peruzzi, A., M. Raffaelli and S. Di Ciolo (2000). Experimental tests of selective flame weeding for different spring summer crops in Central Italy. Agricoltura Mediterranea, 130, 85-94.

Raffaelli, M., M. Fontanelli, C. Frasconi, M. Ginanni and A. Peruzzi (2010). Physical weed control in protected leaf-beet in central Italy. Renewable Agriculture and Food Systems, 25, 8-15.

Raffaelli, M., M. Fontanelli, C. Frasconi, F. Sorelli, M. Ginanni and A. Peruzzi (2011). Physical weed control in processing tomatoes in Central Italy. Renewable Agriculture and Food Systems, 1-9.

REGULATION, (EC), No, 1107/2009, OF, THE, EUROPEAN, PARLIAMENT, AND, OF, THE, COUNCIL, of, 21 and October. (2009). concerning the placing of plant protection products on the market and repealing Council Directives 79/117/EEC and 91/414/EEC. Web Page: http://eur-lex.europa.eu.

Teixeira, H. Z., S. M. Ulloa, A. Datta and S. Z. Knezevic (2008). Corn (Zea mays) and soybean (Glycine max) tolerance to broadcast flaming. RURALS.

UE/Directive. (1991). n° 91/414.

Ulloa, S. M., A. Datta, C. Bruening, B. Neilson, J. Miller, G. Gogos and S. Z. Knezevic (2011). Maize response to broadcast flaming at different growth stages: Effects on growth, yield and yield components. European Journal of Agronomy, 34, 10-19.

Ulloa, S. M., A. Datta, S. D. Cavalieri, M. Lesnik and S. Z. Knezevic (2010a). Popcorn (Zea mays L. var. everta) yield and yield components as influenced by the timing of broadcast flaming. Crop Protection, 29, 1496-1501.

Ulloa, S. M., A. Datta and S. Z. Knezevic (2010b). Growth stage impacts tolerance of winter wheat (Triticum aestivum L.) to broadcast flaming. Crop Protection, 29, 1130-1135.

Ulloa, S. M., A. Datta, G. Malidza, R. Leskovsek and S. Z. Knezevic (2010c). Timing and propane dose of broadcast flaming to control weed population influenced yield of sweet maize (Zea mays L. var. rugosa). Field Crops Research, 118, 282-288.

van der Weide, R. Y., P. O. Bleeker, V. T. J. M. Achten, L. A. P. Lotz, F. Fogelberg and B. Melander (2008). Innovation in mechanical weed control in crop rows. Weed Research, 48, 215-224.

Vanhala, P., D. A. G. Kurstjens, J. Ascard, B. Bertram, D. C. Cloutier, A. Mead, M. Raffaelli and J. Rasmussen (2004). Guidelines for physical weed control research: Flame weeding, weed harrowing and intra-row cultivation. Prodeedings 6th EWRS Workshop on Physical and Cultural Weed Control, 208-239.

Perception and analysis

Hyperspectral imagery to discriminate weeds in wheat

Gilles Rabatel*, Farida Ougache, Nathalie Gorretta* and Martin Ecarnot*****

**UMR ITAP – Cemagref Montpellier*
361, rue J-F Breton, BP 5095 – 34196 Montpellier Cedex 5, France

(e-mail: gilles.rabatel@ cemagref.fr)

***Université Montpellier II, place Eugène Bataillon*

34095 Montpellier cedex 5, France

****UMR AGAP - INRA Montpellier*
2 PLACE VIALA, 34060 Montpellier cedex 1, France

Abstract: The problem of weed and crop discrimination by computer vision remains today a major obstacle to the promotion of localized weeding practices. The objective of present study was to evaluate the potential of hyperspectral imagery for the detection of dicotyledonous weeds in durum wheat during weeding period (end of winter). An acquisition device based on a push-broom camera mounted on a motorized rail has been used to acquire top-view images of crop at a distance of one meter. A reference surface set in each image, as well as specific spectral preprocessing, allow overcoming variable outdoor lighting conditions. The spectral discrimination between weeds and crop, obtained by PLS-DA, appears particularly efficient, with a maximal error rate on pixel classification lower than 2%. However complementary studies addressing robustness are still required.

1. Introduction

The Precision Agriculture concept relies on the spatial modulation of crop processing operations, for a better adaptation to heterogeneities inside the parcel. This concept, which raised more than twenty years ago, is now currently applied in nitrogen input management, allowing a better control on yield and product saving.

However, for weeding operations, despite considerable environmental and economical issues, the common practice until now is still to apply an assurance strategy: herbicides are uniformly spread all over the parcel whatever is the actual level of infestation.

The reason is mainly technological. Actually some devices are proposed on the market to operate localized spraying of herbicides on bare soil (the vegetation

being detected by photocells). However, no commercial setup addresses localized weeding operations after crop emergence, because it requires a perception system based on computer vision, able to discriminate weeds from crop.

Indeed, the identification of species inside vegetation is today the main obstacle to localized weeding. Numerous scientific studies have addressed this problem, and can be classified in two main approaches (Slaughter, D et al. 2008):

- the spectral approach, which focuses on the plant reflectance, and involves multispectral or hyperspectral imagery (Feyaerts and van Gool, 2001) (Vrindts et al. 2002). In this case, the difficulty consists in establishing spectral differences that are robust with respect to variable lighting conditions.

- the spatial approach, which relies on spatial criteria such as plant morphology (Chi, Y et al. 2003, Manh et al. 2001), texture (Burks, T et al. 2000) or spatial organization (Gée et al, 2008). In this case, the natural complexity and variability of vegetation scenes are the main difficulties.

The study presented here comes within the first approach, in the particular case of durum wheat crop. The objective was to evaluate, as a first step, if the leaf reflectance contains enough spectral information to make a reliable discrimination between crop and dicotyledonous weeds. For this purpose, hyperspectral images of crop scenes have been acquired during the weeding period. Then specific correction procedures have been applied to overcome the variability of lighting conditions and of spatial orientation of leaves in natural crop scenes. Finally, a PLS-DA discrimination model has been calibrated and tested on the resulting hyperspectral images, and the discrimination results are presented and discussed.

2. Material and methods

2.1 Image acquisition

Hyperspectral images of durum wheat have been acquired in an experimental station (INRA, domaine de Melgueil) near Montpellier, south of France, in March 2011. Images were acquired using a device specially developed by Cemagref for in-field short-range hyperspectral imagery. The device consists in a push-broom CCD camera (HySpex VNIR 1600-160, Norsk Elektro Optikk, Norway) fitted on a tractor-mounted motorised rail (Fig. 1). The camera has a spectral range from 0.4 µm to 1 µm with a spectral resolution of 3.7 nm. The first dimension of the CCD matrix is the spatial dimension (1600 pixels across track) and the second dimension is the spectral dimension (160 bands).

Each image represents about 0.30 m across track by 1.50 m along track seen at 1 m above the canopy, the lens and the view angle being fixed. The spatial resolution across track is 0.2 mm. The spatial resolution along track, depending on the motion speed, has been adjusted consequently.

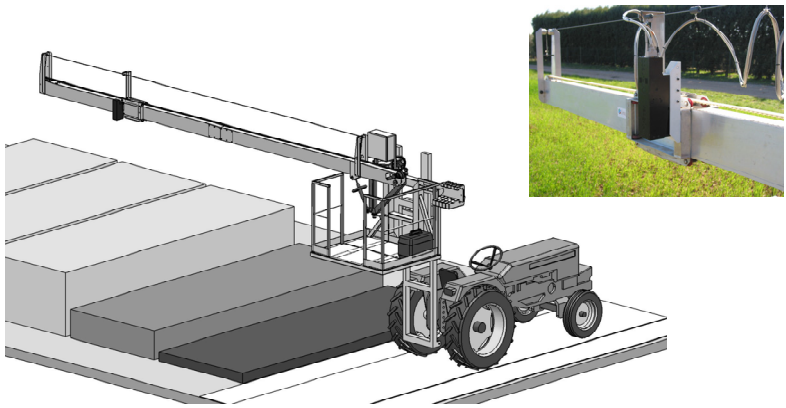

Fig. 1. Cemagref hyperspectral imaging device Computer Aided Design (CAD) general view and camera detail

Data are digitalised on 12 bits, giving a digital number (DN) between 0 and 2^{12}-1 = 4095. In order to preserve the signal-noise ratio (SNR) while avoiding signal saturation, the CCD sensor integration time has been adjusted for each image so that the average raw signal value for vegetation is around 2000 in the near-infrared domain (where it is maximal). Nevertheless, some pixels are saturated: pixels for which at least one band has a value greater than 4000 have been considered as saturated pixels and their spectra have been automatically set to a null value. They will not be used for further treatments.

In the following, hyperspectral image are shown with false colours, i.e. using 3 bands respectively at 615, 564 and 459 nm as R, G, and B channels.

2.2 Image correction

Luminance correction

Because the CCD sensor has not a uniform spectral sensitivity (it is more sensitive in the visible domain than in the NIR domain), the raw signal must be corrected with data provided by the camera constructor, in order to obtain absolute radiometric data not depending on the instrument. At this stage, other instrumental effects are also taken into account, such as the dark current (which is automatically measured before each image shot with the lens shutter closed), and the relative sensitivity of each CCD pixel. The detailed correction is given by (1)

$$CN[i,j] = \frac{DN[i,j] - BG[i,j]}{RE[i,j].S[j]} \quad (1)$$

where DN[i, j] is the digital number (raw signal), with *i* referring to the first (spatial) dimension of the CCD matrix ($i \in$ [0, 1599]) and *j* referring to the second (spectral) dimension ($j \in$ [0, 159]). BG[i, j], RE[i, j] and S[j] are respectively the dark current,

the relative response matrix for each detector element (or pixel) and the camera spectral sensitivity. The resulting float type value CN[i,j] for each line pixel is then a luminance signal. It will be noted *L(x,y,λ)* in the following, where x is the spatial coordinate *i* in the line, y is the spatial coordinate of the line along track, and λ is a given wavelength.

This luminance correction can be made by post-processing, or in real-time during image acquisition. An example of corrected spectrum is given in Fig. 2.b.

Reflectance correction

In order to be able to compare spectral data collected in different outdoor conditions, we need to have hyperspectral images independent of illumination, i.e. reflectance images. The reflectance of a given material is the ratio of reflected light to incident light. So, we need to know solar lighting at each acquisition time. To this end, Spectralon™ (Labsphere, Inc., New Hampshire, USA.) is generally used because it is a lambertian surface and it reflects 99 % of received signal whatever the wavelength. Therefore, it provides a good approximation of solar incident light in outdoor conditions. However, in our case, we have chosen to use a commercial ceramic plate, which is more robust to damage or dirt due to field experiment conditions. Also, since integration time is optimised for vegetation, a grey ceramic plate was required, in order to avoid saturated ceramic pixels. This plate has been set in the field of view for every image acquisition (see Figs 5 and 7).

The bidirectional reflectance distribution function (BRDF) of the ceramic has been measured in laboratory. As for many ordinary materials, it is the summation of a lambertian term and a specular term (shininess), this last one depending on the incident and viewing angles. However, because the specular term is directive enough, it can be totally neglected in our field operating conditions (horizontal plate observed with a zenithal view under non zenithal solar lighting incidence, according to the latitude and season). We can thus consider the ceramic plate as a lambertian material with a known hemispheric reflectance *Rc(λ)*.

Finally, for a given luminance image, the average luminance *Lc(λ)* measured on the ceramic plate can be used to compute the horizontal irradiance *E(λ)* on the scene:

$$E(\lambda) = Lc(\lambda) / Rc(\lambda) \quad (2)$$

This allows to apply the following reflectance correction to every pixel in the image:

$$R(x,y,\lambda) = L(x,y,\lambda) / E(\lambda) = \frac{L(x,y,\lambda).Rc(\lambda)}{Lc(\lambda)} \quad (3)$$

where (x,y) are the pixel coordinates.

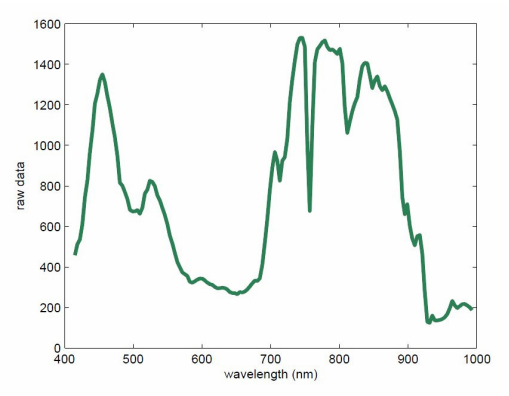

a)

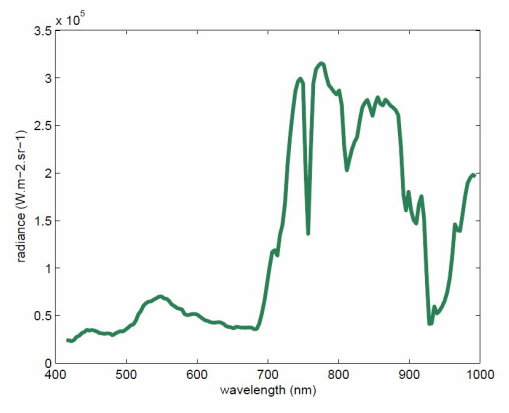

b)

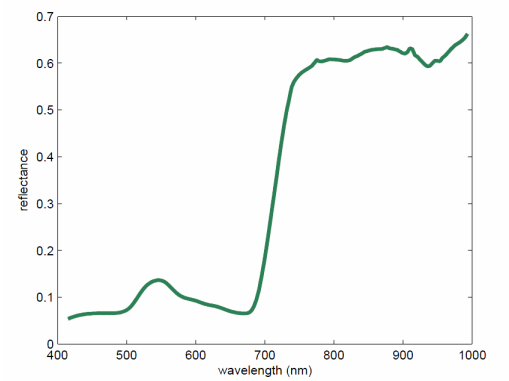

c)

Fig. 2. Example of 12 bits raw spectrum (a), luminance spectrum (b) and reflectance spectrum (c) for a vegetation pixel

The effect of successive luminance and reflectance corrections on a vegetation pixel are given in Fig. 2. The reflectance spectrum clearly shows how lighting

spectrum specificities are removed, e.g. the absorption peak near 750 nm due to oxygen in the atmosphere.

Leaf-orientation-effect correction

The reflectance correction specified in (3) takes into account the irradiance E*(λ)* measured by means of an horizontal plate. However, leaf surfaces in the vegetation scene are not horizontal. Therefore, their irradiance can be higher or lower than the ceramic plate's one, according to the cosine of the angle between their surface normal and the lighting incidence (Fig. 3.a). This introduces an unknown multiplicative factor *k1* on the pixel spectrum collected in the reflectance image, with respect to the real leaf reflectance.

Moreover, as already mentioned for the ceramic plate, the BRDF of leaves includes a specular term (Bousquet L. et al, 2005). But in this case, due to a random spatial orientation, this specular reflection may be directed toward the image sensor (Fig. 3.b). Because the specular light is not spectrally modified by the material, it contributes to the apparent reflectance as an additive term *k2*.

As a summary, the leaf pixel values in the reflectance image do not correspond to the actual leaf lambertian reflectance *Rf(x,y,λ)*, but to an apparent reflectance:

$$Rapp(x,y,\lambda) = Rf(x,y,\lambda).k1 + k2 \quad (4)$$

where *k1* and *k2* are unknown terms.

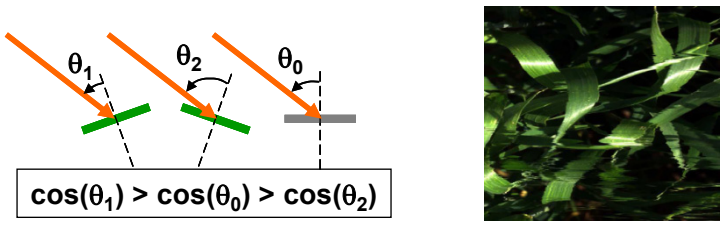

a b

Fig. 3. Leaf orientation effects. a) effect on irradiance level; b) specular reflection

In order to remove these unknown terms, a Standard Normal Variate (SNV) transformation will be systematically applied to every spectrum before any further processing. It consists in centring the spectrum and setting its standard deviation equal to one (Fig. 4).

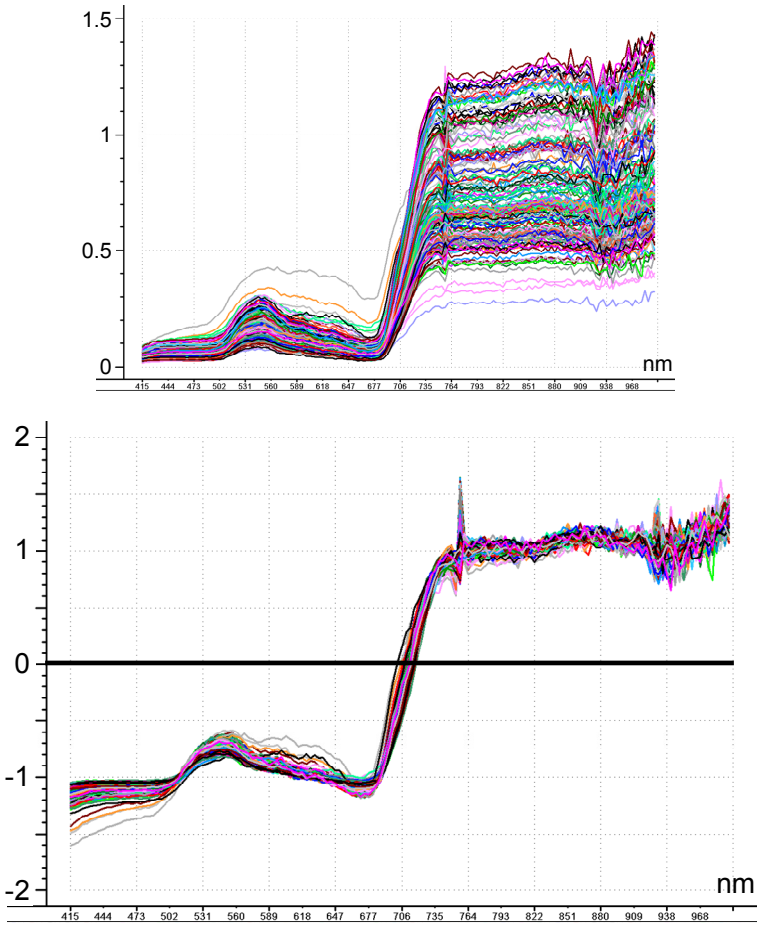

Fig. 4. SNV transformation applied to a set of wheat spectra

2.2 Spectral discrimination model

Calibration set

In order to build a discrimination model, we need a calibration set, i.e. a set of spectrum samples for each of the material classes that we want to discriminate. For this purpose, we have selected manually a total of 335 pixels in a reflectance image, according to three classes: durum wheat (157 pixels), dicotyledonous weeds (60 pixels) and soil (118 pixels).

The calibration image is shown in Fig. 5, as well as the position of the samples. It has been obtained with an integration time of 100 ms per line.

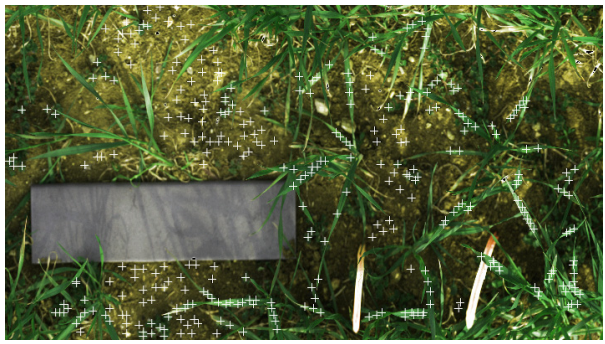

Fig. 5. Calibration image and sample positions

PLS-DA discrimination model

Because they contain accurate information about the chemical content of materials, reflectance or transmittance spectra are often used for quantitative evaluation of component concentration, or for material discrimination. However, due to the high dimension of spectral data (hundreds of variables), classical multivariate regression or discrimination tools are not directly usable, and a first step of dimension reduction is generally required. In this context, the Partial-Least-Square regression (PLS) has become a very commonly used tool, thanks to its ability to determinate a pertinent subspace for a given regression problem (unlike other dimension reduction methods like the Principal Component Analysis, the PLS takes into account the covariance of both inputs and outputs to determine the subspace components, called “latent variables” or LV).

The PLS addresses the following linear regression problem: given a set of p calibration spectra $Xp = [S1(\lambda), \ldots, Sp(\lambda)]$ and the corresponding outputs $Yp = [y1, \ldots, yp]$, one wants to define a linear regression model B so that for any input spectrum S, the corresponding output y can be estimated by:

$$y = B.\ S \qquad (5)$$

(notice that the standard solution $B = Yp\ .\ Xp^{+}$, where Xp^{+} is the pseudo-inverse of the matrix Xp, is generally undefined due to the high dimensionality of Xp).

The PLS is an iterative method, where a new LV is built at each step. The optimal number of latent variables (LV) is usually determined using an independent test set, or by a leave-one-out procedure (cross-validation).

Though the PLS usually addresses linear regression, it can also be use in discrimination analysis (PLS-DA). In the present case, we have chosen the following PLS-DA procedure:

i) 3 targeted output functions y1, y2, y3 have been defined as the membership level for each of the three classes, with the following values for the calibration set :

y1 = 1 for the wheat class, and 0 otherwise
y2 = 1 for the weed class, and 0 otherwise
y3 = 1 for the soil class, and 0 otherwise

ii) 3 regression models B1, B2, B3 have then been computed by PLS, so that for a given input spectrum S, the membership levels can be estimated by:

$$y1 = B1.S \; ; \qquad y2 = B2.S \; ; \qquad y3 = B3.S$$

iii) the chosen class for the input spectrum S is then the class *i* for which the membership degree y*i* is the higher.

3. Results and discussion

In order to illustrate the classification procedure, the three estimated membership values for all the samples are given in Fig. 6. As it could be expected, the best membership estimation is obtained for the soil, and requires only two LV (soil could be discriminated easily from vegetation using a few spectral bands).

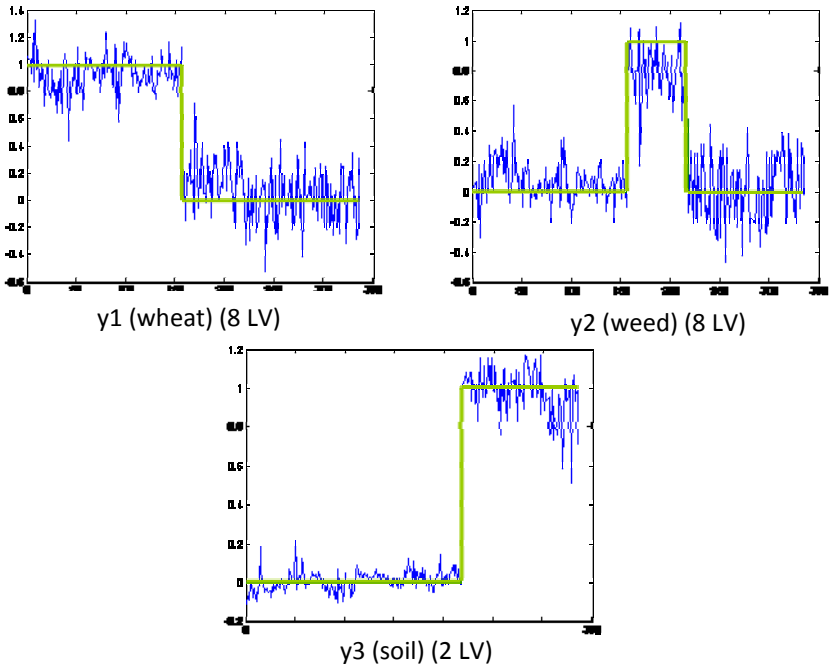

Fig. 6. Membership degree functions estimated by PLS for the 335 samples
on the abscissa: sample number (samples are sorted by class)
in green: targeted binary values

As explained above, the classification procedure consists, for a given spectrum, in choosing the class with the highest estimated membership degree. It has first been

applied on the calibration set itself, i.e. according to the function values shown in Fig. 6. The resulting confusion matrix is given in table 1. The classification performances are very good, with a maximal error rate of 1.7 % (dicotyledonous classified as wheat).

Table 1. confusion matrix for the whole sample set

	Classified as wheat	**Classified as weed**	**Classified as soil**
Wheat	156 (99.4 %)	1 (0.6 %)	0
Weed	1 (1.7 %)	59 (98.3 %)	0
Soil	0	0	118 (100 %)

Finally, the classification procedure defined above has been applied to a complete test image. This image has been acquired one hour after the calibration image, with an integration time of 50 ms. The original image as well as the corresponding classification results are given in Fig. 7.

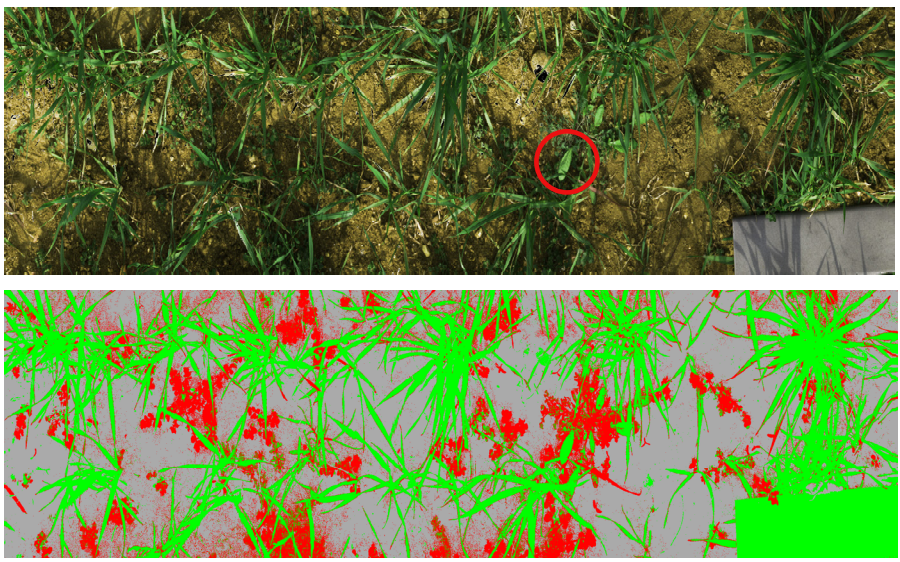

Fig. 7. Original test image (up) and classification results (down). Pixels classified respectively as wheat, weed and soil are colored in green, red and gray. The red circle show a dicotyledonous weed classified as wheat.

This test image confirms the high quality of classification and its robustness with respect to variable local lighting conditions (leaf orientation and shadowed areas). As an exception, a dicotyledonous weed (red circle in Fig. 7 up) has entirely been

classified as wheat: the reason is that this weed specie was not represented in the calibration set, so that its classification is arbitrary (as well as the classification of the ceramic pixels).

4. Conclusion

The results obtained above show the remarkable ability of detailed spectral information to discriminate vegetation species, provided the influence of lighting variability has been overcome using a reference material, and provided efficient chemometric tools such are PLS are involved. However, the classification error in the test image for a weed specie that had not been sampled before, underlines the importance of the calibration set sufficiency. Moreover, the high number of required latent variables (up to eight) indicates that very tiny differences in the spectral shapes are taken into account to achieve an accurate discrimination.

For these reasons, the robustness of such a discrimination model must still be assessed in extended experimental conditions (different days, different parcels, etc.). If the results are satisfactory, the following step will be to evaluate the possibility to reduce the number of required bands, e.g. through a detailed study of the latent variable shapes. It would open the door to an operational device based on multispectral image acquisition.

Acknowledgement

The research leading to these results has received funding from the European Union's Seventh Framework Programme [FP7/2007-2013] under Grant Agreement nº 245986.

References

Bousquet L., S. Lachérade, S. Jacquemoud and I. Moya (2005). Leaf BRDF measurement and model for specular and diffuse component differentiation, *Remote Sensing of Environment*, 98(2-3):201-211.

Burks, F.T, S.A. Shearer and F. A. Payne (2000). Classification of weed species using color texture features and discriminant analysis. *Transactions of the ASAE* 43: 441-448.

Chi, T.Y, C.-F. Chien and T.-T. Lin (2003). Leaf shape modeling and analysis using geometric descriptors derived from Bezier curves. *Transactions of the ASAE* 46: 175-185.

Feyaerts, F. and L. van Gool (2001). Multi-spectral vision system for weed detection. *Pattern Recognition Letters* 22(6-7): 667-674.

Gée, C., J. Bossu, G. Jones and F. Truchetet (2008). Crop/weed discrimination in perspective agronomic images. *Computers and Electronics in Agriculture* 60(1): 49-59.

Manh, A.-G., G. Rabatel, L. Assemat, M.-J. Aldon (2001). Weed Leaf Image Segmentation by Deformable Templates. *Journal of Agricultural Engineering Research* 80(N°2): 139-146.

Slaughter, D.C., D.K. Giles and D. Downey (2008). Autonomous robotic weed control systems : A review. *Computers and electronics in agriculture* 61: 63 - 78

Vigneau, N., M. Ecarnot, G. Rabatel, P. Roumet (2011). Potential of field hyperspectral imaging as a non destructive method to assess leaf nitrogen content in Wheat. *Field Crops Research* 122(1): 25-31.

Vrindts, E., J. De Baerdemaeker and H. Ramon (2002). Weed Detection Using Canopy Reflection. *Precision Agriculture* 3(1): 63-80.

Strategies for video sequence stabilisation

Angela Ribeiro*, Nadir Costa*, Gonzalo Pajares, Maria Guijarro****

**Centre for Automation and Robotics (CSIC-UPM), Crtra. Campo Real Km 0.2. 28500 Arganda del Rey, Madrid, Spain*

(e-mail: angela.ribeiro@car.upm-csic.es).

***Facultad de Informática. Universidad Complutense de Madrid (UCM), C/ Prof. José García Santesmases, s/n.*

28040 Madrid, Spain

(e-mail: pajares@fdi.ucm.es)

Abstract: This paper describes a stabilisation method applied to a precision agriculture scheme for weed control in crop fields. The method uses the centres of the crop rows as the characteristic elements to be detected and tracking across frames to compensate for the lateral movement of the camera. The inverse perspective transform is used to obtain a bird's-eye view of the original image recorded at the field. The transformation allows us to keep the centres of the three central crop rows centred on the screen for further processing. The proposed algorithm has been tested on image sequences of different fields and recorded at different times and under different lighting conditions. Lateral displacements of up to 66% of the inter-row spacing have been suppressed.

1. Introduction

Precision agriculture (PA) can be defined in many ways, but the underlying concept is always the same: the use of a management strategy that allows inputs to be varied with the aim of adjusting the crop management methods to the soil variations as well as the different conditions presented across the same crop. When the focus is weed control, PA can be thought of as a process that involves gathering field data (mapping) and the application of appropriate treatments based on the information gathered (actuation). In other words, the efficacy of a treatment (application of herbicides or other means of weed control) in a PA scheme is highly dependent on the accuracy of the information available about the crop to be treated. Weed mapping is an essential stage of the PA approach, but it is also currently the most expensive one; it is associated with a greater cost than "classic" weed control (i.e., treating the entire crop with the same herbicide dose). In other words, weed mapping is the Achilles heel of the PA when the costs of classic weed control are compared with the costs of the selective weed control

proposed by PA. In summary, it is extremely important to obtain the weed maps by automation (no operator intervention) and develop low-cost procedures for accomplishing the tasks involved in weed mapping: field data acquisition and both processing and interpretation of the data collected in the field. The aim is to automatically generate an accurate weed map of the target crop.

Weed mapping has traditionally been performed manually, using, among other things, random sampling techniques with a team of experts working in the field and performing in situ visual estimations. An alternative to this difficult task, which requires the transportation of several experts to the field with its consequent associated cost, is taking photo samples with and without controlled lighting (Ribeiro et al., 2005). The idea is that once photo sampling has been performed in the field by an operator, one or several experts in the laboratory can estimate the weed density and the crop growth stage from the images. This procedure avoids the subjectivity associated with the evaluation process in situ, in which experts tend to adjust the assessment of the weed amount to a global situation (Andujar et al., 2010). Nevertheless, it is clear that this kind of photographic sampling is not suitable for obtaining weed maps in real fields, which are often several hectares in size.

The automation of the information acquisition process in the field can be viewed as the integration of the inspection equipment (mainly cameras) onto mobile platforms that record continuous information (video). Possible approaches include the following: 1) the integration of a camera into a conventional tractor, with video acquisition occurring while other tasks are being performed in the field, or 2) an approach focused on inspection, in which an autonomous platform (mobile robot) is designed and developed exclusively for the inspection task. In either approach, obtaining quality images (video frames) is a significant challenge due to the uneven terrain, which results in undesirable movement of the mounting system of the camera, leading to the blurring of the images and making the discrimination of elements of interest more and more difficult, even to expert eyes. Due to the particular roughness of the terrain common to PA tasks, motion in the video sequences can include vibration, sway, roll and pitch, which reduces the image quality and makes the tracking of the elements of the scene a very complex task. It is, therefore, necessary to include a procedure for image stabilisation to eliminate the unwanted effects caused by the tractor's movements. The current paper describes a method for image sequence stabilisation in crop fields; it was developed specifically for use on maize crops but is also useful for many other wide-row crops.

2. The generation of a weed map from a sequence of video images

The generation of a weed map can be accomplished using a process that consists of three steps. The first step is the segmentation of the vegetation cover against the background (including soil, shadows, and sky) in each frame; the second step is the

integration of the information contained in each segmented bird's-eye view into a complete map of the entire field length; and the third step handles weed discrimination in each frame and the identification of the infested zones on the map.

2.1 Vegetation cover segmentation

Most cameras today use the RGB colour space, which is based on a combination of three different colour luminance signals (red, green and blue), such that each pixel obtains its specific colour by combining intensities (values in the range of 0-255) of the three planes. The segmentation of the vegetation cover can be achieved from the information supplied by these three colour planes. For example, Yang et al. (2003) consider each pixel in which the intensity in the green plane exceeds a certain threshold to be part of the vegetation cover, as long as the intensity of the green plane is also greater than those of the red and blue planes. This threshold is necessary to avoid false positives produced by pixels with a very low value of intensity in the three planes of colour (i.e., shadows).

Segmentation generally classifies a pixel as associated with the vegetation cover based on the value provided by a linear combination of the RGB planes. In this case, the primary issue is to choose adequate values for the constants to be multiplied to the matrices R, G and B. Hereafter, these constants will be denoted by *r*, *g* and *b*. Woebbecke et al. (1995) propose an excess green index (ExG) that assumes the following values for the constants: r = -1, g = 2, and b = -1. These values are empirically set. This index has been used with good results on images taken from the ground (Van Evert et al., 2006). Burgos-Artizzu et al. (2008) propose other values obtained from a set of 126 images of wheat taken in different places and with different lighting conditions, using an optimisation procedure based on an evolutionary algorithm. The adjusted values show a better performance in the discrimination of vegetation cover than those proposed by Woebbecke (Burgos-Artizzu et al., 2010). Following (Burgos-Artizzu et al. 2010), the colour image is transformed into a monochrome (grey level) image by (1):

$$image_{grey}(i,j) = r \cdot image_{red}(i,j) + g \cdot image_{green}(i,j) + b \cdot image_{blue}(i,j) \quad (1)$$
$$\forall i \in rows \wedge \forall j \in columns$$

Where $image_{red(i,j)}$, $image_{green(i,j)}$, and $image_{blue(i,j)}$ are the red, green and blue intensities (in the interval [0,255]) at pixel *(i,j),* respectively. To finish the segmentation procedure, a threshold function is applied to convert the grey-level image into a binary image in which the white pixels correspond to vegetation cover and the black pixels represent the rest. Several methods were tested to obtain the most appropriate threshold, including Otsu's method, which tends to set the threshold slightly above average in intensity, resulting in an overestimation of the

vegetation in the image. Ultimately, the threshold proposed by Burgos-Artizzu et al. (2008) was selected for its simplicity and its good average performance.

2.2 Integration of the field information in a map

The aim of this step is to build a map of the crop field using the recorded video sequences. Therefore, the information contained in each segmented bird's-eye frame has to be integrated into a complete map of the entire field length. This map consists of a matrix of specific dimensions, with each of its elements corresponding to a cell of a given size in the real field, enabling the selection of an adequate scale factor depending on the precision and field size required. The values of the matrix elements are determined by how many times vegetation cover is found in the cell that the element represents; higher values correspond to those cells in which vegetation cover was found in a larger number of frames. When a white pixel is found in the segmented frame, the matrix element corresponding to that field location (cell) is increased by one unit. Because the vehicle on which the camera is mounted moves forward, each new frame covers a slightly different field area, and the map's frame of reference must be updated. The distance in pixels that the reference moves between frames depends on the speed of the vehicle, i.e., the treatment speed. Once a particular field area has been mapped, the map contains different values (ranging from zero to a previously determined maximum) that refer to the number of frames containing vegetation cover (weeds and crops) in the corresponding field cell. In this manner, a higher number implies a higher level of certainty that the corresponding field cell contains vegetation cover.

After mapping, the matrix can be converted into a grey image in which higher values are lighter (white) colours and darker grey or black pixels represent lower values. Applying a threshold here retains only those cells in the map in which vegetation definitely occurs.

The proposed strategy uses bird's-eye view images, but when a camera is placed on a tractor, the acquired images have perspective, which must be removed before applying the mapping method. Fig. 1 shows an example of the videos acquired from the field, as well as the position of the camera. The next section explains the approach applied to obtain the bird's-eye images. A selection of video sequences recorded from an autonomous tractor in a real spraying operation (approximately 6 Km/h speeds) will be employed to explain the different elements of the proposal and to test its performance.

2.3 Inverse perspective transformation

Inverse perspective mappings have been discussed widely in the literature (Barnard 1983, Mallot et al., 1991, Bevilacqua et al., 2008, Sonka et al., 2008). Through the use of homogeneous coordinates, nonlinear perspective mapping can be written as a linear transformation between two planes: the horizontal plane (field plane) and

the camera or image plane. According to Barnard (1983), a point with homogeneous coordinates *u=(u,v,w)* in the field plane can be projected into the image plane using (2):

$$u' = sHu \tag{2}$$

where *s* is a scale factor, u′ are the homogeneous coordinates of the image point, u are the coordinates of that same point in the field plane and *H* is the 3×3 homography matrix. The determination of *H* allows the computation of the projection of points from one plane to the other. In computer vision, a commonly used method to calculate the homography is based on point correspondences that are defined as sets of *n* pairs of points $(\boldsymbol{u}_i, \boldsymbol{u'}_i)$, such that a point $\boldsymbol{u}_i$ in the field plane corresponds to $\boldsymbol{u}_i'$ in the image plane. Therefore, a system with $n(d+1)$ equations and $n + (d+1)^2 - 1$ unknowns can be obtained. *H* can be determined up to an overall scale factor by using $n = d + 2$ point correspondences, as long as no more than *d* of them are collinear. For 2D planar images (i.e., *d=2*), at least four point correspondences are required, and no more than two can be collinear.

(a)

(b)

Fig. 1. (a) Position of the video camera on top of the tractor;(b) An example of a framer corded in the video.

In the case of field video frames, points in the perspective image can be selected from the centres of the crop rows. If the points selected in pairs are in different rows, the non-collinear requirement will be kept. Therefore, points can be chosen as the vertices of a trapezoid, as shown in Fig. 2a.

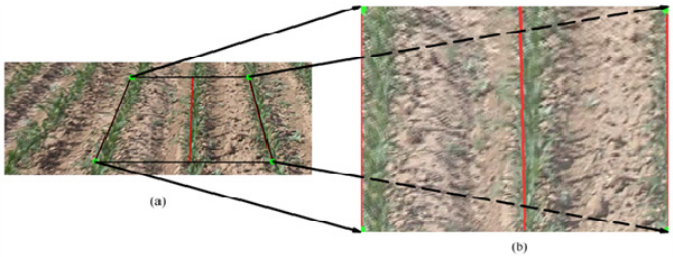

Fig. 2. (a) Perspective view (original image). (b) Bird's-eye view (transformed image).

On the other hand, the corresponding points in the transformed image are chosen as the vertices of a rectangle of selected dimensions (Fig. 2b). The width of this rectangle will correspond to twice the inter-row spacing (usually approximately 0.75 m in maize crops), and its height will determine the vertical scale factor of the transformation, which must be calibrated by the measurement of a known object and the treatment speed, approximately 6Km/h in the provided example.

Once the homography matrix is computed, the entire image can be warped by applying inverse perspective mapping to each pixel, producing a planar crop field image or bird's-eye view in which parallel rows remain parallel, and, once calibrated, distances can be measured.

Therefore, the essential elements to accomplish the inverse perspective transformation are the crop rows. It is crucial to develop techniques to discriminate the crop rows in each frame, such as the method described in the next section.

2.4 Detection of the crop rows

Fig. 3 graphically summarises the process followed in crop row detection. The process begins with vegetation cover segmentation, using the method described in subsection 2.1 (Fig. 3b). Next, morphological operations are applied to reduce the cover between rows (i.e., weeds), and the image is divided into four bands of fixed width (72 pixels) in which the *y*-coordinates are centred vertically (see Fig. 3c). The average intensity of the pixels in each band and each column in the band is then calculated; all the intensities of all the pixels in a column are added up, and the result is divided by the total number of pixels in the column, i.e., 72. Using this computation, an average intensity for each band is obtained, determining a grey level for each column. Different grey levels indicate different percentages of vegetation cover; darker columns indicate a lower vegetation cover, while whiter columns correspond to areas with a higher vegetation cover. The centres of the crop rows are, therefore, more densely covered (close to 100% vegetation coverage). By applying a threshold, it is possible to isolate the blocks that represent the crop rows (Fig. 3d). The resulting binary image contains broad blocks

representing the crop rows; on some occasions, it may also contain some narrow blocks belonging to weed patches, but these rarely affect more than one band. The blocks are then chosen by their width and position in the image among those blocks that are more likely to belong to one of the three central rows of the crop. The horizontal centres are calculated for the selected blocks and used as the *x*-coordinates of the points to be used to build the lines that define the crop rows (Fig. 3e). The last step is a linear regression used to build the three straight lines that define the direction of the crop rows (Fig. 3f).

Fig. 4 shows the results of applying the entire process described above to two videos of approximately 300 frames. In the analysed video sequences, the typical values for the matrix elements (the number of frames where weeds were present in a particular cell) ranged from 0 (no weeds in the area in any frame) to 17. To eliminate false vegetation cells in the map due to segmentation errors in particular frames, a threshold corresponding to approximately 25% of the maximum value was selected. Thus, any value below 4 in the map matrix was considered a vegetation-free cell in the final map.

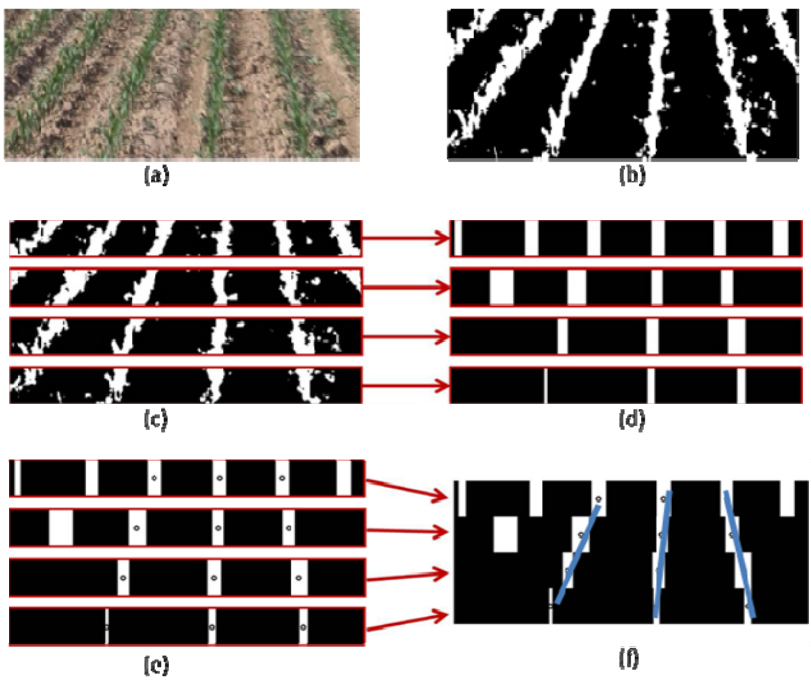

Fig. 3. Steps followed to discriminate the crop row in a video frame.

The maps shown in Fig. 4 do not present the perfectly straight rows that exist in the real crops. This discrepancy is caused by the effect of camera movement caused by the uneven ground on the images, a problem mentioned earlier in this document. The first video sequence (Fig. 4a) was recorded on a sunny day in a field more with a more or less regular surface, while the second (Fig. 4b) was recorded on a partially overcast day over rough terrain. The next section discusses the problem of stabilisation and describes an appropriate solution.

3. The stabilisation method

With the aim of assessing the importance of video stabilisation, the distance between the image's horizontal centre and the calculated position of the central crop row in the lower part of each frame was measured in all the recorded video sequences. In this area, the central crop row of a stabilised sequence should remain close to the horizontal centre of the frame, even with perspective. However, the measured deviations vary from 26 pixels to the left of the centre to 93 pixels to the right, with an average distance of 20 pixels and a standard deviation of 28.9 pixels.

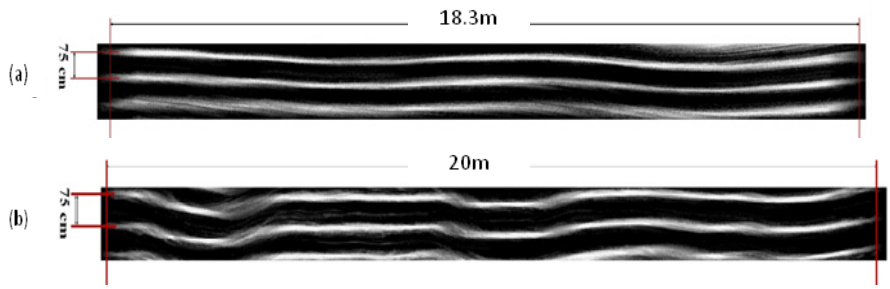

Fig. 4. (a) Crop map obtained from a video sequence recorded on a sunny day on a field with low weed cover and slightly uneven terrain. (b) Crop mapping from a video sequence recorded on an overcast day on a field with low weed cover and an uneven terrain.

The problem of image stabilisation has been assessed by a number of researchers (Morimoto, 1996; Irani, 1994; Censi, 1999; Viéville, 1993, Hansen, 1994; Ertürk, 2002; Vella *et al.,* 2002). Different techniques are used in the literature, mostly based on sparse feature tracking. Some have used Kalman filters to predict the motions of the features from frame to frame (Censi, 1999). In the study by Ertürk (2002), Kalman filters are used to estimate the camera's velocity and acceleration vectors for each frame using linear camera motion models. Hansen (1994) and Morimoto (1996) make use of Laplacian pyramid images to estimate the optical flow field and compute the required affine transformation. In Irani (1994), the 3D

motion of the camera is computed by first calculating the image flow of a 2D planar region and then subtracting it from the whole image flow, resulting in a rotationless optical flow. This rotationless image sequence is considered stabilised for all relevant purposes. In Viéville (1993), nearly vertical segments in the image are used to compute the transformation required to make them vertical lines and correct the camera rotation. Vella *et al.* (2002) use block motion vectors to estimate the motion between consecutive frames.

All these methods attempt to compensate for all instances of motion and are rather complex and computationally demanding. Most of them use discrete features (i.e., corners or segments) and attempt to keep these features fixed in relation to a reference frame. These solutions are not possible in the current case, in which there are no permanent features, even for a constant reference frame, as the portion of the field recorded by the camera changes constantly as the vehicle travels through it. In the context of wide-row crops, other characteristics of the images can be exploited; in particular, the fact that crop fields present an approximately constant pattern of evenly spaced parallel rows. In other words, the stabilisation of the lateral sway of the camera requires the selection and tracing of some sort of feature in every frame; the aim is to calculate the compensation required in each frame to obtain as steady an image sequence as possible. Because the vehicle is constantly moving, there is no horizon line in the images. However, the crop rows are present in every frame of the video sequence and are, therefore, ideal candidates to be tracked.

With the inverse perspective transformation (subsection 2.3), the parallelism between the crop rows is recovered, making it possible to shift the images in all directions, both transversely and longitudinally (the depth in the original image with perspective). Furthermore, the correspondence between the selected vertices of the trapezium (Fig. 2) and the same four corners of the bird's-eye image is always determinable. This correspondence allows us to accomplish perspective rectification and stabilisation to remove the effects of the unwanted camera movements in one operation. The selected points of interest will always be located on the same central rows of the crop, even when the rows oscillate laterally or change their positions.

Fig. 5 shows the effect of the previously applied stabilisation method on the video sequences shown in Fig. 4. It is evident that a tracking error occurred in this first sequence around the middle of the crop field. In this area, the vegetation density in the left crop row is reduced due to sowing errors, and some isolated weed patches were misidentified as the real crop row, causing the tracking error.

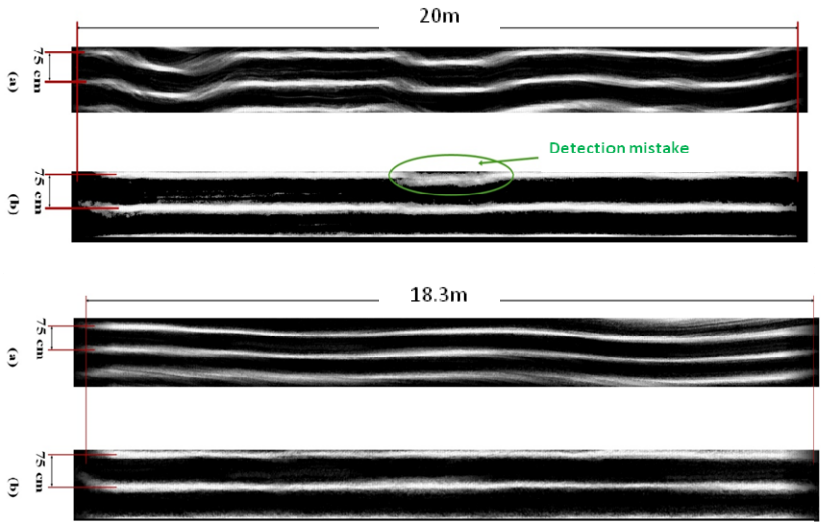

Fig. 5. Results obtained with the proposed stabilization approach. The (a) images correspond to the crop maps obtained without stabilizing the original frame. The (b) images show the results after stabilization.

Trials conducted on various sequences of videos of the field taken at different times and under different lighting conditions showed that the distances between some reference features, such as the central crop row and the horizontal centre of the frame, remained invariant once the video sequence was stabilised. Lateral displacements of up to 66% of the inter-row spacing were suppressed.

A similar mechanism can be used when the perspective is not unaltered. In this case, after the first frame calculations, the crop row centres are stored in an array. A new frame is processed in the same way, but this time, the stored centres from the previous frame are used as the origins around which the system searches for the crop row centres in the current frame. This enables the algorithm to search for a given centre in a window of a specific width around the last known position of the same centre; therefore, the system is able to find the centres of the same crop rows in every frame, even if they move laterally from frame to frame. This is consistent to a certain extent; if the feature displacements between one frame and the next are too abrupt, the algorithm will not be able to find that same feature in the next frame. However, frame-to-frame displacements are almost always small because the frames come from video sequences recorded at 25 fps (or 40 ms per frame).

Finally, Fig. 6 shows some of the weed patches (vegetation zones between rows) that appear in the obtained map.

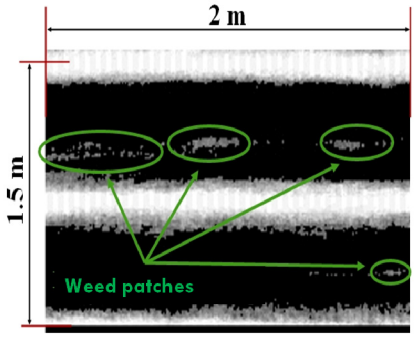

Fig. 6. Appearance of the weed patches in the maps obtained from the video sequences by means of the proposed approach.

4. Conclusions

In precision agriculture, and in weed control in particular, precise knowledge of the weed distribution is essential to achieving efficient weed treatment. A useful strategy to obtain information on the crop and weeds in a field could be to place a camera on a tractor and record visual information (video) while other operations are being accomplished. If the tractor is moving over a smooth surface, the video taken by the camera will also be smooth; however, agricultural terrain is irregular, and this provokes camera movements that result in unsteady video sequences. Many stabilisation methods extract characteristic points in the initial frame and attempt to find the same points in the next frames of the video, using these characteristic points to stabilise the whole video sequence. However, in crop fields, with the cameras constantly moving and facing slightly downwards towards the ground and without the presence of permanent features, the problem of stabilisation is not trivial.

The only elements that can be considered permanent are the crop rows. This paper presents a stabilisation approach based on detecting and tracking crop rows. The proposed approach has been proven to supply good performance, stabilising several video sequences recorded in various fields under different lighting conditions. The crop rows are detected and tracked, and the lateral camera sway is removed by keeping the region of interest centred on the screen. Furthermore, the distances between some reference features, such as the central crop row and the horizontal centre of the frame, remain invariant once the video sequence has been stabilised. Lateral displacements of up to 66% of the inter-row spacing are suppressed.

The proposed approach fails in cases in which the weed infestation is high or when there are sowing errors. In both cases, the crop row is obscured, and the method is unable to find it. Moreover, when the infestation is very high, this method tends to

confuse the weeds with the crop. These problems are usually not common in a well-managed commercial field, but they should be taken into account in future versions of the method. One way to improve the approximation method is to include some sort of memory in the stabilisation system so that it can use information from previous frames to eliminate ambiguities or compensate for a lack of knowledge.

Acknowledgements

The Spanish Ministry of Science and Innovation and the European Union have provided full and continuing support for this research through projects PLAN NACIONAL AGL2008-04670- C03-02/AGR and UE-CP-IP-2-45986-2-RHEA.

References

Andujar, D., A. Ribeiro, R. Carmona, C. Fernández-Quintanilla, J. Dorado (2010). An assessment of the accuracy and consistency of human perception of weed cover. *Weed Research*, 50, 638-647.

Barnard, S.T. 1983. Interpreting perspective images. *Artificial Intelligence*, 21, 435-462.

Bevilacqua, A., A. Gherardi, L. Carozza (2008). Automatic perspective camera calibration based on an incomplete set of chessboard markers. *Sixth Indian conference on computer vision, graphics & image processing, ICVGIP '08*, 126-133.

Burgos-Artizzu, X.P, A. Ribeiro, A. Tellaeche, G. Pajares (2008). Optimisation of Natural Images Processing Using Different Evolutionary Algorithms. *Proc. IEEE Congress on Evolutionary Computation*, 1268-1275.

Burgos-Artizzu, X.P., A. Ribeiro, A. Tellaeche, G. Pajares, C. Fernandez-Quintanilla (2010). Analysis of natural images processing for the extraction of agricultural elements. *Image and Vision Computing*, 28, 138-149.

Censi, A., A. Fusiello, V. Roberto (1999). Image Stabilization by Features Tracking. *International Conference on Image Analysis and Processing*, 665-670.

Ertürk, S (2002). Real-Time digital image stabilization using Kalman filters. *Real-Time Imaging*, 8, 317-328.

Hansen, P., P. Anandan, K. Dana, G. VanDer Wal, P. Burt (1994). Real-time scene stabilization and mosaic construction. *Proceedings of the Second IEEE Workshop on Applications of Computer Vision*, 54-62.

Irani, M., B. Rousso, S. Peleg (1994). Recovery of ego-motion using image stabilization. *Proceedings of the 1994 IEEE Computer Society Conference on Computer Vision and Pattern Recognition*, 454-460.

Mallot, H. A., H.H. Bülthoff, J.J. Little, S. Bohrer (1991). Inverse perspective mapping simplifies optical flow computation and obstacle detection. *Biological*

Cybernetics, 64, 177-185.

Morimoto, C., R. Chellappa (1996). Fast Electronic Digital Image Stabilization for Off-Road Navigation. *Real-Time Imaging*, 2, 285-296.

Ribeiro, A., C. Fernanadez-Quintanilla, J. Barroso, M.C. Garcia-Alegre (2005). Development of an image analysis system for estimation of weed. *Proceedings of the Fifth European Conference on Precision Agriculture*, 169-174.

Sonka, M., V. Glavac, R. Boyle (2008). Image processing, analysis, and machine vision. *3rd Ed. Thomson Learning*. Hilda Gowans, 553-565.

Van Evert, F.K.; G. Van Der Heijden, L. Lotz, G. Polder, A. Lamaker, A. De Jong, M. Kuyper, E. Groendijk, J. Neeteson, T. Van Der Zalm (2006). A mobile field robot with vision-based detection of volunteer potato plants in a corn crop. *Weed Technology*, 20, 853-861.

Vella, F., A. Castorina, M. Mancuso, G. Messina (2002). Digital image stabilization by adaptive Block Motion Vectors filtering. *IEEE Transactions on Consumer Electronics*, 48 (3), 796-801.

Yang, C.C., S.O. Prasher, J.A. Landry (2003). Development of an image processing system and a fuzzy algorithm for site-specific herbicide applications. *Precision Agriculture*, 4, 5-18.

Woebbecke, D., G. Meyer, K. Vonbargen, D. Mortensen (1995). Colour indices for weed identification under various soil, residue and lighting conditions. *Transactions of the American Society of Agricultural Engineers,* 38 (1), 271–281.

How the spatial resolution can affect the quality of mosaics and assessment of optimum number of tie points necessary to obtain good quality images

David Gómez-Candón*, Sylvain Labbé, Montse Jurado-Expósito*, José M. Peña-Barragán*, Gilles Rabatel** and Francisca López-Granados***

**Institute for Sustainable Agriculture (CSIC), Av. Menendez Pidal s/n*

Campus Alameda del Obispo, 14080 Cordoba, Spain

(e-mail: dgomez@ias.csic.es)

***Cemagref, Maison de la télédétection*

500, rue Jean-François Breton. F-34093 Montpellier, France

(e-mail: Sylvain.Labbe@teledetection.fr)

Abstract: Orthorectification and mosaicing are two important steps in the design of input application strategies for precision agriculture. Images with low spatial resolution and big georreferencing errors are not useful to obtain good quality maps. In this paper we tried to compare the usefulness between two different pieces of software for orthorectificacion and mosaicing of remote images. Furthermore, we studied the spatial resolution requirements and minimum number of tie points/GCPs needed to obtain good quality orthomosaics. These orthomosaics have to be ready to be used to detect weeds in crops and to obtain high precision prescription maps.

1. Introduction

A new era of remote sensing is emerging with the arrival of unmanned aerial vehicles (UAVs) for civil applications. Scientific interest in this type of platforms is growing, and a number of experiences have already been reported. Miniaturization and cost reduction of inertial sensors, GPS devices, and embedded computers have enabled the use of a new generation of autopilots for inexpensive model aircrafts (Esposito et al, 2007).

With the development of high-spatial-resolution imagery, the impact of errors in geographic co-registration between imagery and field sites has become apparent and potentially limiting for classification application, especially those involving patchy target detection (Weber et al. 2008).

Images taken from Unmanned Aerial vehicles (UAVs) normally cover a smaller area than the study parcels. For this reason, it is necessary to take several images during one or several flights to acquire a **sequence or collection of images** and later combine them to form **one unique image of the field**. Each image shows distinct point of view and viewing angles, leading to geometric distortion of each image. For this reason, combining all the images to obtain a complete **orthophoto** of the field requires a process of **orthorectification** to make a **mosaic** image of the area. This orthophoto should have the **high-quality landscape metric**, minimum geo-reference errors and accurate correlation matching, which must guarantee imagery inter-operability from consecutive flights executed over the same field.

Direct geo-referencing is the process of registering an image frame to a map coordinate system through direct measurement of the image exterior orientation parameters by a GPS (Global Positioning System) and IMU (Inertial Measurement Unit) at the moment of exposure. Such direct geo-referencing further incorporates a predefined model of the sensor's interior orientation parameters. These parameters include location of the image sensor relative to a map coordinate system (x, y, z) and its perspective orientation (i.e., pitch, yaw, and roll) around that point (Skaloud 1999). The model for transforming between the image coordinate system and map coordinate system, including correction for bore-sight misalignment, was developed by Grejner-Brzezinska (1999).

There is some available software to achieve the orthorectification and mosaicing processes, and two of the main are Erdas-LPS and MICMAC. LPS is one of the most used and powerful available software and MICMAC is other of the available photogrammetric tool able to complete the process and indeed is free software.

The main objectives of this work are:

- To test some of the main available software for orthorectification and mosaic remote images.
- To transform the spatial resolution of a sequence of images over an agricultural area in order to orthorectify and to mosaic them by using ERDAS-LPS.
- To determine the effects of spatial resolution over the quality of remote imagery mosaics.
- To assess the number of tie points required to mosaic remote images in agricultural areas at every of the spatial resolution essayed.

2. Tested software

2.1 ERDAS-LPS

LPS is a complete suite of photogrammetric production tools for triangulation, generating terrain models, producing orthomosaics and extracting 3D features. It

supports panchromatic, colour and multispectral imagery with up to 16 bits per band. This software works as an ERDAS' module.

LPS maximizes productivity with automated algorithms, fast processing, and a tight focus on workflow. A unique workflow toolbar guides users through projects from beginning to end (Figs. 1 and 2). The LPS Project Manager enables easy monitoring of the progress of all projects, whether they are completed step-by-step or with extensive use of LPS' batch processing functionality.

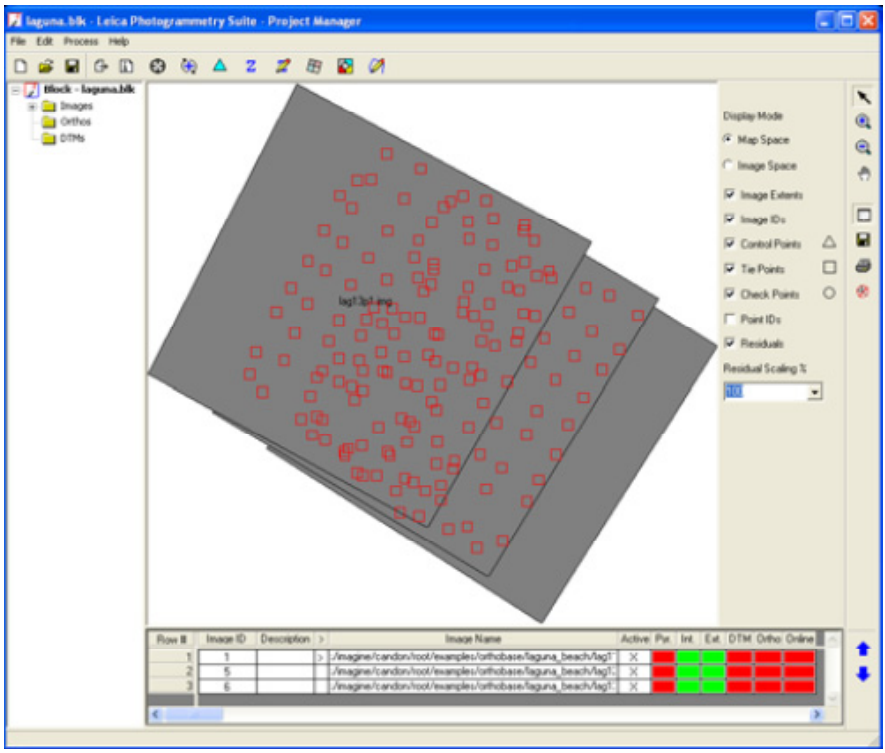

Fig. 1. Main interface of the LPS software

LPS increases accuracy through state-of-the-art photogrammetric and image processing algorithms for automatic point measurement, triangulation, automatic terrain extraction and sub-pixel point positioning.

How the spatial resolution can affect the quality of mosaics and assessment of optimum number of tie points necessary to obtain good quality images

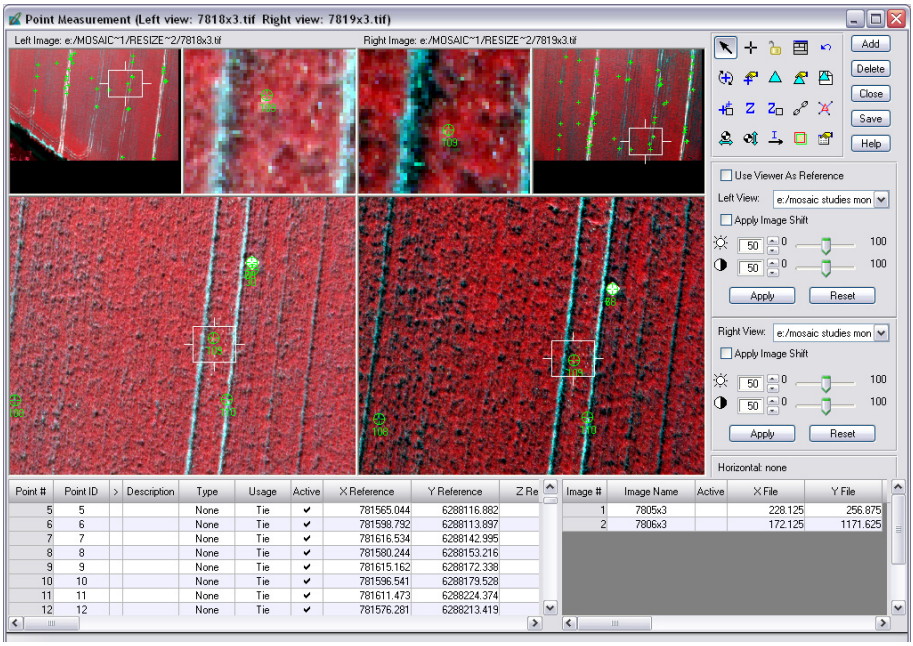

Fig. 2. Auto-Tie Point generation interface of the LPS software

2.2 MICMAC

This is a set of software photogrammetric tools written in C++ that, under certain conditions, allow computing a 3D modeling from a set of images.

MICMAC is a tool for image matching made by the French National Geographic Institute (IGN). It is a general purpose tool. One of its expected advantages is its generality. It has been used in a lot of different contexts, for example:

- Digital terrain model in rural context from pairs of satellite images, with exact or approximate orientation;
- Digital elevation model in urban context with high resolution multi-stereoscopic images;
- Detection of terrain movements;
- 3D modelization of objects (sculptures) or interior and exterior scenes;
- Multi-spectral matching of images registration.

This generality comes with a price: it requires a lot of parameterization which sometimes turns to be quite complex. For 3D computation, MICMAC works only with oriented images like the ones resulted from classical aero-triangulation process (Fig. 3).

```
- <ParamMICMAC Subst="@$#1" NameDecl="@$#1" NumC="@09375" NumMin="@09375" NumMax="@09379">
  - <Section_Terrain>
    - <IntervAltimetrie>
        <!--  Mandatory but unused  -->
        <ZIncCalc>0.0</ZIncCalc>
      </IntervAltimetrie>
    - <IntervSpecialZInv>
        <MulZMin>0.3</MulZMin>
        <MulZMax>5</MulZMax>
      </IntervSpecialZInv>
      <Planimetrie />
    </Section_Terrain>
  - <Section_PriseDeVue>
      <GeomImages>eGeomImageOri</GeomImages>
    - <Images>
        <Im1>img${NumC}.tif</Im1>
        <ImPat>img_[0-9]{4}.tif</ImPat>
      - <Filter>
          <Min>img${NumMin}.tif</Min>
          <Max>img${NumMax}.tif</Max>
        </Filter>
      </Images>
    - <NomsGeometrieImage>
      - <FCND_Mode_GeomIm>
          <FCND_GeomCalc>KeyStd-Assoc-Im2Orient@-Correl</FCND_GeomCalc>
        </FCND_Mode_GeomIm>
      </NomsGeometrieImage>
    </Section_PriseDeVue>
  - <Section_MEC>
      <ChantierFullImage1>true</ChantierFullImage1>
    - <EtapeMEC>
        <DeZoom>-1</DeZoom>
        <SzW>1</SzW>
        <AlgoRegul>eAlgo2PrgDyn</AlgoRegul>
        <GenImagesCorrel>true</GenImagesCorrel>
        <ZPas>0.5</ZPas>
        <ModeInterpolation>eInterpolMPD</ModeInterpolation>
        <ZDilatAlti>3</ZDilatAlti>
```

Fig. 3. Main interface of the MICMAC software

Using this software the photogrammetric processing chain follows three main major phases:

- Matching pictures with the module PASTIS: this step detects in each image a set of points using SIFT algorithm (Lowe 2004) which will automatically search for counterparts other images of the site.
- The calculation of calibration and aerial triangulation with the module APERO: this module allows calibrating the cameras and determining the positions and orientations of the different peaks of shots.
- The correlation with the dense module MICMAC: this software allows using the previous data recorded and images to generate depth maps and clouds of points.

Therefore, it is s necessary to use tree different software to complete the process (Fig. 4).

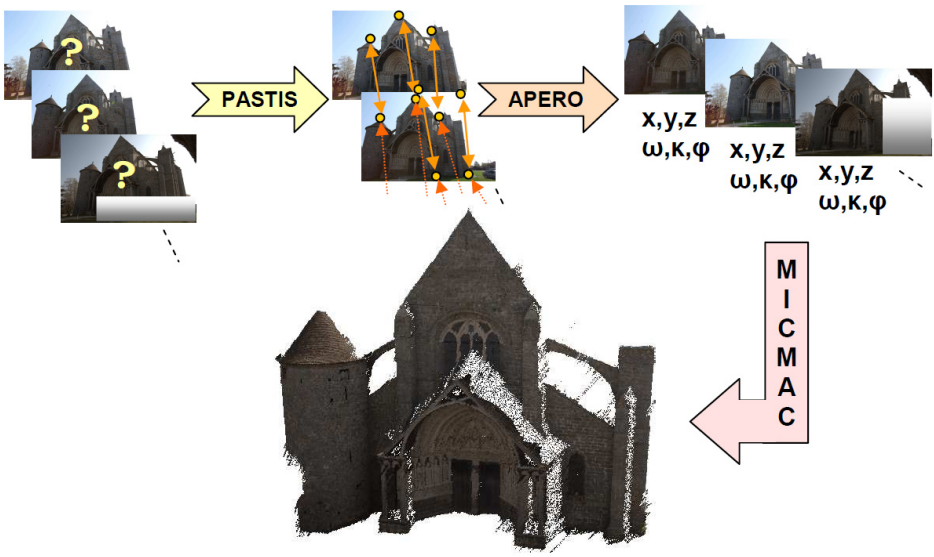

Fig. 4. Step by step process using MICMAC software

MICMAC is open source software, under the CeCILL-B license (an adaptation to the French law of the L-GPL license).

3. Area of study and Materials

A sequence of aerial imagery was taken by L'Avion Jaune Company on 20-May2011 at Castries (Montpellier) (Fig. 5 and 6). Flights were at low altitude in order to simulate a usual UAV way of workCharacteristics of the images:

- Flying area: Castries (France).
- Focal length: 50 mm.
- Flying altitude: 150 m.
- Image size: 5870x3888 pixels.
- Original image size: 6080+4048.
- Pixel Size (PS): 5.940 µm.
- Optical centre: 105/80.
- Projection:
    - ~ Lambert_Conformal_Conic (GCS-RGF-1993).
    - ~ Datum: D_RGF_1993.
    - ~ France transformation grille: RGF93 / Lambert 93 (2154)
- Number of images: 19 (named from 7804 to 7823).

Fig. 5. Castries study area (Montpellier, France)

Fig. 6. Sequence of six images (numbered from 7818 to 7823) taken at Castries. Image contours are marked in purple and image overlapping in white

4. Methods

The following steps were carried out:

First of all, to select the proper images from Castries (May 20th) according to a criteria based on sufficient overlapping and a similar flight direction between them.

Secondly, to transform the original images selected in the previous step from a three bands (RGB) and one band (NIR) formats to a four bands (B, G, R and NIR) final images.

Then, to combine the image pixels (1 x 1; 3 x 3; 6 x 6; and 11 x 11 pixels) in order to obtain four sequences of images at different spatial resolutions (1.8; 5.3; 10.7; and 19.6 cm) each one, according to the following equation:

$$\frac{f}{H} = \frac{PS}{GSD} \quad (1)$$

where:

f= Focal length (mm)

H= Aircraft altitude (m)

PS= Pixel size on the camera lens (mm)

GSD= Spatial resolution of the image (m)

Finally, to orthorectify and mosaic the four sequences of images using the aerotriangulation method by mean of LPS software and geo-referenced ground-truth field data or ground control points (GCPs).

5. Results and discussion

5.1 Software comparison

-Kind of Interfaces.

There are roughly three kinds of interfaces for software:

a. User friendly graphical interface, with intuitive menu and window etc. Its advantage is that it may be usable by all final user; the drawback of this solution being the cost for the developer;

b. API or application programming interface. Using this level of interface requires that you can use one of the programming language the API is functioning with; one of the drawbacks of these API is that they require a lot of documentation;

c. A set of programs that you can call on a command line, with parameters being added on a command line or included in a file.

The tools needed to manage LPS are of the first kind of interface; however MICMAC use the third kind one (although a friendly graphical interface of MICMAC is under development). For this reason, it is not easy to manage MICMAC.

- Price: While LPS is commercial software, MICMAC is free software. This has become the main reason to choose MICMAC.

- Operative System: LPS can be used in Windows OS while MICMAC can be used in Linux-Ubuntu. Both OS are well known and are planned to be used in RHEA.

- Usually, it is necessary to take some manual tie points using LPS; however MICMAC does not offer the chance to do it manually if it is necessary.

- Working in batch mode is easier using MICMAC than LPS.

- Practical management: in our own experience, we were able to start using LPS after three days of training. On the other hand, after one week course and one month more of practising, we hardly can finish the first step of the three needed to use MICMAC.

- Other characteristics: while LPS having the possibility to fix manually the overlapping fails and can homogenise differences between images, MICMAC has not a similar tool.

There is a brief resume of the main characteristics on Table 1.

Table 1. Comparison between tested software

	Interface	Price	Operative System	Tie point generation	Batch mode	Practical management
ERDAS-LPS	User friendly	Commercial software	Windows	Manual + Automatic	Yes	Easy to use
MICMAC	Command line	Free software	Linux	Automatic	Yes	Not easy to use

5.2 Image mosaicing

The selected images where: 7818-7819-7820-7821-7822-7823 and all of these were resized to the selected spatial resolutions (Fig. 7).

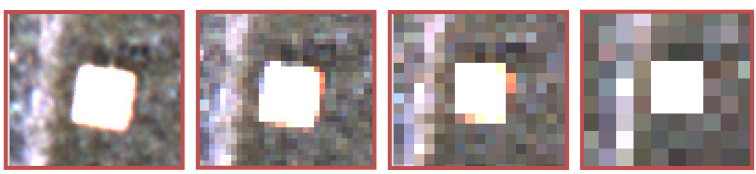

Fig. 7. Example of transformed images at different spatial resolutions: 1.8, 5.3, 10.7 and 19.9 cm, from left to right respectively

In every sequence of images, no automatic tie points were generated by LPS software unless that two pairs of tie points were taken manually for every pair of adjacent images. The Table 2 shows the number of tie points per image that were generated automatically by the software. The number of tie points varied from 35 in the image with higher spatial resolution to 0 in the images with lower resolution. That shows that it was more difficult to find tie points in the images with lower spatial resolution (pixel > 19 cm).

Table 2. Number of tie points automatically generated by LPS software per single image at the different spatial resolutions essayed

	Image Number					
Spatial Resolution (cm)	7818	7819	7820	7821	7822	7823
1.8	13	34	31	27	35	18
5.3	15	30	29	29	31	16
10.7	6	14	8	4	7	3
19.6	3	3	0	0	0	0

The minimum number of tie points needed by the software to achieve the aerotriangulation process is 6 per image. This is because with less than 6 points there is no enough relative orientation between images. However, not every image at every spatial resolution has reached this minimum number. So that, some tie points had to be taken manually to obtain the number of tie points needed.

To obtain a geo-referencing error (Root Mean Square Error, RMSE) lower than 2 cm, the number of tie points had to be increased (Table 3). For this purpose, we used the “tie point generation menu” several times. In the sequences of images with 1.8 and 5.3 m spatial resolution, new points were generated by the software; however, for the 10.7 and 19.6 m pixel sequences, no more points were automatically generated again and therefore, they had to be taken manually.

The Table 3 shows the number of pairs of tie points required to obtain a good orthorectification by LPS (RMSE lower than 2 cm). The number of tie points increased from 32 to 165. It was necessary to use more tie points in the images with higher spatial resolution, but a number of 16 tie points was acceptable to obtain convergence between images in any of the studied images.

Table 3. Number of pairs of tie points needed to obtain a good orthorectification (RMSE <2 cm) at every spatial resolution essayed and using 16 GCPs

Spatial Resolution (cm)	1.8	5.3	10.7	19.6
Tie points	165	122	32	32

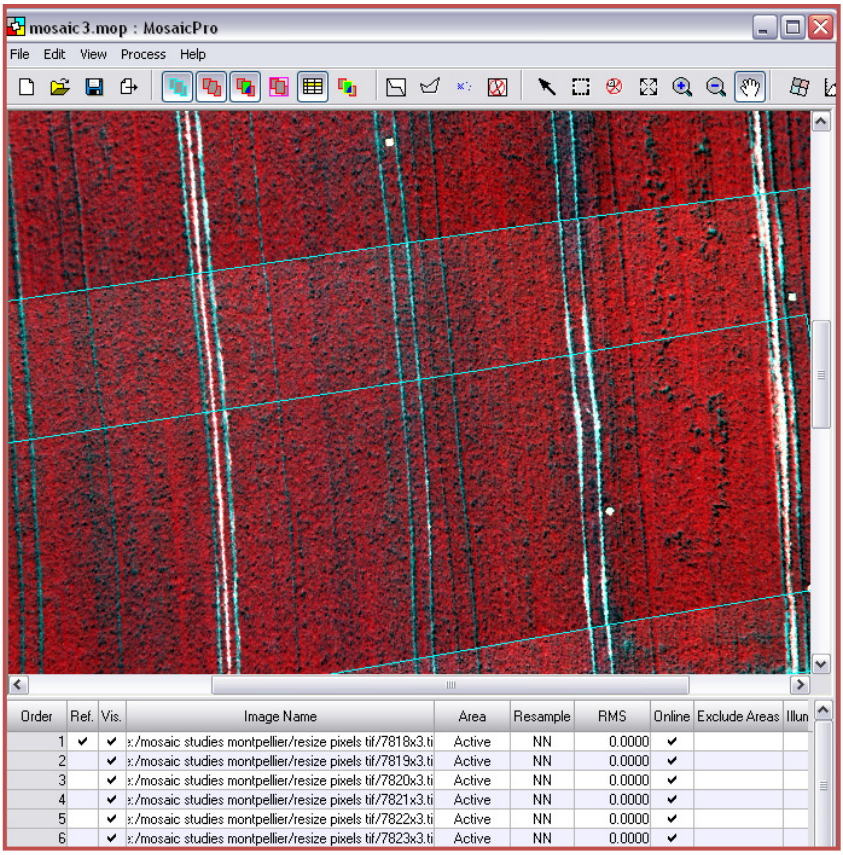

Fig. 8. Example of mosaic (5 cm of spatial resolution)

6. Conclusions

Two different kinds of software have been tested and there are some reasons to decide for one or other, but most of them are in the LPS side.

At lower spatial resolutions is more difficult to distinguish the smaller objects in the images. This is due to the images taken in crop scenarios become more monotonous and present serious limitations to find the tie points between pairs of adjacent images.

Images with higher spatial resolution are more complex than the others, and it is necessary to use a higher number of tie points to carry out the orthorectification and mosaicing processes.

The number of ground control points used (16) was adequate to orthorectify and mosaic every sequence of images at every of the spatial resolution studied.

Acknowledgement

The research leading to these results has received funding from the European Union's Seventh Framework Programme [FP7/2007-2013] under Grant Agreement nº 245986.

References

Esposito, F., Rufino, G. and Moccia, A. (2007). 1st mini-UAV integrated hyperspectral/thermal electro-optical payload for forest fire risk management. *in Proceedings of the AIAA Infotech Aerospatial Conference,* 1, 653–665.

Grejner-Brzezinska, D.A. (2000). Direct Exterior Orientation of Airborne Imagery with GPS/INS System: Performance Analysis. *Navigation*, 46, 261-270.

Lowe,D.G. (2004), Distinctive Image Features from Scale-Invariant Keypoints. *International journal of computer vision*, 2, 91-110.

Skaloud, J. (1999). Problems in Direct-Georeferencing by INS/DGPS in the Airborne Environment. *ISPRS Workshop WG III/Barcelona*, 1, 25-26.

Weber, K. T., Theau, J., and Serr, K. (2008). Effect of co-registration error on patchy target detection using high-resolution imagery. *Remote Sensing of Environment*, 112, 845–850.

Camera System geometry for site specific treatment in precision agriculture

Martín Montalvo*, José M. Guerrero*, María Guijarro*, Juan Romeo*, Pedro J. Herrera, Ángela Ribeiro** and Gonzalo Pajares ***

**University Complutense of Madrid. Facultad Informática. Madrid. Spain 28040 Madrid, SPAIN*

(e-mail: pajares@fdi.ucm.es).

***Centre for Automation and Robotics (UPM-CSIC), Crtra. Campo Real Km 0,2 28500 Arganda del Rey, Madrid, Spain*

(e-mail: angela.ribeiro@car.upm-csic.es).

Abstract: A visual perception system, on board a ground mobile unit, is used for detecting rows in maize crops. Camera-based system geometry, under perspective projection, is exploited to guide the image analysis. The aim is to apply prior knowledge to facilitate the detection and location of weeds in crops. This knowledge is used to determine where the crop rows should be located to the search for plants (crop and weeds), thus reducing the computational cost from the point of view of image processing, i.e. oriented toward real-time image processing. From the point of view of crop/weed identification the most suitable configuration is one that achieves maximum image resolution for an identical area in the field, since with higher resolution better decisions can be made about crop/weed detection. In this paper we study and compare two camera devices, based on image geometry, to verify their behaviour with different intrinsic and extrinsic parameters. This allows us to identify the best geometric image configuration from the point of view of highest image resolution, making the main contribution of this work.

Keywords: crop row, intrinsic and extrinsic parameters, camera geometry, focal length.

1. Introduction

Nowadays soil pollution in agriculture is increasing considerably as a result of the abundant use of chemical products, particularly herbicides which are applied to eliminate weeds in crops. Precision Agriculture (PA) is an approach for solving this

problem. Numerous technologies have been developed to make agricultural products safer and to reduce their adverse impact on the environment. The goal is to reduce the use of such products and apply them only when required. This implies the correct identification and location of areas infested with weeds.

Thanks to the increasing development of autonomous ground mobile units equipped with machine vision sensors, the above goal has become more feasible. However, it requires image analysis to identify and locate crop and weeds, under conditions made difficult by outdoor illumination and other adverse factors.

As most crops are cultivated in rows, major efforts have been made to extract lines derived from plant structures. Most of the methods described in the literature use algorithms to detect crop rows. Fontaine and Crowe (2006) have studied a set of synthetic rows under controlled lighting conditions, with and without simulated weeds. They proposed four algorithms for line detection, allowing them to determine the position and the angle of the camera with respect to a base reference system.

A common technique to determine lines identifying crop rows is based on the Hough transform (Hough, 1962). This technique has been extensively used in many agricultural applications due to its usefulness and robustness. It allows the detection of simple predefined shapes forming alignments in images, which is the case of crop rows. Gee et al. (2008) proposed a new method for detecting the crop row based on the identification of the vanishing point taking the opportunity to exploit the perspective projection which allows the scene to be mapped onto the image. Åstrand and Baerveldt (2005) have developed a method based on the Hough transform for real-time automatic guidance following the crop lines. The method proposed by Bakker et al. (2008) also applied the Hough transform to merge images obtained from three sections of the grey-scale image which involved less data and retained the information on three crop rows.

Reid and Searcy, 1987) applied a binarization thresholding approach based on the well-known Bayes classifier to segment plants at different growth stages and in different soil in cotton fields. Han et al. (2004) applied a robust algorithm which included row segmentation using the *K*-clustering algorithm. Crop row detection is carried out through what they call the moment algorithm and guidance line selection based on the cost function. Brivot et al. (1996) concludes that the segmentation of plants, weeds and soil according to infrared images offers good results. Also using this approach, Olsen (1995) used a near infrared sensor, obtaining images with the optical axis perpendicular to the soil to minimize the effect of perspective projection. To find rows all grey values are summed up column-wise to obtain a histogram of the crop rows and then a low-pass filter is applied to it.

Jinlin and Weiping (2010) use mathematical morphology to identify the crop rows, based on the least-square method, according to the centroids of individual target

crops and the central points of several pixel rows of crops with a continuous region in the image. To identify the location of the cotton plants among weeds, the method used by Slaughter et al. (1999) applies a new technique which performs a segmentation of the 24-bit true colour image into a binary image with stochastic pattern recognition.

A common feature of the above methods is that they analyse the image content applying certain constraints derived from system geometry and require sufficient image resolution of the specific area in the image being processed. Indeed, because the intrinsic and extrinsic parameters of the vision system are known, only specific plant alignments and geometrical area limitations are expected. In short, crop row detection is based on an exhaustive search over the whole image by applying geometrical constraints. This implies that imaging geometry becomes an important issue. Unlike the above approaches, in this study we pay special attention to system geometry, which guides the image analysis and focuses on achieving the highest image resolution under specific geometric configurations. This is justified by the fact that in the RHEA project (RHEA, 2011) crop row location is identified as an important problem, where real-time image processing becomes another major constraint. A trade-off must be established between the real-time requirement and the highest image resolution possible.

The application of geometry, under perspective projection, guiding the subsequent real-time image analysis under maximum image resolution, constitutes the main contribution of this paper. For this purpose we apply system geometry to locate crop rows and compare the performance of two camera devices provided by different manufacturers with the goal of achieving areas of interest with maximum image resolution and the lowest processing time possible.

This paper is organized as follows: section 2 describes the approach to detecting crop rows in maize based on the geometric model. In section 3 simulated experiments are described, and the different results obtained with two real camera devices are shown. Finally, conclusions are provided in section 4.

2. Crop row detection

One of the main problems we face is how we can cover, with the camera installed on board the mobile unit, an appropriate number of crop rows to obtain as much information as possible.

Undoubtedly, one of the most common problems in PA consists in recognising the crop rows and their subsequent location, distinguishing the correct number of rows with the highest image resolution possible. We approach the problem by applying image system geometry.

In RHEA (RHEA, 2011) one of the crops to be analysed is maize. In maize, crop lines are parallel and spaced 0.75m from each other. Under the RHEA specifications, six

crop rows are to be treated simultaneously. This means the area to be treated is 4.5m wide. This can be carried out by considering a unique camera covering the width of the full area to be treated or two cameras each covering half the width of the area, i.e. 2.25m. In this study we have chosen the latter option, i.e. two cameras. This choice is justified on the assumption that we can achieve higher image resolutions in the half area than with the full area, using specific settings of the geometrical parameters. This method is supported because these half areas can be processed in parallel with multicore processors. The real-time requirement can thus be easily achieved with relatively simple processing technologies providing sufficient image resolution.

The system studied in this paper is therefore designed with two cameras, each covering an area 2.25m wide and three crop rows. It is assumed that the intrinsic (focal length) and extrinsic (camera orientation and pose) parameters associated with the system geometry are known. This allows the mapping of the expected crop rows over the image, i.e. their location and identification.

The next step is to determine the best dimension in length of the area to be examined, so that we can obtain maximum image resolution with as little computational time as possible to fulfil RHEA real-time requirements, as mentioned before. Maximum resolution is desirable to analyse the area with the greatest possible accuracy. This will allow us to make better decisions during the weed/crop identification phase, also involved in the RHEA project but outside the scope of this study.

In section 2.1 an overview of the general system geometry is provided and in section 2.2 its specific configuration from the viewpoint of RHEA.

2.1 Geometric model: extrinsic and intrinsic parameters

Fig. 1 displays the camera geometry with respect to the absolute coordinate system (*X*, *Y*, *Z*). The camera system has its own local system defined by (*x*,*y*,*z*) and can take images with a pitch-angle α which represents the rotation around the *x*-axis of the image plane, this being the angle between the axes *Y* and *y*. In the normal operating mode, during image acquisition, angles roll, θ, and yaw, β, should be null. This situation could change due to terrain irregularities that induce deviations in those angles. The above factors define three extrinsic parameters which are known during the process (except for induced movements). The fourth extrinsic parameter related to our system is the height of the camera with respect to the absolute coordinate system (X_0), i.e. with respect to the ground. The most relevant intrinsic parameter is the focal length (*f*) characterizing the optical system. The sizes of sensors are also considered as intrinsic parameters, to be studied in the next section.

Given a generic point in 3-D space with coordinates (*X*, *Y*, *Z*), in our case placed on the ground where crops and weeds are present, the goal is to obtain the set of

equations that allow us to map such a point into the image plane. This represents a simple transformation between coordinate systems (Fu et al., 1988).

Assume the image plane aligned with the (*O*, *X*, *Y*, *Z*) system and its optical centre coinciding with the origin *O*. We can displace the optical centre along axes *X*, *Y* and *Z*, some distances defined by X_0, Y_0 and Z_0 respectively. In this position we can apply three elemental gyros with angles α, θ and β around the corresponding axis.

Using this simple transformation we obtain equations (1) and (2) where the 3-D point (*X*, *Y*, *Z*) is transformed into the image point (*x*, *y*).

$$x = -f\left(\frac{(X-X_0)\cos\beta\cos\theta+(Y-Y_0)\cos\beta\sin\theta\cos\alpha+(Z-Z_0)\cos\beta\sin\theta\sin\alpha+\ldots}{(X-X_0)\sin\beta\cos\theta+(Y-Y_0)\sin\beta\sin\theta\cos\alpha+(Z-Z_0)\sin\beta\sin\theta\sin\alpha-\ldots}\right.$$

$$\left.\frac{\ldots+(Y-Y_0)\sin\beta\sin\alpha-(Z-Z_0)\sin\beta\cos\alpha}{\ldots-(Y-Y_0)\cos\beta\sin\alpha+(Z-Z_0)\cos\beta\cos\alpha+f}\right) \quad (1)$$

$$y = -f\left(\frac{-(X-X_0)\sin\theta+(Y-Y_0)\cos\theta\cos\alpha+\ldots}{(X-X_0)\sin\beta\cos\theta+(Y-Y_0)\sin\beta\sin\theta\cos\alpha+\ldots}\right.$$

$$\left.\frac{\ldots+(Z-Z_0)\cos\theta\sin\alpha}{\ldots+(Z-Z_0)\sin\beta\sin\theta\sin\alpha-(Y-Y_0)\cos\beta\sin\alpha+(Z-Z_0)\cos\beta\cos\alpha+f}\right) \quad (2)$$

The above image coordinates (*x*, *y*) are referred to the centre of the plane or equivalently to the optical centre. They are expressed in length units, but from the point of view of image analysis a conversion to image pixel coordinates is required. This is carried out by considering the specifications of the corresponding sensor provided by each manufacturer. A sensor is characterized by its size in terms of number of pixels in the horizontal and vertical dimensions. We call them *H* and *V* respectively and the camera resolution is *H x V*, expressed in pixels. Each pixel in the image is obtained from a physical element in the full CCD sensor; the size of each element is *h x v* expressed in length units, normally as *μm*. Finally, the coordinates in the image, expressed in pixels are computed as follows,

$$x_i = x/h \text{ and } y_i = y/v \quad (3)$$

2.2 Setup of system geometry in maize fields

Once the geometrical model is established, the next step consists in the location of crop rows based on exclusively geometric considerations.

The area to be examined comprises three crop rows. The final goal of any perception system is to determine the density of green plants, including crops and weeds, considering the crop rows as the central part guiding the process. Based on this consideration, we can arrange the system as shown in Fig. 1, where three crop rows fall within the field of view of the camera plus an additional surface to the left and right.

As mentioned before, maize crop lines are parallel and spaced b = 0.75 m from each other. Depending on the RHEA real-time requirements, not addressed in this paper, the size of the area in length could vary depending on the number of pixels to be processed. We have established a measurement unit, defined by the parameter a. So, according to the scheme in Fig. 1, the size of the area to be treated, from the point of view of the site specific treatments in PA, is $2a \times 3b$. This covers a surface of 4×2.25 m^2 in the soil.

Also according to Fig. 1, this area is at a distance c from the origin of the global coordinates system (O, X, Y, Z); so the value of the straight line in the XZ plane delimiting the area to be treated is Z = c, i.e. with $Y = 0$.

In maize crops the parameter b is fixed and imposed by the nature of this crop, but the remaining parameters can be varied, depending on a series of factors, one of the most important is related to the real-time requirements. Indeed, we need to process the image with times that allow for subsequent decisions and also to allow the actuators to respond according to the needs of the treatment to be applied. This requires the setting of the remaining intrinsic and extrinsic parameters involved in the process. They are: a, c, Y_0, f and α. Depending on their values the imaged area in the field could vary considerably.

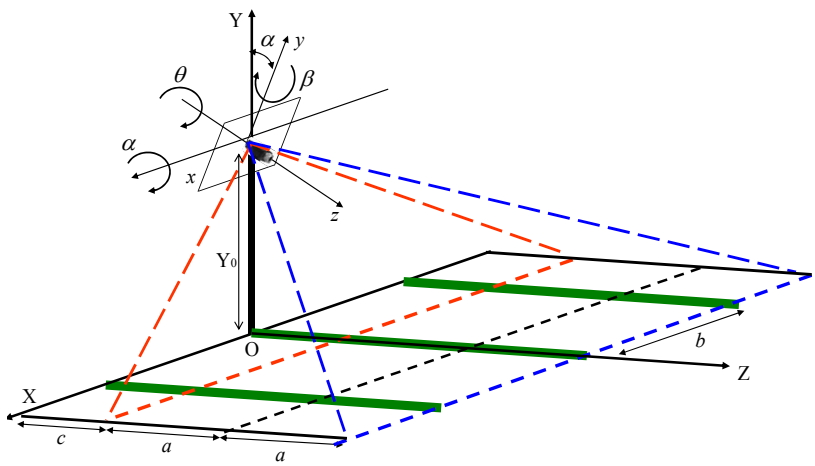

Fig. 1. Camera system geometry, crop row arrangement and area to be treated

3. Experiments

Based on the system geometry and other considerations specified above, we have carried out several experiments in order to determine the number of pixels in the image to be processed coming from the area in the field demanding treatment.

The full images are captured under perspective projection and the mapping of the rectangular area in the field is like that shown in Fig. 2, i.e. with a trapezoid form, which is defined as the Area of Interest (AOI). The areas outside the AOI are not considered from the point of view of image analysis, and are excluded from the specific treatment in the field. Figure 2 shows the image of the area in the maize field, which represents the AOI or study area.

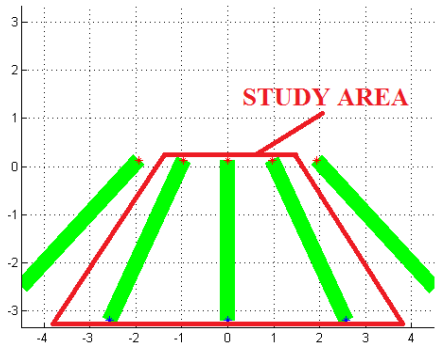

Fig. 2. Image obtained from the field area displayed in Fig. 1

The sensors used in our experiments are the BASLER 17FC 1400 and PROSILICA GB1380C with the specifications shown in Table 1.

Table 1. Sensor specifications.

Device	**Sensor type**	**Image resolution (*HxV*)**	**Pixel size (*h x v*)**
BASLER 17FC 1400	CCD Colour	1392 *x* 1040 pixels	6.45µm *x* 6.45µm
PROSILICA GB1380C	CCD Colour	1360 *x* 1024 pixels	6.45µm *x* 6.45µm

From the point of view of image analysis the best solution is that with the maximum number of pixels in the AOI with this area imaged as near the bottom part of the image as possible. These factors represent a combined measurement of the image resolution for the AOI, which is to be considered. An important issue concerning the number of pixels in the AOI is that the processing time must be enough for making decisions and taking effective actuations. In this study we have not analyzed processing times because they depend on the type of image process applied. Our interest is focused on analysing the number of pixels contained in the

AOI and also the number of pixels in the bottom part of the image of the area of interest.

To prevent the number of combinations of the different parameters involved in determining the best image resolution becoming too large, we have fixed parameters c and a at $2m$ and vary Y_0, f and α for each camera device analyzed.

Tables 2 and 3 display the number of pixels in the AOI for the BASLER and PROSILICA devices and for each setting, the percentage of pixels in the AOI with respect to full image resolution and the distance (in pixels) from the bottom of the image to the AOI.

Table 2. BASLER device: number of pixels in the AOI, percentage of valid pixels in the image and distance from the bottom part of the image.

BASLER 1400 17FC	**HEIGHT (Y_0)**							
	1 m				**1.5 m**			
***f*/α**	**10º**	**15º**	**20º**	**25º**	**10º**	**15º**	**20º**	**25º**
4.5 mm	70410	68214	67666	68716	96818	90178	86140	84315
	4.88	4.72	4.68	4.76	6.71	6.25	5.79	5.84
	311	376	438	499	166	239	307	372
6 mm	125016	121136	120179	122059	171898	160131	152977	149751
	8.66	8.39	8.32	8.45	11.91	11.09	10.60	10.37
	243	329	412	493	48	146	237	223
8 mm	221877	215035	213375	216750	N/A	284236	271581	265891
	15.37	14.90	14.78	15.02		19.7	18.82	18.42
	151	266	376	485		22	144	259

Table 3. PROSILICA device: number of pixels in the AOI, percentage of valid pixels in the image and distance from the bottom part of the image.

PROSILICA GB1380C	**HEIGHT (Y_0)**							
	1 m				**1.5 m**			
***f*/α**	**10º**	**15º**	**20º**	**25º**	**10º**	**15º**	**20º**	**25º**
4.5 mm	70410	68214	67666	68716	96818	90178	86140	84315
	5.05	4.89	4.85	4.93	6.95	6.47	6.18	6.05
	304	369	431	492	159	232	300	365
6 mm	125016	121136	120179	122059	171898	160131	152977	149751
	8.97	8.69	8.62	8.76	12.34	11.49	10.98	12.75
	236	322	405	486	41	139	230	316
8 mm	221877	215035	213375	216750	N/A	284236	271581	265891
	15.93	15.44	15.32	15.56		20.40	19.50	19.09
	144	259	369	468		15	137	252

From the results in tables 2 and 3 we can infer that the best configuration in terms of maximum resolution with the shortest distance to the bottom part corresponds to the following values Y_0 = 1.5m, f = 8 mm and α = 15º. They are obtained in both cameras. This similar behaviour is due to their similar specifications, as displayed in table 1.

The best image resolution should be that with the AOI covering the full image; nevertheless this will affect the image processing time considerably. A suitable trade-off between the AOI image resolution and real-time processing must be established once the processing algorithms are chosen.

Moreover, from the point of view of the RHEA project, which can be extended to any real applications, the mobile ground units work on real terrain, probably with irregularities. There are also vibrations coming from the motor of the mobile ground unit. This means that angles α, θ, and β could vary from their ideal values, affecting the mapping of the area in the field and producing a different AOI from that expected. To overcome this problem, the size of the image plane must be greater than the AOI so that the latter is always mapped inside the image plane for subsequent analysis and treatment.

Figures 3 (*a*) and (*b*) display two representative images captured with the BASLER and PROSILICA camera devices respectively. Both were captured in a maize field, during May 2011 in Arganda del Rey, Madrid, Spain, with the following extrinsic and intrinsic parameters: Y_0 = 1.5 m, f = 8mm and $\alpha = 15^{o}$. Three crop rows define the AOI over a surface 2.5m wide and 4m long. Both cameras were placed 2m away from the base of the area in the field, i.e. c = 2 in Fig. 1. Using the above geometric configuration the mapping is represented in the image with the superimposed lines. In Fig. 3(*b*) the mapped area in the field is displayed, delimited with insulating tape. As we can see in both images, the mapping of the expected lines coincides with the real crop rows, particularly in image 3(b), where the starting and end points of such lines match the border lines in the delimited area.

An additional problem arises from optical lens quality: lens distortions lead to an effect known as barrel distortion because aberrations. It can be seen in Fig. 3(*b*) and is more significant in the bottom part of the image. The effect can be corrected by improving the quality of the lens so that this distortion is minimised or by applying camera calibration where some intrinsic parameters can be estimated including the focal length and distortion coefficients (Tsai et al., 1987).

The image in Fig. 3(*b*) displays an interesting situation. As mentioned before, three crop rows are considered: a central one and two lines placed to its right and left. Theoretically they must be spaced 0.75 m from each other. This is true for the central and right lines, but due to sowing errors this does not occur with respect to the central and left lines, which are separated by a distance greater than 0.75 m. Because of this fact, based on geometric considerations, we obtain an expected

crop line in an erroneous location. In this case, additional image processing is required to identify the correct crop row in the image. This is outside the scope of this study but is addressed in the RHEA project through a correction process. Nevertheless, crop line location is very useful during the crop row correction process.

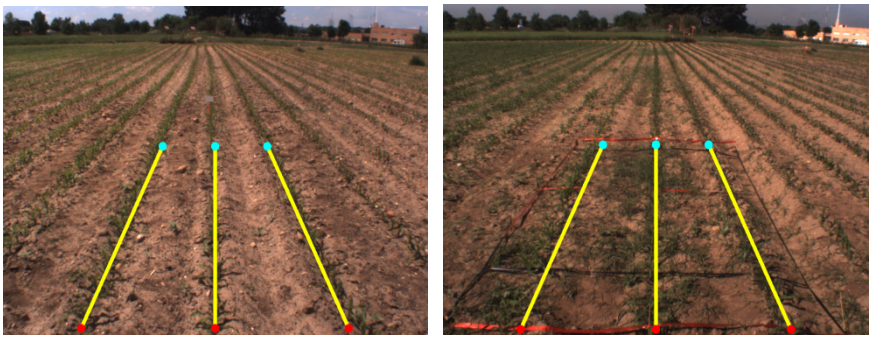

Fig. 3. Mapping of the expected lines on images based on the system geometry defined above: (a) PROSILICA; (b) BASLER

4. Conclusions

In PA an important problem is that of crop row location, so that the positions of green plants, including crops and weeds, can be estimated in a subsequent process, also addressed in RHEA. This task can be accomplished by considering camera geometry. Indeed, based on the setting of intrinsic and extrinsic parameters, we can map the expected crop row locations on the image. This makes the search for crop lines easy, although when they are mapped there may be deviations due to irregularities of terrain and vibrations in the mobile ground unit which affect some parameters. Geometric mapping can be useful to search for correct crop lines even if sowing errors appear in the maize field.

To do this, we consider an area in the maize field which is mapped as an AOI in the image. The AOI must be suitably processed and we search for geometric parameter settings to achieve maximum AOI resolution so that better image analysis can be carried out.

We have tested geometric settings with two specific camera devices, but this study can be extended to other camera sensors from different manufacturers with different specifications. Also, three crop rows have been considered, but a different number of crop rows can easily be studied.

The application of geometric constraints is also useful for methods based on the identification of crop rows by the alignment of green pixels, which are assumed to be crop rows. The performance of some such techniques could be improved by

applying geometric constraints where image resolution is to be considered for image analysis.

Acknowledgement

The research leading to these results has received funding from the European Union's Seventh Framework Programme [FP7/2007-2013] under Grant Agreement nº 245986.

References

Åstrand, B. and Baerveldt, A. (2005). A vision based row-following system for agricultural field machinery. Mechatronics, vol. 15, no. 2, pp. 251-269.

Brivot, R., Marchant, J. A. and Chalabi, Z.S. (1996). Segmentation of plants and weeds using infrared images. Acta Hort. 406, 165–172.

Fontaine, V. and Crowe, T. G., (2006). Development of line-detection algorithms for local positioning in densely seeded crops. Can. Biosyst. Eng. 48 (7), 19–29.

Fu, K.S., Gonzalez, R. C. and Lee (1988). C.S.G., McGrawHill, Madrid.

Gee Ch., Bossu J., Jones G. and Truchetet F. (2008). Crop/weed discrimination in perspective agronomic images. Computer and Electronics in agriculture 60, 49-59.

Hough, P.V.C. (1962). A method and means for recognizing complex patterns. U.S. Patent Office No. 3069654.

Jinlin, X. and Weiping, J. (2010). Vision-based Guidance Line Detection in Row Crop Fields. 2010 International Conference on Intelligent Computation Technology and Automation. DOI 10.1109/ICICTA.2010.400.

Marchant, J. A. and Brivot, R. (1995). Real-time tracking of plant rows using a Hough transform. Real-Time Imag1995:363–71.

Olsen H. J. (1995). Determination of row position in small-grain crops by analysis of video images. Comput Electron Agricult;12:147–62.

Reid J. F.; and Searcy, S. W. (1987). Vision-based guidance of an agricultural tractor, IEEE Control Systems Magazine, vol. 7, no. 12, 39-43.

RHEA, (2011). http://www.rhea-project.eu/.

Slaughter, D. C., Chen, P. and Curley, R. (1999). Vision guided precision cultivation. Precision Agriculture, vol. 1, no. 2, pp. 199-216.

Han, S., Zhang, Q., Ni, B. and Reid J. F. (2004). A guidance directrix approach to vision-based vehicle guidance systems. Computers and Electronics in Agriculture, vol. 43, no. 3, pp. 179-195.

Bakker, T., Wouters, H., van Asselt, K., Bontsema, J., Tang, L. and Muller, J. (2008). A vision based row detection system for sugar beet. Computers and Electronics in Agriculture, vol. 60, no., pp. 87-95.

Tsai, R.Y. (1987). A Versatile Camera Calibration Technique for High-Accuracy 3D Machine Vision Metrology Using Off-the-shelf TV Cameras and Lenses. IEEE Journal of Robotics and Automation, vol. 3, no. 4, 323-344.

Techniques for Area Discretization and Coverage in Aerial Photography for Precision Agriculture employing mini quad-rotors

João Valente, David Sanz, Jaime del Cerro, Claudio Rossi, Mario Garzón,

Juan D. Hernández and Antonio Barrientos

Centre for Automation and Robotics (UPM-CSIC),

Universidad Politécnica de Madrid

C/ José Gutiérrez Abascal, 2

28006 Madrid, Spain

(e-mail: joao.valente@upm.es).

Abstract: Remote sensed imagery acquired with mini aerial vehicles, in conjunction with GIS technology enable a meticulous analysis from surveyed agricultural sites. This paper sums up the ongoing work in area discretization and coverage with mini quad-rotors applied to Precision Agriculture practices under the project RHEA.

1. Introduction

In recent years, precision agriculture (PA) researchers have found that the use of unmanned aerial vehicles (UAV) based on quad-rotors could significantly help in improving research in agricultural sciences. Their motivation was conceived by its availability, simple assemblage and maintenance, as well as their low cost compared with traditional tools (e.g. Satellites or conventional aircrafts).

The main aim of an aerial survey is to obtain aerial images of the field, which can be used for generating generate a map of the surface though mosaicking procedures, those maps can also be post-processed to extract interesting information (e.g. biophysical parameters, shape and features detection).

Therefore, the aerial vehicles have to cover the full area to be surveyed by following a continuous and smooth trajectory and avoiding obstacles or prohibited areas. In order to ensure a minimum completion time for the survey, it is desirable to minimize the number of changes in direction and avoid revisiting points. Furthermore, not all areas are suitable for taking off or landing with aerial vehicles, so the trajectory has to ensure starting and ending locations that fulfill all the requirements (e.g. safety margins, space enough for operation, pick up and drop

ability, accessibility). The problem of covering an entire area, subjected to constraints established by the platform itself and by the workspace, is known as the Coverage Path Planning (CPP) issue.

Aerial robots are mainly employed in agriculture for crop observation and map generation through imaging surveys (Herwitz et al.,2004). The maps are usually built by stitching a set of georeferenced images (i.e. orthophotos) through mosaicking procedures. Typically, they rely on the information about the biophysical parameters of the crop field.

Moreover, the agricultural experiments reported with aerial vehicles fall mainly in waypoints based navigation (Nebiker et al.,2008; Zarco-Tejada et al.,2008; Valente et al.,2011), where the drones navigate autonomously through a pre-defined trajectory, composed by a set of points in the environment.

This paper have been written as follows: After this brief introduction, Section 2 introduces the conceptual aerial framework with all their components and workload. Section 3 presents the techniques of area decomposition, Section 4 explains the area coverage approach, Section 5 presents some case studies and Section 6 provides an improvement for the coverage path planning with multi aerial robots. Finally, Section 7 reviews the issues summed up.

2. Aerial Framework

The conceptual aerial framework is denoted as a set of actions and components (i.e. software and hardware) that provide the achievement of a task inside a particular context in a feasible fashion. Hence, the framework intends to support area coverage missions with aerial robotic systems in PA practices. This is a preliminary phase in the design of a robotic system that can be seen as a top-down approach for solving the problem (i.e. through a step-wise design). Abstractly speaking: Breaking up of overall goal, individualizing the requirements, coming up with a concept, and finally starting the design phase.

As it was introduced in section 1, there is an agricultural task demand and a fleet of aerial and ground robots to carry out the proposed task is assumed. To make the concept description easier to follow, let's assume that there is a general weed control task. This task falls mainly in two sub-tasks: the perception system (i.e. identify the weed species and patches over a wide agricultural area) and the actuation system (i.e. kill the weeds). The second sub-task will not be discussed since it is not considered in the framework design.

In order to identify the weed species and patches, the agricultural field has to be previously surveyed with an image sensor. In this way, the aerial framework will be responsible for performing this operation.

The main components of the framework are: Aerial vehicles, Operation or Control station, and Mission planner.

The framework must be able to provide the operator in charge with the required tools to carry out the mission. This is made up of an aerial vehicle with way-points navigation features, a visual sensor, a control station with tools to define and monitor the mission, and finally a mission planner to generate the aerial trajectory. The general inputs for the mission are: Number of aerial units available, field map characteristics (e.g. coordinates, undesired areas), and images resolution and overlapping. The step-by-step mission can be summed up follows:

1. The aerial units and the control station are setup near the target agricultural site

2. The operator introduces the before mentioned inputs to the mission planner

3. The operator launches the mission planner

4. The mission planner computes an aerial trajectory and sends it to the operator

5. If the operator does not agree with the generated path, the procedure will jump back to 2.

6. Otherwise, the plan is sent to the aerial vehicles, the execution starts, and the operator supervises the mission until finished.

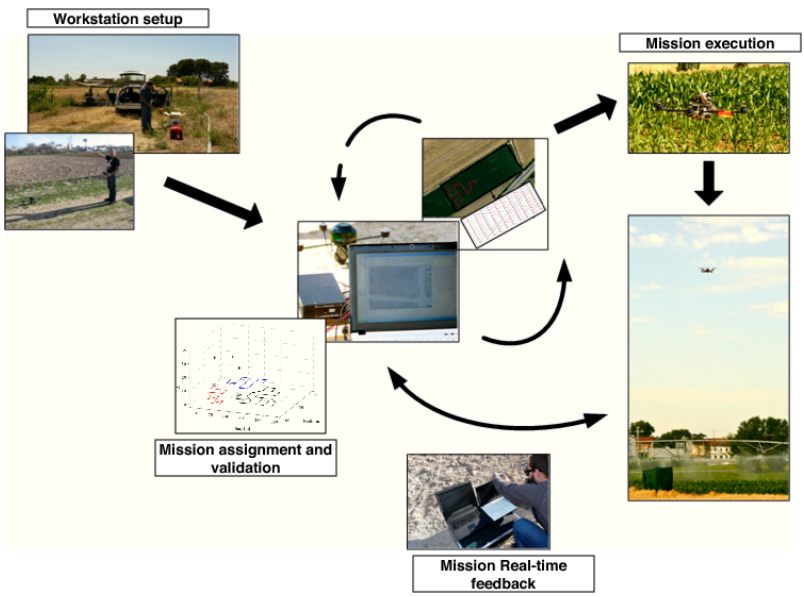

Fig. 1. Mission workflow

3. Workspace definition and sampling

A user with access to a geographic information system (GIS) could easily obtain information corresponding to the field to be surveyed. The first step herein is to obtain a geo-referenced image of the agricultural site. That image should provide information enough to obtain the geographic coordinates from the bounds of the field and therefore the field dimensions.

The second step is to define an image resolution and overlapping for the image survey. Once those parameters are defined, the image sensor resolution that better suits the goal then chosen.

After those two steps the number of images to be taken by the robots and the corresponding geographic position within the field are obtained.

The workspace decomposition in the very end is defined as an approximate cellular decomposition, following the taxonomy proposed by (Choset, 2001), which means that the workspace is sampled like a regular grid. This grid-based representation with optimal dispersion is reached by dividing the space into cubes (i.e. cells and therefore image samples), placing a point in the center of each cube (i.e. centroid of each image, and therefore a geographic coordinate denoted as a way-point). The geographic coordinates from each photograph are computed with the accurate geodesics Vincenty's formulae (Vincenty, 1975).

The last parameter required for the aerial mission is the height of the aerial robots height above the ground. This parameter is computed by considering the cell dimension in the world, and the digital sensor characteristics.

Another advantages of having a grid-based decomposition is that it directly maps the robot workspace into a kind of unit distance graph, denoted as grid graph G(V,E)$\boldsymbol{G}_{<V,E>}$ where V denotes the vertices and E the edges. Each vertex represents a waypoint and each edge is, the path between two waypoints u and v such that u ~ v.

4. Area coverage approach

The approach proposed split into in two sub-problems: 1) the area sub-division and the robot assignment problem are handled. 2) the coverage path planning problem is considered. In Fig. 2 the proposed approach is shown schematically where the sub-problems are also decompose in two stages.

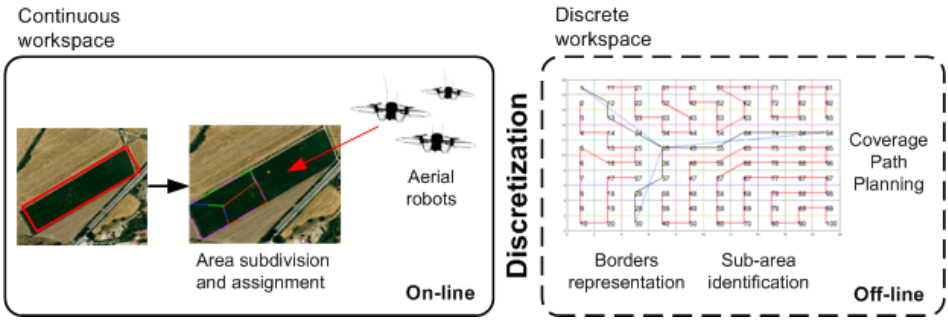

Fig. 2. Overall approach

4.1. Area sub-division and the robot assignment problem

The multi coverage path planning problem is formalized by assuming that there is a top level procedure that handles the area division and robots assignments (Rossi et al., 2009). For a better understanding an example is shown in Fig. 3. The agricultural field depicted has an irregular shape, and has been decomposed in three sub-areas, assuming that there is a robot per area with different characteristics and/or parameters.

Fig. 3. Example from the area-subdivision approach

After applying this approach the result must be mapped on the robots workspace as previously defined. Since the robot workspace is discrete and this method provides a continuous result, a rasterization method is applied on the grid-based workspace. In order to solve this issue a solution based on slightly modified Bresenham's line algorithm (BLA) (Bresenham, 1965) is employed. The borders representation algorithm is depicted in Fig. 4. Algorithm 1 shows the procedure employed where l stands for line segment, ε is an error term and δ stands for cell

size. Let's consider P as the end-point of a line segment l. The leftmost and rightmost end-points of l are denoted respectively by Pl and Pr.

Algorithm 1 Borders representation

```
1: for all l ∈ L do
2:     x ← x_l ∨ y ← y_l
3:     Δ_x ← xr − x ∨ Δ_y ← yr − y
4:     if Δ_y < 0 then
5:         Δ_y ← −Δ_y ∨ step_y ← −δ_h
6:     else
7:         step_y ← δ_h
8:     end if
9:     if Δ_y < 0 then
10:        Δ_x ← −Δ_x ∨ step_x ← −δ_w
11:    else
12:        step_x ← δ_w
13:    end if
14:    if Δ_x > Δ_y then
15:        ϵ ← 2 × d_y − d_x
16:        while x <= x_r do
17:            if ϵ >= 0 then
18:                y ← y + step_y ∨ ϵ ← ϵ − 2 × d_x
19:            end if
20:            x ← x + step_x ∨ ϵ ← ϵ + 2 × d_y
21:        end while
22:    else
23:        ϵ ← 2 × d_x − d_y
24:        while y <= y_r do
25:            if ϵ >= 0 then
26:                x ← x + step_x ∨ ϵ ← ϵ − 2 × d_y
27:            end if
28:            y ← y + step_y ∨ ϵ ← ϵ + 2 × dx
29:        end while
30:    end if
31: end for
```

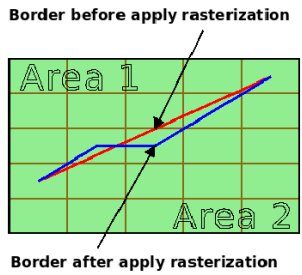

Fig. 4. Borders representation algorithm based on the BLA

4.2. Coverage path planning

In order to obtain a complete coverage path with the minimum number of turns, subject to a pre-defined initial and goal position, and without re-visited points within the workspace, heuristic and non heuristic algorithms are employed.

The distance transform function is applied on the grid by employing a Bread-first search (BFS) on the graph induced by the neighbourhood adjacency of cells. As a result, the coverage path can be easily found from any starting point within the environment to the goal cell by choosing the nearest neighbour cell in gradient ascendant order instead of the common descendant order.

Then, a Deep-limited search (DLS) to build a tree with all possible coverage paths is applied in order to find a complete coverage path that passes only once through all nodes in the adjacency graph. Using this approach, the search length can be limited to the number of vertices, and consequently, the search neither goes around in infinite cycles nor visits a node twice.

During the gradient tracking, the algorithm finds more than one neighbour to choose from with the same potential weight. Additionally, the bottleneck caused by the local minimal can also block the search. In order to solve these issues, a backtracking procedure was employed.

Finally, the coverage path with the minimum number of turns is chosen through the following cost function,

$$\Gamma = \sum_{i=1}^{m} \gamma_k^{\{i\}}, \qquad k \in \{135°, 90°, 45°, 0°\}$$

Where,

$$\gamma_{\pm 135°} > \gamma_{\pm 90°} > \gamma_{\pm 45°} > \gamma_{0°}$$

The algorithm pseudo code is shown in Fig. 5.

Algorithm 2 Coverage Path Planning algorithm

1: Initialize $FiFo = \emptyset$
2: $G_{<V,E>} \leftarrow ConvertToGraph(\Phi)$
3: $G'_{<V,E>} \leftarrow Wavefront(G_{<V,E>})$
4: **while** $\exists P \in \Phi$ **do**
5: $P \leftarrow DLS_{w/Backtracking}(G'_{<V,E>})$
6: $FiFo \leftarrow FiFo + P$
7: **end while**
8: $P^* \leftarrow min\{\Gamma(FiFo)\}$
9: Return P^*

Fig. 5. Coverage path planning algorithm. Φ is a field sampled in a finite number of way-points, P is a complete coverage path

Although the gradient-based approach does not ensure an optimal solution, it provides a simple and fast way to obtain a near optimal coverage solutions, in both regular and irregular fields, with and without obstacles within, subject to the aforementioned restrictions.

5. Demonstration and Results

In order to prove the efficiency of the proposed approaches two experimental scenarios with different characteristics were chosen. The fields considered are a maize field (Fig. 6) with an area approximately of 20000 m² and a vineyard parcel (Fig. 7) with an area of approximately 63765 m², both located in Madrid, Spain.

Fig. 6. Maize field (red square) and UPM-CSIC headquarters (green circle).

Fig. 7. Vineyard parcel.

5.1 Aerial Coverage Metrics

The approaches proposed are evaluated through the following metrics: total of area coverage (%), coverage time (s), computational time (s).

For the total of area covered a Quality of Service (QoS) index was defined, and indicates the percentage of the remote sensed field. The QoS index is given by Ub/(N.M)(%), where Ub is the upper bound of the number of unvisited cells, in a NxM dimension grid.

5.2 Maize field (regular shape)

The first experiment was simulated, and based on a regular shape field. The simulation was performed in two phases: First of all, subdividing the entire area into subareas and then assigning a geo-referenced image of that obtained area to each robot. The robots have to negotiate the sub-areas to be covered based on a set of parameters that address their physical characteristics and sensing capabilities. As a result, those parameters where randomly generated for the present experiment. The result is shown in Fig. 8.

Fig. 8. Result from the negotiation between the robots.

The sub-division is then rasterized over the sampled workspace, and for each sub-area, a coverage path is computed. The final result is shown in Fig. 9.

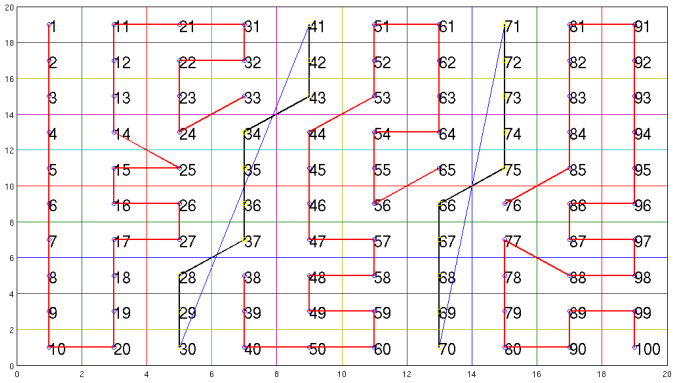

Fig. 9. Borders representation and CPP computed for each sub-area.

In the first sub-area, this is from cell 1 to cell 33, a minimum number of 14 turns were achieved. In sub-area 2, of cell 38 to cell 65, the total number of turns was 15. Turns. And in sub-area 3, cell 76 to cell 100, 14 turns were required. The computational time required for computing each coverage path for each of the sub-areas was approximately, 0.82s, 0.34s, and 0.50s, respectively. With regard to the QoS index, there is an upper bound (Ub) of 20% of non covered cells defined as security strips, therefore a QoS of 80% was achieved in this experiment.

5.3 Vineyard parcel (irregular shape)

The same principles have been applied to the vineyard parcel with irregular shape. Nevertheless, this type of field is more challenging to employ the proposed approach compared to a rectangular field. Since, in an irregular field, not only the borders that break down the overall area have to be discretized, but also the contour of the overall area (i.e. which separate the area of interest to cover from the area of non interest).

Considering a step forward of the study, a real mission has been set up with three mini aerial robots, denoted as quad-rotors. The goal of this mission was to measure the coverage mission time, considering the short mission range of each drone. The quad-rotors considered in this mission were two Hummingbirds, and one Pelican, from the German company, Ascending technologies.

The results from the sub-area decomposition are shown in Fig. 10 where the characteristics and parameters of three real quad-rotors have been considered.

Fig. 10. Sub-area decomposition considering three real aerial vehicles (quad-rotors)

The output shown in Fig. 10 has been rasterized once again in a grid workspace (10x10 cells). For each sub-area, a starting point (e.g. take-off) and final goal point (e.g. landing) locations have been predefined before computing each coverage path. All trajectories have been computed in less than 20s. The computed coverage trajectories are shown in Fig. 11. A minimum number of turns ranging from 8 to 20 have been obtained. The average coverage time of the three robots is 222s at a velocity of 5 m/s. The average battery consumption during the coverage task was approximately 15% for each robot. The QoS achieved in this experiment is 82% with a Ub 18% uncovered cells from.

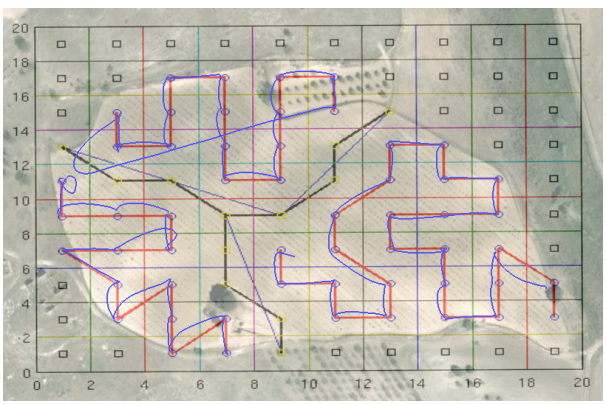

Fig. 11. Rasterization and area coverage in an irregular field

6. Discussion about the amount of area covered

The rasterized borders represented in a multi robot workspace are of great importance, since they work as security strips, where vehicles are not allowed to enter. However, as seen before, a considerable percentage of area when using them remains uncovered. The metric that address the percentage of area covered is the QoS index. Therefore, borders have to be considered so as to improve the QoS but at the same time, safety for the robotic system has to be ensured. A Risk Analysis (RA) has been carried out with the purpose of improving this index.

Defining risky situation as a situation where two or more aerial robots are located in adjacent cells, which makes the distance between them beyond a certain value. Lets denote Pn(Xn; Yn; Zn) the 3-dimensional position of a n aerial robot in an aerial fleet with N elements. A risk condition can be written as,

$$\forall n \in N, \quad \exists \Delta_n^{\{i\}} \leq \delta, \quad i = 1, 2, ...j$$

where i is the ith neighbour robot and j the length of a certain neighbourhood. Finally, Δ is the distance between the robot n and a neighbour robot i, and δ a stipulated minimum safety distance that has to be defined.

The first point to be analyzed is the number of occurrences found during a coverage trajectory (two or more robots are in neighbouring). From the analyses of 8 different coverage trajectories in 2 different crop fields it can be concluded that 37.5% of the times a robot is in an adjacent cell to the other robot. Moreover, up to 12.5% of the times three robot are flying adjacently. This non exhaustive analysis allowed to give an idea of the number of times that this situation occurs.

Secondly, let's suppose that a robot is adjacent to another (i.e. neighbour cells). For example, the vineyard has an area of approximately 63765 m² which corresponds to 195m length and 327m width. Let's assume that the aerial robot carries a commercial digital camera that provides image resolutions up to 10.4 mega pixels. Moreover, if choose the best image resolution to sample the field is chosen, it corresponds to an image size from 3368x3088 pixels. If the mission requires a certain percentage of overlapping, the effective size of the image will be reduce in same percentage. If a spatial resolution of 1 pixel/cm is required, a grid resolution of 6x10 cells (each cell will have a dimension of 32.7x32.5m)is obtained.

With these magnitudes a collision between two aerial robots would hardly ever occur. Even considering a position accuracy of 3m and wind speeds of 10m/s, there is no possibility that two aerial robots collide.

In conclusion, whenever a coverage mission where the cells dimension are above a margin of 2 times the robot position accuracy, the security strips can be removed from the planner and a QoS of 100% is achieved. Figure 12 shows the same

coverage path computed in Fig. 11 but without borders, where the borders have been distributed to each sub-area in a load balancing fashion.

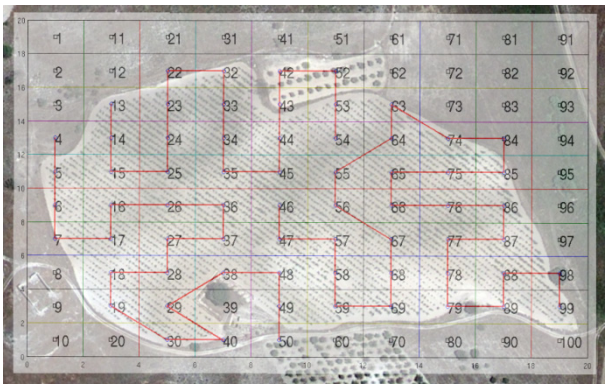

Fig. 12. Multi robot coverage without borders.

7. Conclusions

This paper provides a set of solutions for area coverage with mini aerial vehicles for Precision Agriculture management. The approaches proposed rely in the combination of simple heuristic and non heurist techniques to be easy to replicate the findings and improve the results obtained at any stage.

These approaches are developed to provide the computation of coverage trajectories in agricultural fields with different shapes. In this way two experimental scenarios with different characteristics were used has case study. The usability of the algorithms were verified in both.

Regarding the coverage algorithm. If a solution exists, it retrieves the best one. However it does not ensure that it is the optimal solution. Nevertheless, an effort has been made to minimize the number of turns of each vehicle. The initial and final position can be pre-defined and, there is no chance that there are revisited way-points. If there are areas to avoid, the algorithm is able to handle this constraints. Furthermore, the running time is acceptable for this kind of problem where the complexity is NP-complete.

Field tests show that tree drones were able to cover a large agricultural field consuming much less than the conventional autonomy (approximately 20min). In this way, it is than defined that two quad-rotors will have the same performance, without need to recharge them during the task.

Although in a first attempt the robots path planning considered safety bounds between them, this strategy was cancelled by analysing carefully the risk of collision within the workspace.

Ongoing work will consist in improve the area coverage algorithm, towards an optimal solution. Acquire images in each way-point in order, to study the need of position correction in the previous workspace sampling, and/or introduce further path planning constraints.

Acknowledgement

The research leading to these results has received funding from the European Union's Seventh Framework Programme [FP7/2007-2013] under Grant Agreement nº 245986.

References

Herwitz, S. R., Johnson, L. F., Dunagan, S. E., Higgins, R. G., Sullivan, D. V., Zheng, J., Lobitz, B. M., Leung, J. G., Gallmeyer, B. A., Aoyagi, M., Slye, R. E. and Brass J. A. (2004). Imaging from an unmanned aerial vehicle: agricultural surveillance and decision support. Computers and Electronics in Agriculture, 44(1):49–61.

Nebiker, S., Annen, A., Scherrer, M., and Oesch, D. (2008). A light-weight multispectral sensor for micro uav - opportunities for very high resolution airborne remote sensing. In The International Archives of the Photogrammetry, Remote Sensing and Spatial Information Sciences, volume XXXVII, pages 1193–1200.

Zarco-Tejada, P. J., Berni, J. A. J., Suárez, L., and Fereres E. (2008). A new era in remote sensing of crops with unmanned robots. SPIE Newsroom.

Valente, J., Sanz, D., Barrientos, A., del Cerro, J-, Ribeiro, A-and Rossi, C. (2011). An air-ground wireless sensor network for crop monitoring. Sensors, 11(6):6088–6108.

Choset, H. (2001). Coverage for robotics - a survey of recent results. Ann. Math. Artif. Intell., 31(1-4):113–126.

Vincenty, T. (1975). Direct and Inverse Solutions of Geodesics on the Ellipsoid with application of nested equations. Survey Review XXIII (176): 88–93.

Rossi, C., Aldama, L. and Barrientos, A. (2009). Simultaneous task subdivision and allocation for teams of heterogeneous robots. In Robotics and Automation, 2009. ICRA '09. IEEE International Conference on, pages 946 –951

Specific Techniques for the RHEA Fleet

Analysis of Engine Thermal Effect on Electronic Control units for "Robot Fleets for Highly effective Agriculture and Forestry Management" (RHEA)

Miguel Garrido, Heidi T. Jiménez-Ariza, Miguel A. Muñoz, Adolfo Moya, Constantino Valero and Pilar Barreiro

LPF_TAGRALIA. Polytechnic University of Madrid (UPM), Avda. Complutense s/n, 28040 Madrid, Spain

(e-mail: miguel.garrido.izard@upm.es).

Abstract: The procedures carried out in order to perform the analysis by engine thermal effect on the electronic control units installed on a ground robot fleet were studied in this work. The objective is to characterize the temperatures on the engine tractor environment for different tasks. In this way, it could be possible to estimate the environmental conditions that the cabinets will be exposed to. Those cabinets, in which the electronic controls of sensors, actuators and power supplies will be stored, will be located aboard the ground robot units.

1. Introduction

Within the European project "Robot Highly Effective Fleets for Agriculture and Forestry Management" (project n ° 245986 of the 7th framework program), defined by the acronym "RHEA", it is intended to carry out the development of a structure in order to store all the electronic boxes of the devices that will be assembled in the ground robot (sensors, communication systems and actuators).

In this work we face firstly the identification of the heat emissions sources on the vehicle, and then the different ways for measuring emissions of heat, as well as the important influence of temperature on electronic devices. As a second step, an experiment was defined and performed to assess the environment of the structure. Several remarks on the results and conclusions are provided for the implementation of the structure in the near future.

1.1 Heat emission of tractors and agricultural vehicles

Any object with a temperature above absolute zero emits energy as an electromagnetic emission. As its temperature rises, the energy emission also increases. All mechanical systems generate thermal energy during normal

operation which could be used to evaluate their operating condition. One of the biggest problems in mechanical systems is due to excessive temperatures. This excessive heat can be generated by friction, cooling degradation, material loss or blockages. An excessive amount of friction can be caused by wear, misalignment, over or under lubrication and misuse.

In relation with the internal combustion engines, it is difficult to reach a maximum efficiency higher than 42%, so large amount of wasted fuel energy is expelled from the engine to the surroundings as heat in several ways, with a significant fraction through the exhaust. A recent study estimated that in a typical 2 l gasoline engine used on passenger cars, 21% of the released energy is wasted through the exhaust at the most common load and speed condition. Current estimates of waste thermal energy from light-duty vehicle systems range from 20 kW to 400 kW, depending on engine size and engine torque-speed conditions. (Wang et al., 2011)

1.2 Measurement of heat emissions

Mobile agricultural machines are becoming more complex due to the combination of work steps and the implementation of systems for additional processing (Kutzbach, 2000). Nowadays, the detection of unusual events and diagnosis of its casual origin are still performed by human operators. This higher complexity and the multivariate character of agricultural machinery processes implies an overload for the operator thus highlighting the need for the introduction of fault detection and diagnostic systems on agricultural machinery processes (Craessaerts et al., 2010)

Fault diagnostic systems have not been given much attention yet in agricultural machinery research. However, these techniques could be of high value at a supervisory control level for agricultural machinery (Craessaerts et al., 2010).

There are dozens of predictive maintenance technologies, and some have become a standard in many industries. The `standard' technologies include vibration analysis, ultrasound, oil analysis, wear particle analysis and thermography (Girdhar, 2004).

In the recent past, various techniques have been developed for studying the thermal aspects of machining and are broadly classified into two, namely, (1) the experimental approach and (2) the numerical approach. With the recent developments in machining automation, various cutting temperature measurement techniques, including tool–work thermocouple, embeded thermocouple, and infrared pyrometer, emerged (Rai and Xirouchakis, 2008).

Literature reveals that the previous experimental techniques have been widely applied in the turning process due to its simplicity. Since it is also tedious to calculate directly the temperatures of some tool-work interface, the inverse heat transfer method was employed for estimating the transient tool-face temperature

and heat dissipation. Recently, various finite-element method (FEM) and finite-difference method (FDM) based numerical models have also been proposed for the determination of the temperature distribution in the workpiece, which were difficult to study by experimental methods (Rai and Xirouchakis, 2008).

1.3 Effect of heat on the electronics

Electronic devices have been developed with a trend toward higher performance and smaller dimensions. These electronic devices normally contain a fairly high energy density.

The reliability of an electronic component is defined as the ability of performing required function under given conditions for a stated time. An electronic device fails to fulfil its intended function when its application or environmental condition exceeds its application limit. A survey from the U.S. Air Force indicates that the percentage of temperature related failures in electronics exceeded 55%. This high percentage evidences that the current cooling methods are inadequate to fulfil the device cooling requirement. Advances in electronic packaging and increases in chip complexity and functionality are responsible for this high percentage. Theoretically, electronic components are very reliable at recommended operating temperatures. However, environmental factors and unusual operating situations greatly decrease the effective operating time (Alawadhi and Amon, 2003). Mithal (1996) studied the effect of temperature on electronic component reliability. The experimental results indicate that a 1 °C decrease in a component temperature may lower its failure rate by as much as 4%. Moreover, the research indicates that a 10 °C to 20 °C increase in component temperature may increases its failure rate by 100%.

When considering electric motors and generators, operating temperatures and thermal patterns can be a valuable key in a predictive maintenance program. All motors have a normal thermal pattern as well as given maximum operating temperature. This temperature is usually stated on the nameplate of the motor and is normally given as a rise in Celsius degrees above the ambient air temperature. Most motors are designed to operate at ambient temperatures that do not exceed 40 °C. Conditions such as inadequate air flow, partial discharge, unbalanced voltage, bearing failure, insulation failure and degradation in the rotor or stator can be identified with a temperature monitoring program. Abnormal thermal patterns can also identify misalignment in couplings when these devices are used in conjunction with motors (Peterson, 2008).

2. Materials and methods

At this point, it comes to specifying the issues in relation to the test conducted for this work. The materials used in order to carry out the analysis of thermal effects derived from the tractor engine on electronic control units are defined below. In turn, the paper also explains the methodology undertaken for the completion of this analysis.

2.1 Tractor

The tractor used during the course of this study consisted of a New Holland tractor "TN70VA" whose characteristics, shown in the table below, were comparable to the tractor "T3050 CVT" that will be used in RHEA project.

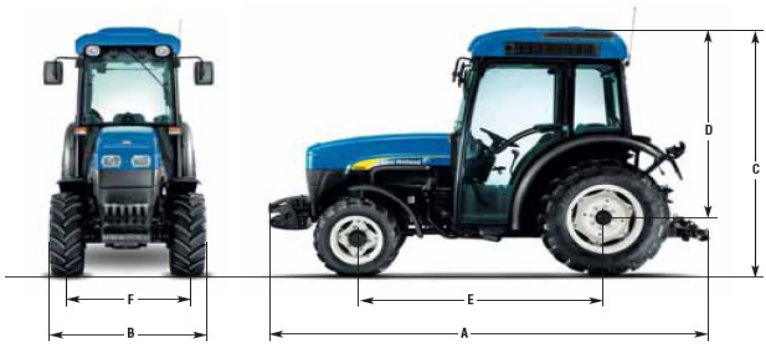

Fig.1. Front and side view of the "TN70VA" tractor

Table 1. "TN70VA" tractor dimensions

Dimensions	
A Total length including pack and rear linkage (mm)	3663
B minimum width (mm)	986
C Total height (mm)	2260
D Height from center of rear axle to top of cab (mm)	1798
E Wheelbase: ST/DT (mm)	2035 / 2064
F width via	
• Front ST min-max/DT min-max (mm)	838 – 1166 / 835 – 1049

2.2 Structure

On the tractor mentioned above, the installation of plates took place, in order to simulate the cabinets' structure, which will be responsible for housing the electronic equipment from the sensors, communication devices, as well as the actuation systems developed for the RHEA project.

The structure consisted of two aluminium plates (100x20 cm) at different heights, joined by profiles for each of the sides. At the same time the profiles of both sides were joined by a transverse profile, providing rigidity to the structure.

The temperature sensor cards were attached to register the temperature in the environment of the assembled framework.

2.3 Temperature sensor cards

The temperature sensor cards used were Turbo Tag Cards ® "T702-B", (Sealed Air, USA) (Fig. 2), which were designed to obtain accurate and efficient data using a radio frequency (RF) communication system. Each card (characteristics shown in Table 2) had an accuracy of ±0.5 °C throughout the operation range. Its data storage limit was an archive file of up to 702 measurements, with a size of a credit card.

Table 2. Specifications of TurboTag ®, "T702-B"

Number of measures:	702
Temperature range:	-55°C to +80°C (-67F to +176F)
Temperature accuracy:	+/- 0.5°C (+/- 0.9 F) with calibration accuzone™ (95%)
Control space of time:	20 minutes minimum, 3 months maximum
Delay control:	0 minutes minimum, 21 days maximum
Rfid interface:	13.56 MHz passive – according to ISO 15693-3
Rfid reading distance:	1 to 30 centimetres (greater distance with antenna booster)
Time data capture:	Less than 2 seconds
Alarms:	High and low alarms set by the user / store time above / below
Means:	Store temperature or mkt arithmetic mean (geometric mean)
Uhf:	Holds 24-character code epc (uhf reader or manually)
Software registration:	Session manager ™ software creates files and / or database records
Lifetime parameters:	Stores the temperature sensitivity based on Arrhenius kinetic model
Lifetime:	Provides remaining information of lifetime at the point of reading

In total, the installation consisted of 69 temperature cards throughout the aluminium structure (Fig. 2).

Fig.2. Turbo Tag® card and framework with all Turbo Tag® cards installed

2.4 Tasks performed

Once the temperature sensors in the structure were installed, and it was joined to the tractor, we proceeded with the development of the tests. These consisted on performing two clearly differentiated tasks, allowing an environmental study of the engine for different conditions.

The tasks performed during the test, which took place in the experimental field of the UPM EIA (4477224.73 m N and 437398.95 m E UTM coordinates), were as follows:

Tillage tasks by using a rotator tiller implement that requires connection to the PTO. The task was carried out on a plot of one third of hectare (Fig. 3).

Transport task of a water tank for irrigation of the trees in the UPM EIA's experimental field. In this case a connection to the PTO it was not required (Fig. 3).

Fig.3. Rotovator task (top left); Irrigation task (top right) and task performed by the tractor during the test (below): red square represent the rotovator tasks and red line the irrigation task

2.5 Principal points of interest

From all points sensed by the installation of the Turbo Tags in the structure, it was interesting to consider which would be the main points of interest. On this line, it was studied both the engine air inlet and the engine air outlet (Fig. 4).

Fig.4.Engine air inlet (blue circumference), engine air outlet (red circumference) and longitudinal and height heat distribution (by red ellipse representing expected warmer places and by blue ellipse the least)

At the same time, were considered as special areas of interest, those which allowed obtaining the distribution of heat within the structure, both longitudinal, lateral and in height (Fig. 4.). The highest temperature was expected in the outlet of the

engine cooling air. Thus, it is expected that the temperature would decrease as moving away from this point.

Thus, the sensor cards that would best represent the main points to consider (outlet and inlet of air into the engine and heat distribution) were differentiated by different colour circumferences in the Fig 5.

The circumference colour represented in each of the selected cards denoted a location in the structure, being the same location for same colour (eg. with red the position of the outlet of the engine air; with grey the inlet of the engine air ...)

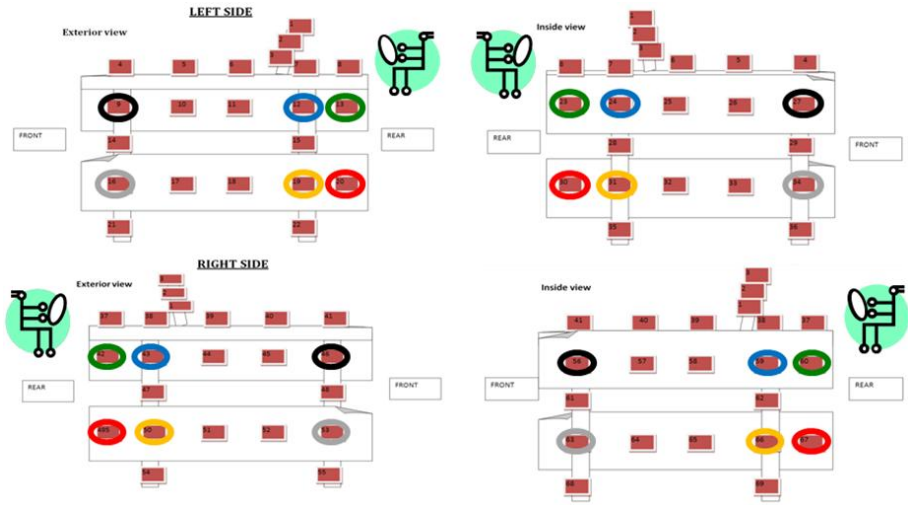

Fig.5. Longitudinal and height heat distribution (by red representing expected warmer places and by blue the least

3. Results

The results obtained during the test for different tasks performed by the tractor show the values recorded by the selected cards. For this purpose the values for each of selected cards were plotted using the representative colour of that location.

3.1 Rotovator test

From rotovator results (Fig. 6), it was observed that lateral factor becomes an important parameter, and at red location (next to the engine air outlet), the higher temperatures were reached on the left side.

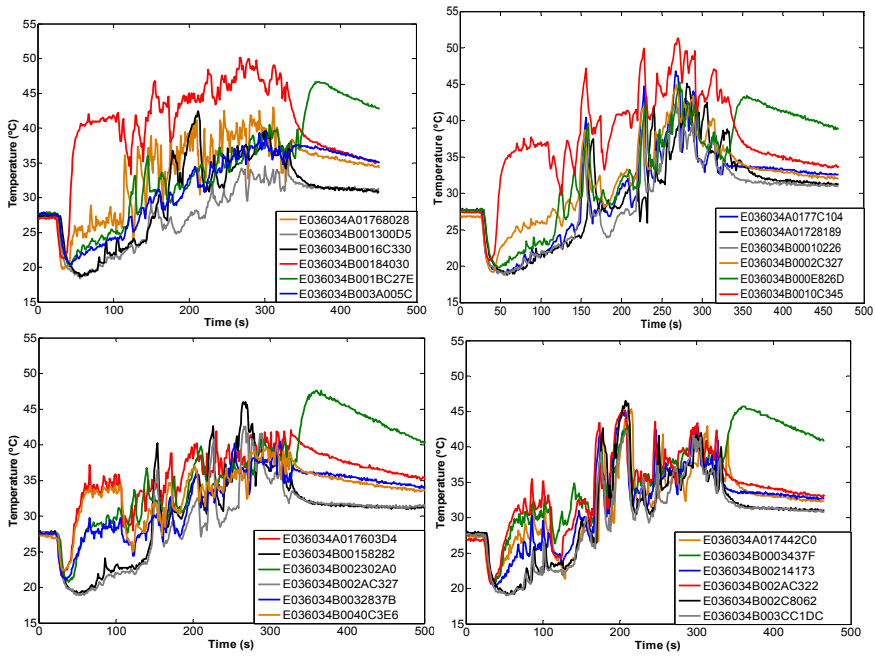

Fig.6. Temperature recorded during rotovator task in the internal left side (above left); external left side (above right) internal right side (bottom left); and external right side (bottom right) of the structure.

3.2 Irrigation test

Similarly, data obtained during irrigation are shown in the following graphs (Fig. 7). In such graphs it can be observed, as mentioned for the rotovator results, that: the lateral factor becomes important, and higher temperatures appear on the left side.

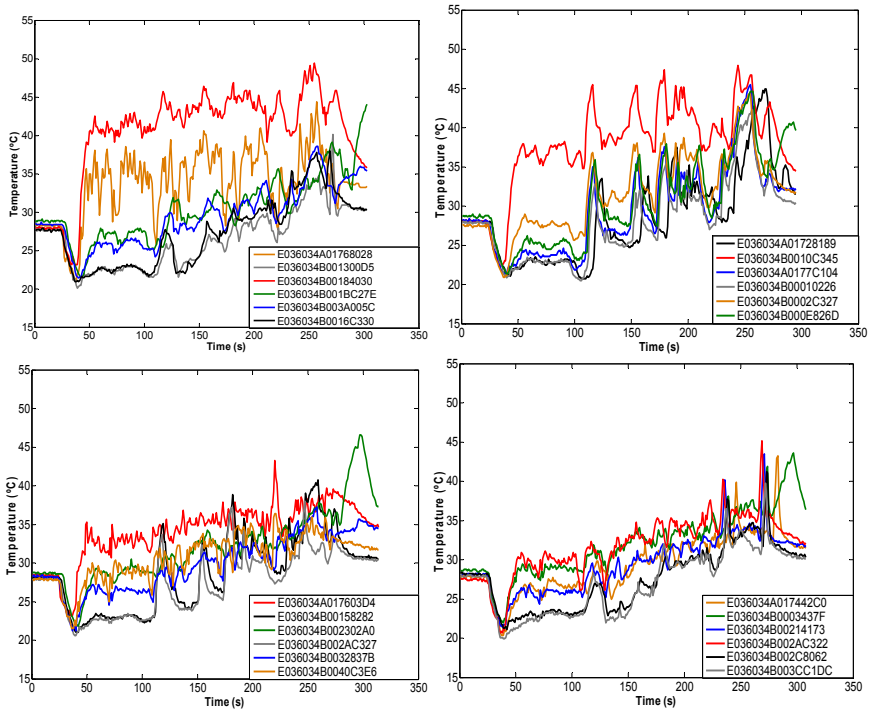

Fig.7. Temperature obtained during irrigation task in the internal left side (above left); external left side (above right) internal right side (bottom left); and external right side (bottom right) of the structure.

3.3 Analysis of variance – mean temperature

An analysis of variance was performed for both mean and variance of the temperatures recorded by the cards. In table 3 the values obtained for the analysis of variance of mean temperatures and variance are shown.

The F values suggest that the most significant factors were longitudinal location (67.2), task performed (29.76), longitudinal location combined with internal or external location (17.12), and the linkage of side and longitudinal location (12, 4); being the remainder factors not significant at 5%.

Table 3. Analysis of variance of mean temperatures and variance recorded during the test.

Source	**Sum Sq. (mean)**	**d.f.**	**F (mean)**	**Sig. level (mean)**	**Sum Sq. (var)**	**F (var)**	**Sig. level (var)**
Task	103.124	1	29.76	***	4015.28	123.38	***
Side	5.657	1	1.63	ns	1264.61	38.86	***
Internal/External	9.031	1	2.61	ns	1134.53	34.86	***
Height	2.945	1	0.85	ns	617.9	18.99	***
Longitudinal location (front/rear)	232.907	1	67.2	***	8.3	0.26	ns
Task* Side	11.421	1	3.3	*	34.61	1.06	ns
Task* Internal/External	0.42	1	0.12	ns	40.53	1.25	ns
Task* Height	3.279	1	0.95	ns	136.83	4.2	**
Task*Longitudinal location (front/rear)	0.29	1	0.08	ns	33.79	1.04	ns
Side* Internal/External	2.377	1	0.69	ns	50.33	1.55	ns
Side*Height	29.409	1	8.49	**	39.21	1.2	0.2752
Side*Longitudinal location (front/rear)	42.991	1	12.4	***	416.35	12.79	***
Internal/External * Height	0.8	1	0.23	ns	0.31	0.01	ns
Internal/External *Longitudinal location (front/rear)	59.341	1	17.12	***	12.39	0.38	ns
Height*Longitudinal location (front/rear)	12.097	1	3.49	*	142.18	4.37	**
Error	325.78	94			3059.16		
Total	806.382	109			10845.99		

*10%; **5%; ***1%

With the aim to simplify the results, it was carried out the elaboration of 2D temperature interpolation of the average temperatures (Fig. 8).

From the figures shown below, it was observed that:

- Rotovator caused more warming, because it was connected to the PTO of the tractor and required a higher power from it.
- A higher warming is produced at the rear, where the outlet of the engine cooling was placed.
- The highest average temperature is recorded at the rear left side.
- The front of the structure showed a higher temperature for the external side compared to the internal side (solar radiation effect).
- Heat transfer and thus temperature recorded were distributed in a fan shape

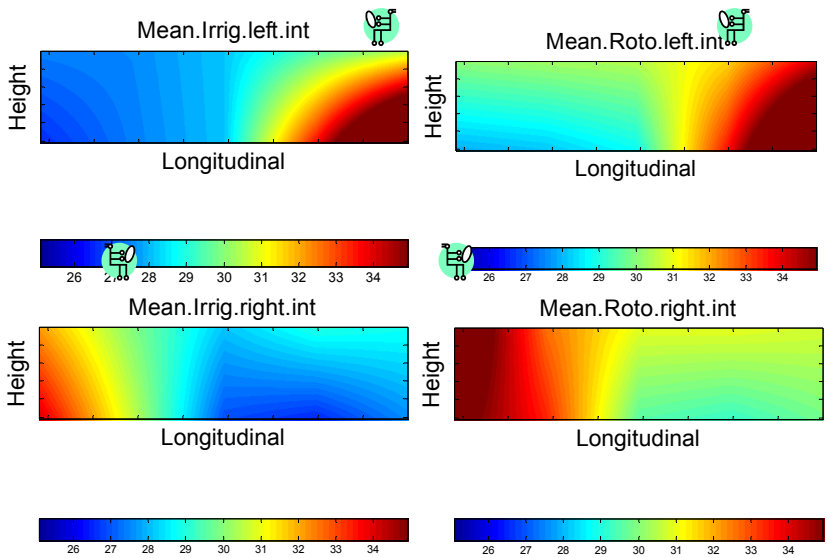

Fig.8. Interpolation of mean temperatures for each task (left figures represent irrigation task, while right figures represent rotovator task), and side (above figures represent left side, while below figures represent right side)

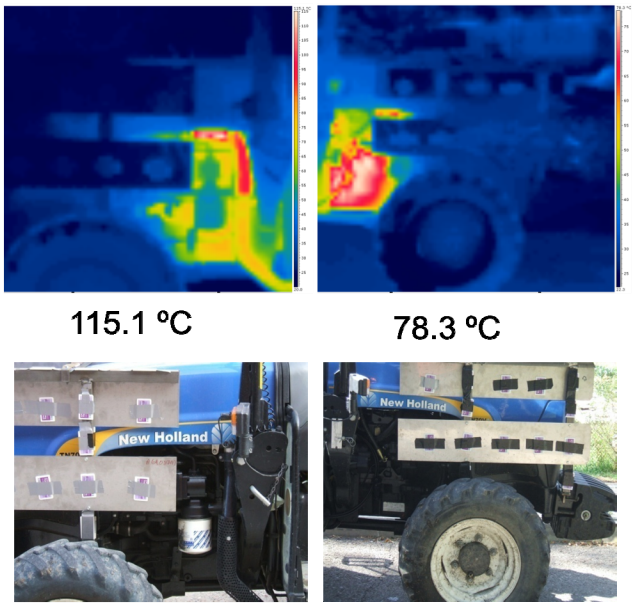

Fig.9. Infrared (FLIR i5, USA) and RGB pictures of left and right side of the tractor during irrigation task

3.4 Analysis of variance – variance of temperature

In the same way as for average temperatures, an analysis of variance of temperatures (table 3) was elaborated. In this case the most significant factors were task various performed (123.38), side (38.86), orientation (34.8), height (18.99) and the linkage of side and longitudinal location (12.79), being the remainder factors not significant at 10%.

Besides, 2D interpolations for each task and side of the interior of the structure were developed (Fig. 10).

So, it was observed that:

- A pattern for each side existed, observing that for different tasks, the pattern of variation was the same.
- The task performed by the tractor generates a higher variation (rotovator task) or lower (irrigation task) of this pattern.
- The rear left side shows higher variations in temperature (at the same place where the mean temperature was higher).
- Greater fluctuations in temperature were produced for the upper, than for lower height; and for external than internal orientation (sensitive to the weather conditions variations).

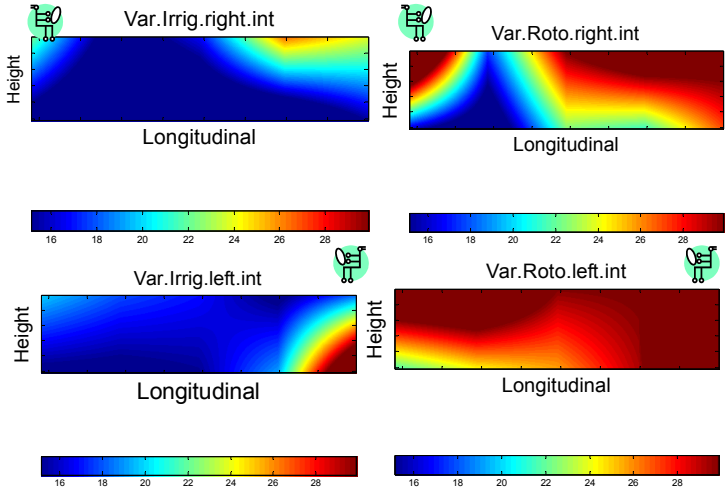

Fig.10. Interpolation of temperatures variance (°C^2) for each task (left figures represent irrigation, while right figures represent rotovator task), and side (above figures represent left side, while below figures represent right side)

3.5 Cabinets' structure applications

With the purpose to apply the knowledge acquired during the course of this test to the cabinets' structure development, which will be responsible for housing both electronic equipment from the sensors, communication devices, as well as the performance systems , it could be said that:

The cabinets' sensitive part of the structure (sensors and others devices) will be placed on the right side of the tractor. Also it will be important to move down a position the DGPS receiver box, leaving free the point of greatest thermal variations.

The cabinets' disturbing part (power supply and actuators) will be placed on the tractor left side, but displacing the power supply position to the front, as this will be the equipment that release more heat.

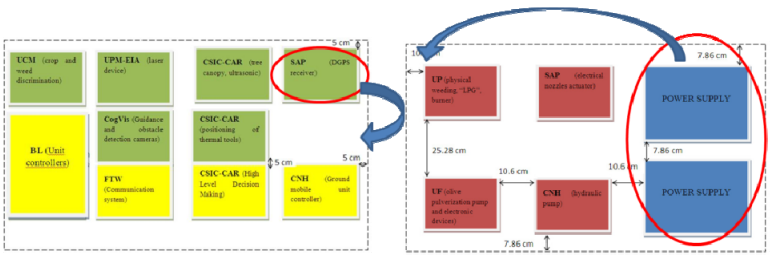

Fig. 11. Representation of the components placed at cabinets' structure, as well as changes in location to be considered after this test

4. Conclusions

It would be desirable to locate the electronic devices that have a greater sensitivity to temperature and temperature variation, as far as possible from components located on the rear left side of the tractor used during this test (hydraulic oil filter, exhaust gas …).

It will be advisable to conduct a similar test in winter, where the effect of solar radiation will be reduced.

Even though temperatures above 50 °C have not been recorded, without taking into account the warming that will produce the electronic boxes, it will be advisable to install a cooling system that attenuates thermal effects, and decreases the possible effect on electronics failure.

Acknowledgement

The research leading to these results has received funding from the European Union's Seventh Framework Programme [FP7/2007-2013] under Grant Agreement nº 245986.

References

Alawadhi, E.M., Amon, C.H. (2003). PCM Thermal control unit for portable electronic devices: Experimental and numerical studies. IEEE Transactions on components and packaging technologies, vol. 26, no 1, march 2003, pag:116-125.

Craessaerts, G., De Baerdemaeker, J. Et al (2010). Fault diagnostic systems for agricultural machinery. Biosystems Engineering 106 (1):26-36.

Kutzbach, H. D. (2000). Trends in power and machinery. Journal of Agriucltural Engineering Research 76 (3):237-247.

Girdhar, P. 2004. Other predictive maintenance techniques. Practical machinery vibration analysis and predictive maintenance. ISBN 0750662751. Elsevier. Pag:221-234.

Mithal, P. (1996). "Design of experimental based evaluation of thermal performance of a flichip electronic assembly", in ASME EEP Proceedings. New York: ASME, 1996, vol. 18, pp. 109–115.

Peterson predict, (2008). Analyzing Mechanical Systems Using Infrared Thermography. Available at:

(http://www.maintenanceworld.com/Articles/petersonpredict/Analyzing-Mechanical-Systems-Using-Infrared-Thermography.html)

Rai, J.K., Xirouchakis, P. 2008. FEM-based prediction of workpiece transient temperature distribution and deformation during milling. Int J Adv Manuf Technil (2009) 42:429-449.

Wang, T., Zhang, Y., Peng, Z., Shu, G. (2011). A review of researches on thermal exhaust heat recovery with rankine cycle. Renewable and Sustainable energy reviews 15 (2011) 2862-2871.

Path-planning of a Robot Fleet Working in Arable Crops: First Experiments and Results

Angela Ribeiro and Jesus Conesa-Muñoz

Centre for Automation and Robotics (UPM-CSIC), Crtra. Campo Real Km 0,2 28500 Arganda del Rey, Madrid, Spain

(e-mail: angela.ribeiro@car.upm-csic.es)

Abstract: Most agricultural tasks require a planning stage to determine the paths to be followed by the mobile platforms. Obtaining the optimal path is a difficult task because of the sheer number of factors that must be considered, and the problem is especially complex when more than one mobile platform is involved. In this paper, path-planning is addressed as an optimisation problem, and a novel approach, based on a genetic algorithm, is proposed. The aim is to establish optimal trajectories in arable crops for a fleet of heterogeneous robots that accomplish weed control tasks when the patch distribution (weed map) is known in advance. The approach is tested over a wide range of different situations, including well known and randomly generated situations. The aim of the study is to verify the performance of the approach and how well it fits with the expected behaviour.

1. Introduction

After sowing, weed control is one of the most important agricultural operations, and depending on the crop, it can be necessary more than once if post-emergency treatment is required. Treatments can be mechanical or chemical, and the selected mode will depend on the weed species to be removed and how the weeds are distributed in the crop.

When performing the treatment, the vehicle must cover the whole field, which requires a lot of attention by the driver, who must often be supported by visible references and even assisted by other operators in charge of changing the location of the references in each pass. This tedious work has motivated many studies to focus on finding the best route to cover the whole crop according to cost criteria.

Indeed, many methods for planning the most efficient route for crop distribution can be found. For example, Visal and Oksanen (2007) propose a path-planning method in which complex fields are divided into smaller and less trapezoidal shapes that are merged together into larger zones when certain conditions are

met. After such mergers, all possible routes are explored, and the most efficient is selected. In other approaches, different areas of the field (work, turning, entry, and exit), as well as a direction in which to cross, are assigned with the aim of obtaining routes that cover all of the areas with the lowest cost in terms of money and effort (Taïx et al., 2006). The best route is found using the best Hamiltonian path and geometric reasoning.

Another method based on a decomposition of the whole field into smaller and simpler areas is proposed by Jin and Tang (2006), who describe a method wherein both the field and obstacles are described as polygons; furthermore, the smaller regions are covered with a Boustrophedon route (Choset 1997). A recursive algorithm is applied to obtain the best cover. Finally, the sub-regions are optimally matched using an approach based on the travelling salesman problem, where the constraints are the entry and exit areas of the field.

In other approaches, prior information about the field, the vehicle and treatment tools, which determine the optimal routes for headings, the main field and the sequence of operational tasks, is used for optimising the driving pattern (Sorensen 2004).

Another possibility to be considered is changing the direction in the headers because of the large amount of time needed for this operation. In fact, Bochtis and Vougiakas (2008) make a distinction among three types of rotation for minimising distances in the non-crop zones. Stoll (2003) calculates the rotation by considering the effective width, the minimum turning radius, the conduction velocity and the rotation acceleration of the vehicle. Furthermore, he considers additional time due to the changes in the direction of rotation.

There is no doubt that the route-planning problem in agriculture is very complex, and it becomes even more complex when a fleet of robots is involved in weed treatment, especially when they are small robots with insufficient capacity to handle the entire field individually.

The problem can be expressed as an optimisation problem in the following way: given a set of robots (*R*) with certain features (e.g., herbicide capacity, motion characteristics, width of the treatment bar), a field with determined dimensions, a crop organised in rows and a map of the weed patches, the aim is to find the subset of robots and associated paths that ensure the cover of the entire weed patch with the minimum cost (1).

$$\left(r_1, c_1, h_1\right), \quad \ldots, \quad \left(r_i, c_i, h_i\right), \quad \ldots, \quad \left(r_n, c_n, h_n\right) \Big| r_i \in R \quad \wedge \quad \bigcup_{i=1}^{n} c_i = C \quad \wedge \quad \sum_{i=1}^{n} h_i = H \quad \forall n \in \mathrm{N} \tag{1}$$

where *R* is the set of all available robots, *C* is the minimum field cover and *H* is the minimum quantity of herbicide that ensures the treatment of all weed patches existing the crop.

In the crop treatment context, two assumptions are made: 1) robots always travel parallel to the crop row and 2) changes in the robots' direction of movement into the crop are forbidden and can only be made in the headers.

Additionally, a third assumption can be made to simplify the problem: fields have rectangular shapes. The third assumption makes the development of the first version of the method easier, and the simplification does not limit further developments to include more complex field shapes. In fact, in a real agricultural context, it is quite common to use strategies that break fields with irregular geometries down into smaller trapezoidal regions (Choset 1997, Oksanen and Visal 2007) to use as building blocks for the whole path plan. The first and second assumptions respond to real situations.

According to our previous assumptions, finding a path plan for the field is equivalent to finding the set of crop rows each robot must cover to perform the treatment task. To understand the complexity of building the optimal path plan, let us suppose a 4-ha field with a width twice its length. If robots are small enough that they can only treat the space between two crop rows (75 cm), the plan that covers the whole field will have approximately 400 parallel routes. Moreover, if the fleet is composed by n_R many robots and each robot can deal with any of the columns, then the number of possible different plans will be n_R^{400}, without taking into account the order in which crop rows are arranged If the order is considered, then the number of possible different plans will be considerably higher. In fact, this more complex problem belongs to the NP-hard (Non-deterministic Polynomial-time hard) problem class.

Due to the combinatorial explosion of possible solutions, the classical optimisation strategies are not able to solve this class of problem. Numerous acceptable, yet non-optimal, solutions have been attained through various computational techniques, including the Genetic Algorithms (GA) technique (Goldberg 1989, Michalewicz 1999).

2. The GA approach

In a GA strategy, each possible solution of an optimisation problem is encoded in a string (called an individual). The search of the best solutions is a process where several individuals are considered in parallel, i.e., in the same iteration of the algorithm. The process usually begins from a population of randomly generated individuals and proceeds in generations. In each generation, the fitness of every individual in the population is evaluated, and multiple individuals are stochastically selected from the current population (based on their fitness) and modified (recombined and possibly randomly mutated) to form a new population. The new

population is then used in the next iteration of the algorithm. Commonly, the algorithm terminates when either a maximum number of generations has been produced or a satisfactory fitness level has been reached for a least one of the individuals of the population. If the algorithm has terminated due to a maximum number of generations, a satisfactory solution may or may not have been reached. Typically, a GA has five basic components (Rawlins 1991): 1) a representation scheme for codifying the problem solutions; 2) a method for generating the initial population of solutions to be explored; 3) a way to evaluate the quality of each solution being explored, i.e., a fitness function; 4) operators that explore the solution space by altering the genetic composition of the individuals to produce new individuals through reproduction; and finally, 5) definitions for values for all of the parameters used to run the GA. In the next subsections, the representation scheme used, the genetic operators selected and the constructed fitness function will be detailed. The method for generating the initial population and the parameters selected for running the GA will be explained in the Results section.

2.1 Representation of a solution

In the proposed approach, the information about the crop and weed distribution is stored and organised in a data structure, a matrix whose dimensions depend on the treatment width. Indeed, the number of columns in the matrix is equal to field_width/treatment_width, whereas the number of rows is equal to field_length/treatment_width. Therefore, each matrix component will represent the herbicide treatment unit, which is denoted as a 'cell' for the rest of the document. Each cell will have a state that corresponds to weed occurrence, thereby specifying whether the cell has to be treated or not.

Keeping in mind the crop and weed representation, each individual of the GA codifies a unique solution as a vector with as many components as columns in the matrix (parallel routes following the crop rows). Each component of the vector contains the identification of the robot devoted to the column treatment. This representation indicates which robot should treat which column but does not explicitly define the order in which the robot should treat the columns. To obtain a complete solution by the decoding of an individual, the vehicle behaviour is defined as follows: 1) for a given a robot, the algorithm determines which of the two outermost columns assigned to the robot is closest to its original position; 2) the robot moves from its initial position to the closest column; 3) the robot treats the column (a crop row); 4) once it has exited the column at the opposite end, the robot advances along the header to the nearest column of the remaining columns; and 5) the robot repeats steps 3 and 4 until there are no more columns remaining.

Through this process, the optimal path for a set of columns is obtained in terms of distance, turns and time. Therefore, by performing the process for each of the robots, the overall path plan for the entire fleet is obtained.

Fig. 1 shows the specific plans for the three robots involved in the individual solution ($r_1,r_1,r_2,r_2,r_3,r_3,r_3,r_2,r_2,r_2$) over a field of 10 columns (10 parallel treatment routes). The first and last matrix rows represent the crop headers where a robot can move freely in a horizontal direction without damaging the crop lines. Cells containing weeds are labelled in green.

This representation avoids the collision of robots or vehicles in the middle of the crop, i.e., within a column. However, collision may be possible in the headers, but it is assumed that headers are large enough for the robots to manoeuvre. Inside these regions, the problem of avoiding other elements is not critical and is easy to solve.

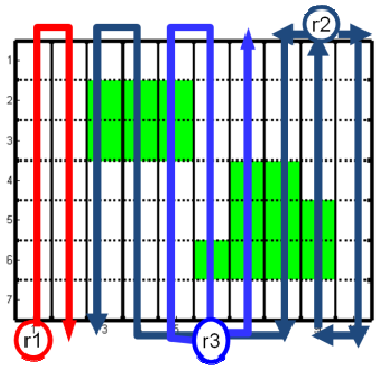

Fig. 1. Plan encodings in the individual solution ($r_1,r_1,r_2,r_2,r_3,r_3,r_3,r_2,r_2,r_2$) for a field with 10 treatment parallel routes. Green cells indicate the presence of weeds. Circles indicate the starting positions

2.2 The genetic operators

Regarding the reproduction stage (the next generation of solutions), the genetic operators used in the recombination are quite common. Two-point crossover has been selected for the recombination step, so two points on the individuals (strings of robot identifiers) are randomly chosen to be crossed; everything between the two points is swapped between the individuals, thereby generating two new solutions. Regarding the mutation, it has been taken into account that solutions (individuals) are codified as vectors of integers instead of vectors of bits. Hence, in the mutation, the probability of reaching each vector component value is *1/m* (where *m* is the number of robots) instead of *1/2*, as in the simple GA. The configuration parameters related to these operators will be explained in the Results section.

Finally, the selection of the individuals used in the recombination stage is performed with a roulette-wheel selection, also known as fitness proportionate selection.

2.3 The fitness function

The fitness function is a particular type of objective function that set the quality of a solution or individual, so it must compute how a particular individual is ranked against all of the other individuals in the population. In this case, the fitness for a fleet of *n* robots is defined by a function (2) where the following factors are taken into account:

- *Distance (moveCostRobot)*: The function attempts to find the shortest path that covers the entire field.
- *Turns (turnCostRobot)*: The path should reduce the number of turns needed because they are expensive for any vehicle.
- *Number of robot used (bootCostRobot)*: Solutions that involve fewer robots are preferred.
- *Herbicide application (sprayCostRobot)*: It is assumed that each robot has a tank with a specific capacity. When a robot sprays a cell, the quantity of herbicide in its tank decreases, so it is possible that a robot expends the entire amount of herbicide in the tank before finishing the treatment of a column. In this case, the robot would have to proceed to a header for refilling the tank before continuing with the weed treatment. Additionally, the column would remain partially treated. This factor is introduced for properly penalising individuals that represent incomplete solutions because not all weeds in a column are treated.

$$Cost = \sum_{i=1}^{n} bootCostRobot_i + \sum_{i=1}^{n} distanceRobot_i \cdot moveCostRobot_i + \\ + \sum_{i=1}^{n} turnsRobot_i \cdot turnCostRobot_i + \sum_{i=1}^{n} herbicideRobot_i \cdot sprayCostRobot_i \quad (2)$$

Expression (2) is normalised by estimating the minimum and the maximum values of the function. The minimum value can be assessed as the total coverage path that meets the following conditions: 1) it passes each cell in the field only once (minimum distance), 2) it makes the least number of turns, that is, two per column (one to enter the column and another to exit it), 3) it uses the minimum number of robots (i.e., one), and 4) it applies the minimum cost for spraying herbicide using the largest possible tank. In a similar way, the maximum value of the function can be approximated by the path that covers the whole crop field using the following conditions: 1) the maximum distances in the transitions between columns, 2) the maximum number of turns, 3) the maximum number of robots, and 4) the highest cost of the herbicide with the minimum tank possible. Finally, the normalised value of the fitness is calculated by (3).

$$fitness = \frac{(Cost - MinimumCost)}{(MaximumCost - MinimumCost)} \quad (3)$$

3. Results and Discussion

In all of the tests carried out, the values of the GA parameters were established as follows: crossover probability is equal to 0.8; mutation probability is equal to 0.2; and the number of individuals or solutions to be explored simultaneously (population size) is equal to 100. In addition, an elitism operator was used to facilitate convergence in such way that the best individual of a generation replaced the worst one of the next generation.

The crop fields used in the trials were approximately 4 ha in size, with a width twice their length. Therefore, a 202x400 matrix was required to represent the weed map. Consequently, vectors (individuals) that encoded the solutions were approximately 400 elements long. In every trial, it was assumed that approximately 30% of the field was covered by weeds, i.e., there were approximately 24,000 cells (matrix components) with a weed occurrence. For obtaining heterogeneous weed distributions similar to real situations, the central positions of the weed patches were randomly generated. Additionally, the starting position for the robots of the fleet was fixed at the middle of the upper header, i.e., in the component (1, 200) of the matrix.

3.1 Test 1

In the first experiment, a large fleet of 10 robots was considered. All of the mobile platforms had the same characteristics except for combustible consumption (Move), as shown in Table 1. This test was undertaken to verify the performance of the proposed method in a well-known case.

Table 1. Assumed costs for the ten robots in the fleet in Test 1

Robot / Cost	1	2	3	4	5	6	7	8	9	10
Boot (€)	200	200	200	200	200	200	200	200	200	200
Move (€/cell)	1	6	11	16	21	26	31	36	41	46
Turn (€)	5	5	5	5	5	5	5	5	5	5
Spray (€/cell)	1	1	1	1	1	1	1	1	1	1
Herbicide (€)	400	400	400	400	400	400	400	400	400	400

It has been assumed that the crop can be treated by only one robot, i.e., all tanks have enough capacity to treat approximately 4 ha (the worst case) or

approximately 80,000 cells. The herbicide cost has been calculated assuming a treatment cost per cell of 0.005 €. In this situation, the best solution should involve only a single vehicle (the cheapest), and our approach obtained this solution, as Fig. 2 shows.

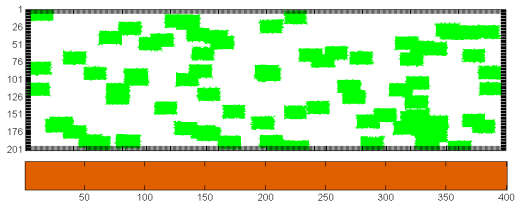

Fig 2. Distribution of weeds in the crop field used for Test 1. The best solution only involved a single robot that was the cheapest to operate

Similar trials have been carried out for nearly homogeneous robot fleets that differ in only one characteristic (different cost for turning or for herbicides). The method always obtains the same result: the robot with the lowest cost is the one selected to cover the whole field.

3.2 Test 2

The second test was designed to check the behaviour of the approach when the costs of booting and herbicides are reduced (see Table 2). In addition, the herbicide each robot carries is insufficient for treatment of the entire field. In fact, all of the robots in the fleet are needed to accomplish the treatment of a crop with a 30% infestation.

Table 2. Costs for each robot in the fleet in Test 2

Robot / Cost	1	2	3	4
Boot Cost (€)	20	20	20	20
Move Cost (€/cell)	1	1	1	1
Turn Cost (€)	5	5	5	5
Spray Cost (€/cell)	1	1	1	1
Herbicide (€)	8	8	8	8

In this case, the best solution is to boot all of the robots in the fleet. This is the solution obtained by the proposed method, as shown in Fig. 3. The four robots are booted and distributed to minimise the number of herbicide refills as well as the total distance travelled. In the solution obtained, robot 1 (in blue) covers 81

columns with 4,863 weed cells, robot 2 (in cyan) covers 107 columns with 5,302 weed cells, robot 3 (in yellow) covers 104 columns with 6,821 weed cells, and finally, robot 4 (in brown) covers 108 column with 7,014 weed cells.

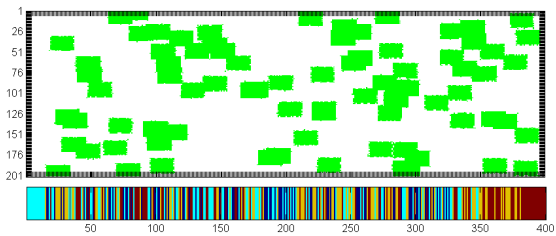

Fig. 3. Weed distribution in the crop used in Test 2. In this case, four robots in the fleet should be booted to minimise herbicide refills

3.3 Test 3

Another well known and interesting situation is when robots have inverse costs for moving and spraying. In this case, the best plan is to use vehicles with a low move cost and a high spray cost to perform the treatment of columns with fewer weeds and to use robots with a low spray cost and a high move cost to perform the treatment of more infested columns. Test 3 has been designed to verify that the proposed method is able to find this kind of solution. The assumed costs in this case are displayed in Table 3.

Table 3. Costs for each robot of the fleet in Test 3

Robot / Cost	1	2	3	4
Boot (€)	200	200	200	200
Move (€/cell)	1	5	10	15
Turn (€)	5	5	5	5
Spray (€/cell)	50	34	17	1
Herbicide (€)	40	40	40	40

Fig. 4 shows the best solution obtained by the proposal. The plan involves just 3 robots. Robot 1 (in blue), with the lowest cost to move and the highest cost to spray, is devoted to covering columns free or almost free of weeds, whereas robot 4 (in brown), with the lowest cost to spray but the highest cost to move, treats the columns with a very high weed infestation. Finally, robot 2 (in cyan) is in charge of the columns with a medium weed infestation because it has a medium cost both to move and to spray.

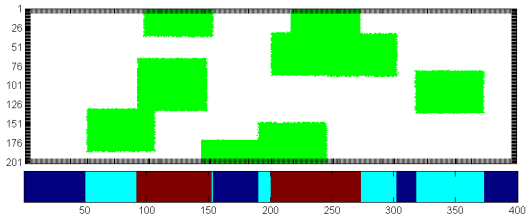

Fig. 4. Distribution of weeds in the crop used in the Test 4. Robot 1 (in blue), robot 2 (in cyan) and robot 4 (in brown) cover columns with a low, medium and high number of weed cells, respectively

Finally, a set of randomly generated trials was tested to measure the mean fitness obtained by the proposed approach. In all cases, the initial fleet comprised five robots. The level of infestation ranged from 10% to 30%, and the number of patches ranged from 1 to 15. Table 5 summarises the most important data from the experiments that were carried out. The best solution of each trial always involved two robots, and the mean fitness was approximately 0.06.

Table 5. Summary of the most important data from the experiments carried out. The trials have been randomly generated

Infestation level (%)	Number of patches	Size of lowest patch (number of cells)	Size of highest patch (number of cells)	Number of robots involved in the solution	The best Fitness
26%	12	1136	10256	2	0.05627
11%	14	400	1240	2	0.05532
27%	3	4812	10065	2	0.05627
29%	14	1167	6572	2	0.05500
24%	10	880	4905	2	0.05554
25%	2	10000	10000	2	0.05610
13%	9	550	1394	2	0.05392
16%	7	1826	2634	2	0.1133
11%	15	369	1228	2	0.0563
26%	11	325	1002	2	0.05123

4. Conclusions

Path-planning in an agricultural context attempts to determine the best path for a vehicle. It is a very complex problem, and several factors have to be taken into account; consequently, it must be well structured to adequately assess the cost of the agricultural task. The problem becomes even more complex if more than one vehicle is involved, i.e., if there is a fleet of mobile platforms able to work alongside each other. This paper presents an approach, based on a genetic algorithm that was designed and developed to offer a way to obtain the best solution not only for a single vehicle but also for a fleet of several vehicles in a weed-control context. The approach takes into account a wide range of parameters for each vehicle, such as the herbicide storage capacity, the number of turns required to cover the entire field and the distance travelled, and determines the best path for performing the weed treatment with the least number of vehicles involved for each situation (output).

To further assess the performance of the proposed method, a varied set of experiments with heterogeneous conditions were tested. In the well known situations, the solutions reached were strong enough to be considered optimal path plans, and in all cases, the results were as expected. Furthermore, for the generated randomly tests, the solution found by the proposed method had a fitness value of approximately 0.06, which is very close to the optimal solution involving only one robot with cost 0 (the minimum of the fitness function).

In summary, a reasonable approach to a complex problem has been designed and implemented. The results presented are part of the first simplified approach but do not influence the effectiveness of the proposed method.

Finally, in future studies, it will be interesting to include time as an additional factor to be considered in the cost computation. A solution that reduces the treatment time also decreases supervision time (the operator cost) and could increase the availability of the fleet for another task, which would be very interesting if a specialised company were providing the weed treatment to the farmer as a service.

Another question to be tackled in future works will be the irregularity of the fields. In this case, the same strategy can be used, but columns with variable lengths, rather than fixed lengths, must be considered. This new approach must be able to correctly deal with the transitions between columns.

Acknowledgement

The research leading to these results has received funding from the European Union's Seventh Framework Programme [FP7/2007-2013] under Grant Agreement nº 245986 (RHEA project).

References

Bochtis, D.D. and S.G. Vougioukas (2008). Minimising the Non-working Distance Travelled by Machines Operating in a Headland Field Pattern. *Biosystems Engineering*, 101(1), 1-12.

Choset, H. and P. Pignon (1997). Coverage Path Planning: The Boustrophedon Decomposition. *In Proceedings of the FSR'97: International Conference on Field and Service Robotics*, edited by Alexander Zelinsky.

Goldberg, D.E. (1989). Genetic *Algorithms in Search, Optimization and Machine Learning*, Kluwer Academic Publishers, Boston, MA

Jin, J. and L. Tang (2010). Optimal Coverage Path Planning for Arable Farming on 2D Surfaces. *Transactions of the ASABE*, 53(1), 283-295.

Michalewicz, Z. (1999). *Genetic Algorithms + Data Structures = Evolution Programs*, Springer-Verlag.

Oksanen, T. and A. Visala (2007). Path Planning Algorithms for Agricultural Machines. *Agricultural Engineering International: the CIGR Ejournal. Manuscript ATOE*, 4.

Rawlins, G.J.E. (1991). *Foundations of Genetic Algorithms*. Morgan Kaufman Publishers.

Sørensen, C.G., T. Bak. and R.N. Jørgensen (2004). Mission Planner for Agricultural Robotics. *AgEng 2004*, 894-895. Leuven Technological Institute, Belgium.

Stoll, A. (2003). Automatic operation planning for GPS-guided machinery. *In: Precision Agriculture '03, Proceedings of the Fourth European Conference on Precision Agriculture* (edited by J.V. Stafford & A. Werner), 657-664. Berlin.

Taïx, M., P. Souères, H. Frayssinet and L. Cordesses (2006). Path Planning for Complete Coverage with Agricultural Machines Field and Service Robotics. *Springer Tracts in Advanced Robotics* (edited by S. Yuta, H. Asama, S. Thrun, E. Prassler, and T. Tsubouchi), 24, 549-558. Springer Berlin / Heidelberg.

Simulation of Communication within the RHEA Robotic Fleet

Mariona Roca and Slobodanca Tomic

FTW Telecommunications Research Center Vienna

Donau-City Straße 1/3, A-1220 Vienna, Austria

(e-mail: ros@ftw.at, tomic@ftw.at)

Abstract: Webots (Webots 2011a; Webots 2011b) is a commercial mobile robot simulation software package, widely used by research groups and universities. It allows the users to simulate the behaviour of the robots in detail. However, it has significant shortcomings in the communication modelling as it provides a simple model of connectivity only based on the distance between the devices. The Network Simulator (NS2) (NS 2011) is on the other hand, an open source network simulator that offers simulation models for a wide range of networks and routing protocols in a structured way.

This paper presents an approach to integrate more realistic model of communication in the Webots platform by introducing the modelling concepts already evaluated with implementations for NS2. As a result, we add new functionalities to the simulator that help the user to understand the impact of communication on the robotic mission..

1. Introduction

1.1. Simulation of the robotic fleet in RHEA

RHEA (Robot Fleets for Highly Efficient Agriculture and Forestry Management) is an EU project dedicated to introducing autonomous robots in the agriculture management so that chemical product utilization, energy and time may be minimized, while the quality of products and safety is maximized.

The robots of the RHEA robotic fleet operate according to a predefined mission description which is created using the information about the field and information about the agricultural tasks and capabilities of the robots. The mission is a product of the mission planning software running on the base station being the main

command centre for the robots. The process of creating the mission also includes the simulation of the mission. The RHEA integrated simulator offers for the mission planner a graphical interface shows the movements of the robots in the field and the tasks that they perform. After the mission is designed the base station distributes the mission specifics to all the robots via wireless interfaces. During the mission the robots actively exchange data with the base station informing the mission supervisor about the state of the mission and receiving the actual corrections to the mission.

Accordingly, it is important to maintain communication of sufficient quality within the fleet during the whole mission, or alternatively, taking into account that wireless interfaces implemented on the robots have some constraints in terms of bandwidth and the coverage, it is important to design a mission in such a way as to assure required quality of communications within the fleet and among the robots and the base station.

This work aims at evaluating the possibility to use more realistic communication model of the wireless interfaces when simulating the RHEA mission, to understand the possible gains of this approach in the mission design, and to test how long such simulations could take.

1.2. Webots overview

Webots is a software package used to model, program and simulate mobile robots. This tool modells a 3D virtual world with physical properties, and allows users to add to it multiple models of simple passive/active mobile robots with a wide range of different properties and characteristics chosen by the user, such as different locomotion schemes or sensor and actuator devices. The user can program each robot individually and once simulated and checked port the software to commercially available physical robotic platforms.

This software tool has been used by a great number of universities and research centres worldwide. However, in the field of communications, some limitations exist as the communication components – the emitter and the receiver device, model only a physical layer communication, omitting more rigurous implementation of the upper layers standards.

This work is focused on modelling the upper communication layers needed to simulate IEEE 802.11a wireless local area network (WLAN) communication standard in the Webots tool, and may be a basis to implement other standards, e.g. ZigBee, in the future.

1.3. Time management in Webots

Webots is a time based simulation tool, while NS2 is an event based simulator. When the Webots simulator runs, each of the modelled robots is launched as a different process. In a synchronous mode all robots share the same virtual time, and so, can interact among themselves: each robot process runs separetelly, but theysynchronize when the function *wb_robot_get_time(TIME_STEP)* is called.

This function makes also the simulator compute the values of all parameters of the virtual world and all the devices and sensors of all the robots after the *TIME_STEP* milliseconds .

So in short, this function makes the virtual time of the simulation move forward one step of time. This concept determines the way in which new functionalities can be added.

1.4. Content and scope

The work presented in this paper is focused on the implementation of the IEEE 802.11a communication standard for the Webots mobile robot simulator tool, to make it possible to test realistic wireless communication between the robots in the simulations. We use the conceptula model already implemented by researchers of the university of the Institute of Telematics of the University of Karlsruhe and the DaimlerChrysler Research Engineering and Design North America Inc. (Chen et al. 2007).

The NS2 approch towards modelling communication system is well structured allowing easy addition of new features. Applying a simmilar approach in Webots we developed a structure in which other protocols can be easily implemented reusing a specific scheduler, transmission units and layer structure created in this work.

2. IEEE 802.11a Model Overview

The IEEE 802.11a wireless standard defines the specifications for the physical layer (PHY) and the Media access control (MAC) layer. The model of the physical layer offers specific functions including keeping track of received RF signals via the power monitor module, and managing the Physical layer operation via the Physical Layer state manager module (Fig. 1). The PHY functionality model assures that the probability of the reception of the packets is related to the transmission power of the packets. The model of the channel introduces the power loss due to the transmission over the air.

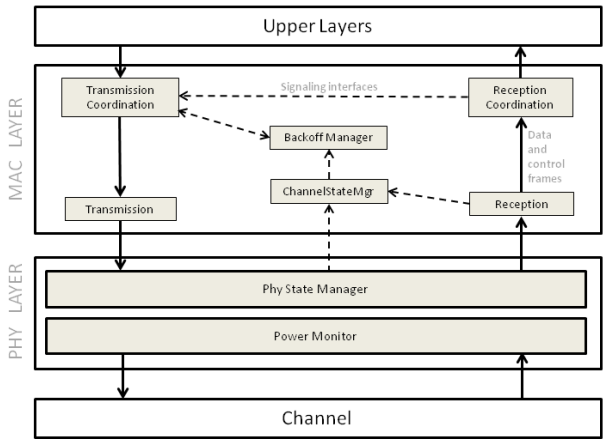

Fig. 2. IEEE 802.11 simulation architecture

The MAC layer is modelled with six modules (Fig. 1), responsible for implementing a Carrier sense multiple access with collision avoidance (CSMA/CA) mechanism for avoiding collisions between packets. As illustrated in Fig. 2, when one node wants to send a packet to another node the Transmission Coordination Module first checks its length to decide whether a Request To Send packet (RTS) is needed or not. In case it is needed, it is generated and processed by the MAC and PHY layer modules to simulate its sending over the air.

Each node that receives the RTS packet examines the address field in the Reception Coordination Module to check if it is the destination of the sent packet. If it is, it will respond with CTS packet after a Short Interframe Space (SIFS) time, if it is not sending or receiving yet. If it is not a destination node specified in the packet, the received packet will be discarded and the Network Allocator Vector will be initialized in the Channel State Manager module and so, the node will not send packets until the packet is transmitted.

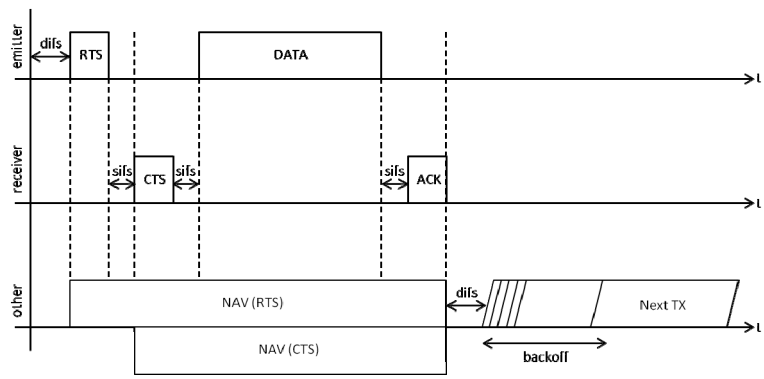

Fig. 3. CSMA/CA mechanism in the MAC layer

When the emitter node receives a CTS packet, it answers with the Data frame. And SIFS time after receiving this Data frame, the receiver will send an ACK packet with which the successful transmission is acknowledged.

In the case that during the time while the media is occupied a node needs to send packets, the node waits DCF Interframe Space time (DIFS) after the end of the previous transmission and then, the Backoff counter (in the Backoff Manager Module) starts running; if meanwhile any other node starts transmitting this counter stops. When it finishes, the packet will be transmitted by using the same procedure explained before.

In our simulation model the frames are generated in the application layer according to a data generation rate, duration and size specified by the user before the simulation starts. This information and other parameters relative to the simulation can be modified through the new added fields of the Emitter node. Default values may be provided. The application layer schedules the first packet of the first flow, and the first packet of the other flows are stored in a Queue List from where the MAC layer will pick the packets up when possible.

When a packet is received through the Webots emitter/receiver devices, it is sent to the scheduler and when it is time to, it is attended by the physical layer according to the 802.11 protocol.

3. Communication Model

3.1. Class and layer structure

As shown in Fig. 3, new implemented layers are the PHY and MAC layers corresponding to the structure of the wireless IEEE 802.11a standard and the concepts of (Chen et al. 2007) and a simple application layer. A pre-reception layer is added to simulate the Wireless Channel.

A Queue List is implemented as an interface for the MAC layer, so just one packet is processed at any time while others are in the queue. The mecanism of picking new packets up from this Queue List is implemented in the MAC layer.

In the MAC layer configuration several parameters can be specified by the user such as Carrier Sense Thresholds, retry number of packets, contention window size, etc. The standard values provided in NS2 according to the model (Chen et al. 2007) are used as default values in our work.

In the Application layer, several information about the transmission is used (starting, ending, transmission data rates and destination of each flow). This information is set by the user according to the desired simulated application, and will be introduced directly through the Webots interface in the Emitter node before the simulation starts.

The layers in our implementation are centrally managed by the Mobilenode object which inherits from a scheduler class that manages how the time evolves. In this approach after a packet is processed by one layer it is put into the scheduler queue. The scheduler takes the packet from the queue according to the time predefined by the last layer which processed the packet and forwards it to the next layer. This way of operation is essential for the implementation of protocols at different layers as the operation of each layer protocol is modelled as a state-event machine. In this way the delay that different layers introduce can also be modelled in the simulation to make it more realistic.

When the packet is finally attended by the PHY layer it is sent to the other robot by using the Webots Emitter/receiver devices, and received by the receiver robot in the Pre-reception layer, that simulates the channel delay. This component sends the packet to the scheduler, so it is received by the PHY layer at the appropriate time.

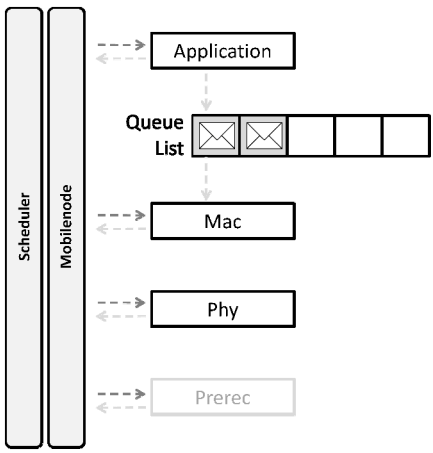

Fig. 4. Implemented Layer Structure

3.2. Basic transmission unit

R_pack is the basic transmission unit. It simulates the packet that travels through the layers of the sending nodes, over the air, and along the layers of the receiving node. In our model not only data packets created by the application layer, but also control packets (like RTS, CTS or ACK) are created in the MAC layer as R_pack instances. In addition, the execution of MAC and PHY state-event machines requires the implementation of timers. The timers are created to simulate the duration of sume actions and also implemented as R_pack objects even though they are not strictly packets.

All the information relative to the communication is included into a R_pack object. For example, a simple timer identifier flag lets the mobilenode distinguish between packets and timers; other information in the packet helps the mobilenode to decide which layer must attend each packet at any time. The size of payload and header, identifiers, attending time, delay, direction, the different header structs, scheduler parameters, transmission and reception stamps with power, position and antenna information are some of the information contained in the R_pack object.

Some of this information will be used while the simulation runs and some other will just be logged in a file when the simulation finishes, so the user will be able to analyse the results.

3.3. Scheduler

In our model we use the event-based operation and the concept of the scheduler similar to NS2. Our scheduler manages all the packets and timers in a linked list of objects. Figure 4 shows its linked-list structure in which the R_pack objects are sorted depending on the time at which they must be attended, from the earliest to the latest. The use of this kind of scheduler requires scanning all the list to find the apropiate entry when inserting and deleting packets. On the other hand, choosing next event for execution requires just trimming the first entry off the head of the list. So while the insertion of new objects is not so efficient, processing of events is very efficient.

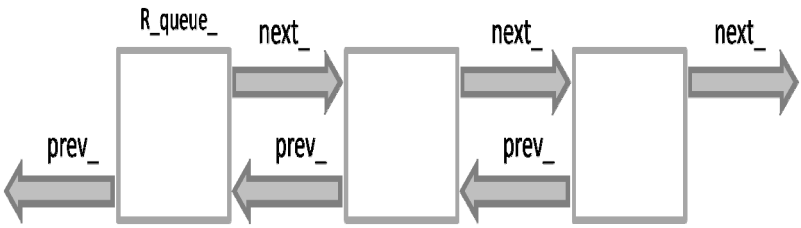

Fig. 5. Linked List Scheduler

3.4. Algorithm in the controller of the robot

The controller is the program that coordinates the behaviour of each robot and makes it interacts with the virtual world in the Webots' environment. We implemented an algorithm by which a controller picks up and attends the packets of the scheduler. In the Fig. 5, a flow chart of this algorithm is presented.

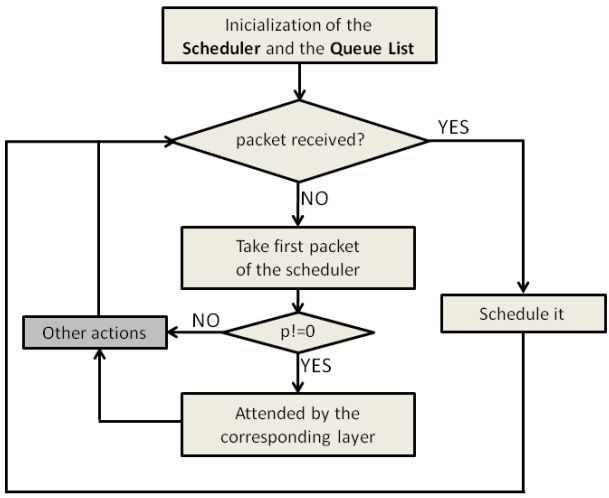

Fig. 6. Algorithm in the controller

First of all, the user must give the simulation specifications through the Webots interface. Appliction layer information about the different flows of data must be specified before the simulation starts. At this point, the scheduler is inicialized with the first packet of the first flow. The first packet of further flows will be stored at the QueueList. The scheduler will be also inicializated with the first Webots event. A webots event is a packet that when attended, calls the function *wb_robot_step(TIME_STEP)* (Section 1.3) and makes the simulation move forward one step. It also sends to the scheduler a new Webots event. In this way each event triggers the following one.

When dealing with data flows, we must have just one packet being processed within the MAC layer at any time. So when the first packet of the first flow placed in the main scheduler list is attended by the mobilenode, it will create the second packet of the flow. This packet will be send to the QueueList instead of to the main scheduler. According to the IEEE 802.11 protocol, when the MAC layer is ready with the first packet, it will check for new packets in the QueueList to be attended by calling the checkQueue() function. If there is a packet available, this will be sent to the main scheduler and the mobilenode will pick it up according to the predefined time. Avoiding the creation of all the packets of an entire flow also reduces the risk of running out of memory before starting the simulation.

After this step, the controller enters into an infinite cycle. It checks if new packets have been received (as the emitter and receiver devices have finite buffers we must give priority to these packets in order not to loose packets for buffer overloading). In case a new packet is received, it will be inmediatelly atended and sent to the pre-receive layer, who schedules the packet, so the PHY layer will be

able to receive it at the apropiate moment. In case there is no new packets, the mobilenode picks up the first packet from the scheduler and attends it. Then, after checking all the fields, the mobilenode passes the packet to the corresponding layer, which after processing the packet sends it again to the scheduler, if necessary.

If the attended packet is a Webots event, the process will be blocked at the webots call wb_robot_step(TIME_STEP) until all the other processes arrive at this function. This way, the Webots software keeps a synchronized tempo within the different robots in the virtual world.

When the packet picked up from the scheduler is already attended, it is time for other actions to be executed such as actions relative to the movement of the robots. After that, the algorithm goes back again to the point of checking if a packet is received.

4. An Illustration of a Concrete Simulation

To make the working procedure clear we will consider the situation of having four robots moving along the rows. Webots allows us to implement paths as well as to get the position of each robot at any time.

As shown in Table 1, after 2.50 seconds from the simulation start, a robot R1 will send a broadcast flow of packets at a rate of 512Kbps during 0.40 seconds (until virtual time is 2.90). At the end of this flow, an other flow of 128Kbps will start from robot R1 to robot R3 until virtual time is 2.95.

Table 2 Flow information

	Start	End	TX rate	Src	Dst
Flow 1	2.50	2.90	512Kbps	1	Broadcast
Flow 2	2.90	2.95	128Kbps	1	3
Flow 3	3.01	6	512Kbps	2	3

Until virtual time is 3.01 no packets will be created at the application layer, and then, a new flow will start again of 512Kbps from robot 2 to robot number 3 until time is 6 seconds.

This three situations are represented in Fig. 6.

Thanks to the Webots simulator tool, it is possible to get the position of the robots at any time. So, any propagation model can be implemented and added to the simulation. At the moment, only free space propagation model is implemented.

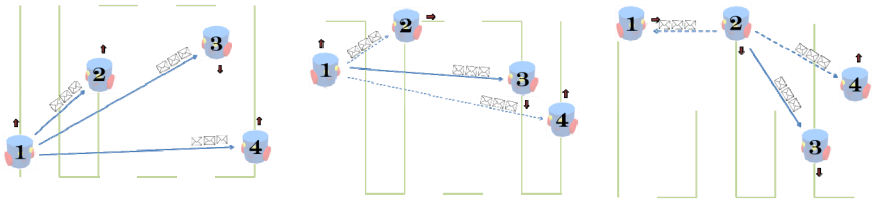

Flow 1 Flow 2 Flow 3

Fig. 7. Considered Scenario

4.1 Webots configuration

The Webots world configuration is not unique. In this case, simulations have been done by creating, in one hand, four mobile robots with a DifferentialWheels locomotion scheeme whose main function is just to recreate the movement of the robots through the rows.

In the other hand, we created four other static Supervisor robots (one per each DifferentialWheels), that will just communicate within themselves by using the new functionalities added to the Webots simulator. These Supervisor robots will keep track of the current position of its corresponding DifferentialWheels. This way, each real robot will be modelled by using two robots in the virtual world: the DifferentialWheels for the movement simulation, and the Supervisor for the communication simulation. Both will be linked by using the Supervisor functions.

4.2. Simulation steps

Following the algorithm for the controller, explained in the section 3.4 of this paper, the user must first of all introduce the information of the communication through the webots interface, as new fields have been added to the Emitter node, in the sceene tree of the simulator. Default values are provided for all the parameters of the simulation. So just information about the differents packet flows are essential for the simulation.

Once parameters are specified, the simulation can run normally. Once the simulation is finished, the user will be provided with a file with traces that will show the results of the simulation through the analysis of the events that have happened (send, receiv, drop, ...).

4.3. Postprocessing of results

During simulation a log file is created which can be used for postprocessing of results. This is a txt file with a set of traces. The obtainable trace format is shown in Fig. 7.

Event type	First time	Time	Node id	Node coord	Layer	Reasn	Src node	Dst node	Pkt type	Hdr size	Pld Size	Flow ini	Uid

Fig. 8. Trace format

The parameters which are logged during the simulation include:

- EVENT TYPE: g (generation), s (send), r (receive), d (drop).
- FIRST TIME [sec]: time packet was first created.
- TIME [sec]: time the event happened.
- NODE ID: Node unique identifier.
- NOODE COORD[m]: Coordinates x,y, z of the node.
- LAYER: APP, MAC, PHY.
- REASON FOR DROPPING:
    - “END”: DROP_END_OF_SIMULATION.
    - “COL”: DROP_MAC_COLLISION.
    - “DUP”: DROP_MAC_DUPLICATE.
    - “ERR”: DROP_MAC_PACKET_ERROR.
    - “RET”: DROP_MAC_RETRY_COUNT_EXCEEDED.
    - “STA”: DROP_MAC_INVALID_STATE.
    - “BSY”: DROP_MAC_BUSY.
    - “NRTE”: DROP_RTR_NO_ROUTE.
    - “TTL”: DROP_RTR_TTL.
    - “TOUT”: DROP_RTR_QTIMEOUT.
- SOURCE NODE: Source node.
- DESTINATION NODE: Destination node. In case the packet has been broadcasted, a B is specified in this field.
- PACKET TYPE: RTS, CTS, DAT, ACK.
- HEADER SIZE [bits].
- PAYLOAD SIZE [bits].
- FLOW INI [sec]: the time of the first packet of the flow at which the registered packet belongs to.
- UID: scheduled paquet unique identifier.

So an example of an obtained trace when a packet of the second flow reaches the application layer in the destination robot, in the proposed escenario, would be the following:

[r | 2.910063 | 2.942542 | 3 | (+0.948531) - (+0.000000) - (-0.449213) | APP | ---- | 2 | B | DAT | 128 | 33 | 1 | 2.900000 | 4]

This trace corresponds to the packet number 4 out of five packets created in this flow. The flow corresponding to this event is the one that started at time 2.90 seconds after the beginning of the simulation. By examining all the fields, we can see that this packet was first created at the time 2.910063 and received by the Application layer of the robot 3 at time 2.942543. As it was not dropped, no reason is specified.

The position of the node at the moment of the event is (+0.948531) - (+0.000000) - (-0.449213), and the size of the header and the payload is 128 and 33 bytes respectively.

5. Conclusions

This paper presents a tool that allows users to add some realistic models of IEEE 802.11a based communication to a mobile robot simulation by using the cyberbotics' Webots software, as a realistic alternative to the simpified model currently used in this simulator. These new added functionalities are based on a modular scheeme already used in the NS2 simulator and proposed in (Chen et al. 2007). Our future work includes defining several RHEA specific simulation use cases and testing with the presented simulator extension to quantify the performance of this approach.

Acknowledgement

The research leading to these results has received funding from the European Union's Seventh Framework Programme [FP7/2007-2013] under Grant Agreement nº 245986.

References

Webots, 2011a, "User guide", http://www.cyberbotics.com/

Webots, 2011b, "Reference manual", http://www.cyberbotics.com/

NS, 2011, "Network Simulator ns-2", http://www.isi.edu/nsnam/ns

Chen, Q., Schmidt-Eisenlohr, F., Jiang, D., Torrent-Moreno, M., Delgrossi, L. and Hartenstein, H., 2007, "Overhaul of IEEE 802.11 Modeling and Simulation in NS-2"

Safety functional requirements for "Robot Fleets for Highly effective Agriculture and Forestry Management"

Pilar Barreiro*, Miguel Garrido*, Adolfo Moya*; Benoit Debilde, Patrick Balmer***, Jacob Carballido****, Constantino Valero*, Nicola Tomatis*** and Bart Missotten****

** LPF_TAGRALIA. Polytechnic University of Madrid (UPM), Avda. Complutense s/n, 28040 Madrid, Spain*

*** Case New Holland Belgium N.V. (CNH). Zedelgem, Belgium*

**** Bluebotics S.A. (BL.) Lausanne, Switzerland*

***** Soluciones Agrícolas de Precisión S.L. (SAP). Cordoba, Spain*

(e-mail: pilar.barreiro@upm.es).

Abstract: This paper summarizes the steps to be followed in order to achieve a safety verified design of RHEA robots units. It provides a detailed description of current international standards as well as scientific literature related to safety analysis and fault detection and isolation.

A large committee of partners has been involved in this paper, which may be considered as a technical committee for the revision of the progress of safety development throughout the progress of RHEA project.

Partners related to agricultural machinery, automation, and application development declare the interest of providing a stable framework for bringing the safety verification level required to be able to commercial unmanned vehicles such as those described in the RHEA fleet.

1. Introduction

This paper aims at establishing the safety specifications of RHEA robots based on current state of the art of safety standards and scientific knowledge.

The amount of authors reflects the wish of integrating a wide scope of points of views on the subject. These authors are committed to set-up a dedicated commission that will help the rest of partners on defining the safety functional requirements for each of those specialized units.

The paper is structured in a number of paragraphs dealing with the typification of actual hazards levels of operated machinery ; a review of the safety standard; the concept of life cycle assessment in the safety of agricultural machines; the assessment of risk; the concept of safety-related control systems for machines; hardware and software specifications; the recommendations towards the elimination of systematic faults and the definition of safety functions; available procedures for fault detection, isolation and prognosis; a review of the safety verification level when designing an agricultural machine; the concept of building blocks for intelligent mobile equipment and finally the steps to be accomplished for RHEA units.

2. Hazard levels in agricultural work

Agricultural machinery is involved in the majority of occupational accidents on farms, as proven by recent extensive scientific studies from the U.S. and Northern Europe (Bunn et al., 2008; Gerberich et al., 1998; Colémont and Van den Broucke, 2008; Thelin, 1998).

Although in absolute terms tractors are widely represented in these occurrences, large self-propelled harvesters are twice as hazardous as tractors. Most accidents occur in elevation or load transport work (21%), attachment and adjustment (20%), or when repairing (17%) machines. There are several variables that are associated to a high accident risk. Therefore, for example, working more than 40 hours a week multiplies this risk by three, as does the fact of the operator being married (risk multiplied by 2), or divorced (risk multiplied almost by 4).

Some factors that are associated to mortal accidents and which are not mutually exclusive are: 49% mechanical (seat belt not used, defective brakes or clutch), 52% type of tractor equipment (no rollover protection structure, use of rotary mowers or insufficient ballasting), or 55 % due to work location (slopes, muddy terrain). The risk of fatality is multiplied by 20 if the tractor rolls over. The lack of a rollover protection structure multiplies this risk by 11, while deficient maintenance multiplies it by almost 7, the same as for brake or clutch problems.

Some studies indicate that the user's perception of self-control is also a contributing factor in the risk of suffering an accident. It also appears that the number of accidents drops when the user has a positive and committed attitude towards the safety standards.

Generally speaking, reducing the presence of an operator without increasing risk would lead to an enormous decrease in accidents. Therefore, becoming autonomous may be more an advantage than a drawback in terms of safety. This argument was first held by Reid (2004a) and should be dearly considered when facing the analysis of safety in autonomous agricultural machinery.

3. Main safety standards for agricultural machinery

Making safe machines has become a top priority goal and in recent years, various standards have been published. It is important to review these standards. Figure 1 shows how the most relevant design and safety standards for general machinery are interlinked: ISO 12100 (safety of machinery, 2003), ISO 14121 (analysis and risk assessment, 2007), ISO 13849 (safety-related parts of control systems, 2003-2006), as well as for this specific field, ISO 25119: safe design for tractors and agricultural machinery(2009), although the general principles and safety requirements are set forth respectively in standards ISO 26322 (2010) and ISO 4254 (2008).

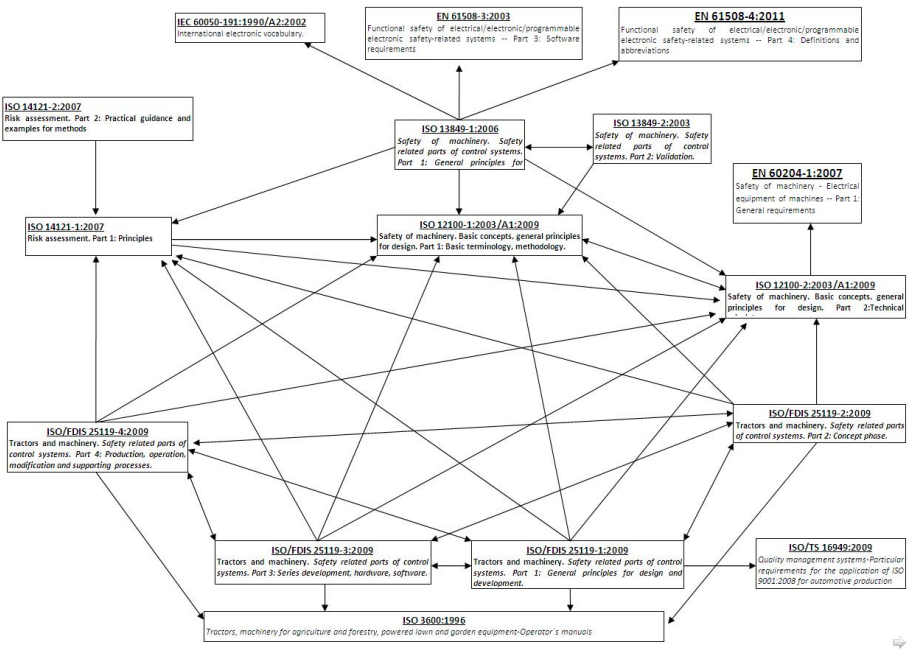

Fig.1. Interlinks between ISO standards related to the safety of machines.

This clearly shows the huge effort that has been made in the last five years towards enhancing safety conditions in the agricultural setting.

3.1 Life cycle analysis in the safety of agricultural machines

There are very close links between the various standards pertaining to safety. In general, the most recent ones tend to incorporate the content of the previous ones. For this reason, the first part of the design standard ISO 25119 offers a more global overview of the entire process in the form of a life cycle analysis, from conceptual development through to mass production or the alterations that are made after a machine enters the mass production stage (see Fig. 2).

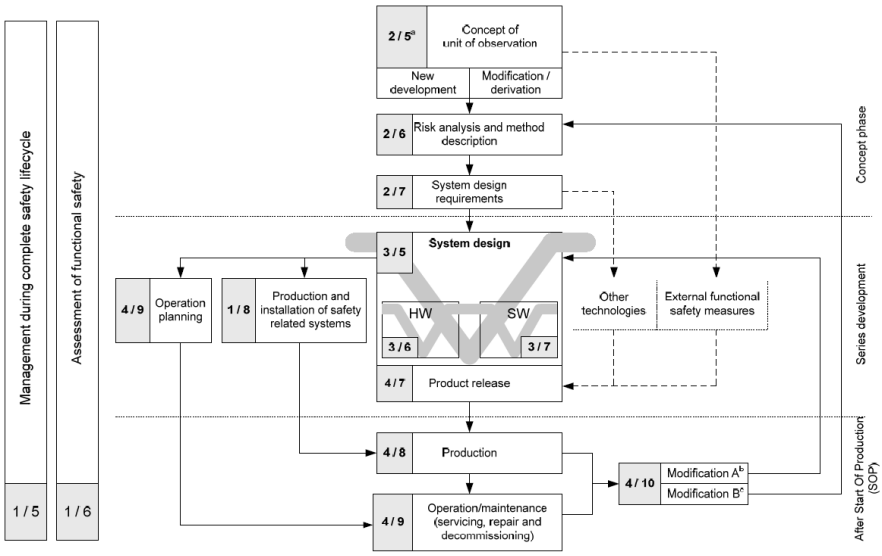

Fig.2. Life cycle analysis in the safety of agricultural machines. (Source: ISO 25119-1)

Figure 2 indicates that when mass production commences, special attention will be paid to the system design, both hardware and software aspects, using the V-model (Fig. 3). The numbers shaded in grey (a/b) respectively encode the part of the ISO 25119 standard and the chapter in which they are contained.

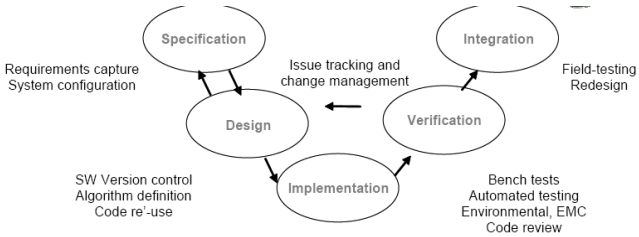

Fig. 3. V-model (Source: Lenz et al. 2007)

It is important to point out that wherever possible the new unit of observation (machine under study) should be defined as an alteration of some pre-existing system of the same or another manufacturing firm, so that it is possible to avail of the legacy of information available in terms of analysis and risk assessment, and the corrective measures associated thereto. It has also been proposed that insofar as possible, a parallel should be drawn between the hardware and software structure for assessment and pre-existing equipment, so that the required agricultural performance levels (AgPL) may be more easily allocatable.

3.2 Risk assessment

This section specifically refers to the ISO 14121 standard: Risk assessment. According to this standard, it is necessary to distinguish between analysis, which consists of determining the limits of the machine, hazard identification and quantitative risk estimation, and evaluation, which is the result of deciding on the need or otherwise to reduce risk by implementing design measures, incorporating protective elements or providing information to the person that may potentially be affected. Figure 4 sums up this process.

Defining the limits of the machine means considering the intended purpose and what kind of incorrect use may reasonably be foreseen, the operating modes (transport, work, maintenance), the level of training expected of users (operators, maintenance personnel, apprentices and members of the general public); as well as the space limitations to be taken into account for the breadth of movements (areas within scope) and the dimensional requirements for people.

In order to identify hazards, as sources of damage, i.e. physical injuries or harm to health, it is necessary to consider the operations and tasks that the machine performs, as well as those that are carried out by the people that interact with it, deciding which are hazardous situations and events, i.e. circumstances and events in which one or more people are exposed to one or more risks. The significance or severity of the damage should be defined: S0 (not significant or only requiring first-aid), S1 (slight to moderate with medical care and full recovery) , S2 (severe with lifelong side-effects but probable survival) and S3 (with side-effects in vital capacities, uncertain survival and/or severe disability); as should the likelihood of the damage occurring: E0 (improbable, maximum once in the machine's useful life, < 0.01%), (rare, annual maximum, 0.01%-0.1%), E2 (sometimes, less than on a monthly basis, 0.1-1%), E3 (frequent, more than once a month, 1-10%), and E4 (very frequent, in almost every operation, >10%) (see Fig. 5).

The ISO 14121-1 standard is thorough in defining types of hazards: mechanical (associated to kinetic or potential energy, and the shape and structure of the elements), electric, thermal, noise-related, vibration-related, radiation-related, caused by materials or chemical substances, hazards associated to a failure to comply with the principles of ergonomics, or the setting in which the machine is used (dust or fog, humidity, mud, snow, etc.). The standard also provides several examples of tasks in relation to the stage in the life cycle of the machine, as well as hazardous situations, which are understood to mean situations that may give rise to damage.

Risk is defined as the combination of the likelihood of damage occurring and its severity and, as indicated previously, the concept of risk analysis contemplates specifying the limits of the machine, hazard identification and risk estimation.

In evaluating risk, the possibility of avoiding or controlling the damage should also be taken into consideration: C0 (easy to control), C1 (simple to control, over 99% of people would know how to control it in over 99% of circumstances), C2 (mostly controllable, over 90% of people would know how to control it in over 90% of circumstances) and C3 (not avoidable by average operator or typical personnel in vicinity) (see Fig. 5).

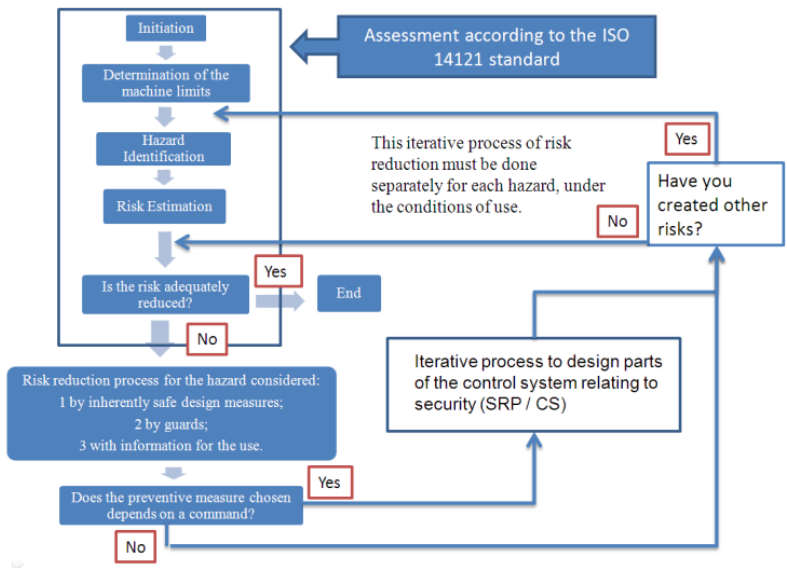

Fig.4. Flow diagram linked to assessing risk in agricultural machines. (Elaborated from ISO13849-1)

The ISO 25119-2 standard defines beyond which combination of severity and likelihood of damage, and control level it is indispensable to include a control system in addition to the inclusion of protection devices or merely informative aspects that are generally covered under the term QM, i.e. quality assurance measures pursuant to the ISO 9001:2000 standard (see Fig. 5).

3.3 Safety-related control systems for machines

For cases in which the quality assurance measures do not suffice, it is indispensable to include risk reduction systems, the features of which should match the performance level. These systems are generally called SRP/CS, i.e. safety-related parts of the control system. The ISO 25119-2 standard provides five performance levels for agricultural equipment (AgPL) identified with the letters "a" to "e" for increasing levels of risk.

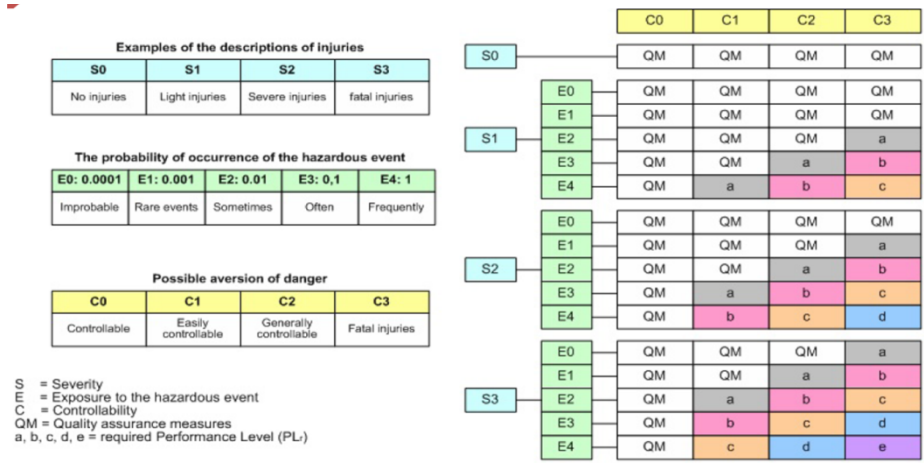

Fig.5. Performance levels for agricultural equipment (AgPL) identified with the letters "a" to "e" for increasing levels of risk. (Source: Benneweis, 2006)

Attaining a particular AgPL depends on a number of factors, such as: the category associated to its hardware structure (B, 1, 2, 3 ó 4), the mean time to a dangerous fault (MTTFd), diagnostic coverage (DC) and common cause faults (CCF). The software readiness levels (SRL) are in turn dependent on the AgPL value that is required, the diagnostic coverage available: low (60 to 90%), medium (90 to 99%) or high (over 99%) and MMTfd: low (3 to 10 years), medium (10 to 30 years) or high (30 to 100 years). The ISO 25119-2 standard defines a simplified procedure for assessment, as shown in Fig. 6.

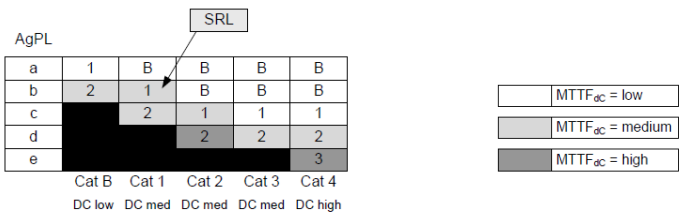

Fig.6. Performance levels and software readiness levels depending on hardware configuration (B, 1, 2, 3 and 4) and the diagnostic coverage level (fault detection capacity). (Source: ISO 25119-2)

3.4 Hardware configurations

According to the ISO 13849-1 and ISO 25119-2 standards, there are five typical hardware configurations (B, 1, 2, 3 and 4) in SRP/CS, which may be displayed in 3 different diagrams (see Fig. 7). The first layout: inputs (I), logical processing (L), outputs (O) corresponds to the typical structures B and 1, with the difference that in the former, the diagnostic coverage is null and the MTTFd for each channel cannot be measured, whereas configuration 1 uses components of proven

efficiency in safety-related operations and may require redundant inputs depending on the diagnostic coverage required (low or medium). The second layout, which corresponds to the type 2 architecture, includes as well as the above elements, other testing equipment (TE, typically man-machine interfaces) and the outputs of the testing equipment (OTE). Finally, architectures 3 and 4 are the third layout, with the difference that for the latter, the diagnostic coverage in monitoring (m) is higher than in architecture 3, and that redundant outputs may be necessary in order to maintain the safety functions.

Another relevant aspect of the standard is that it also defines how to calculate the performance level when there are several SRP/CS attached in series. Generally speaking, when there are more than 2 or 3 SRP/CS in series with the same minimum AgPL level, the global value drops by a level, e.g. from level AgPL d to AgPL c.

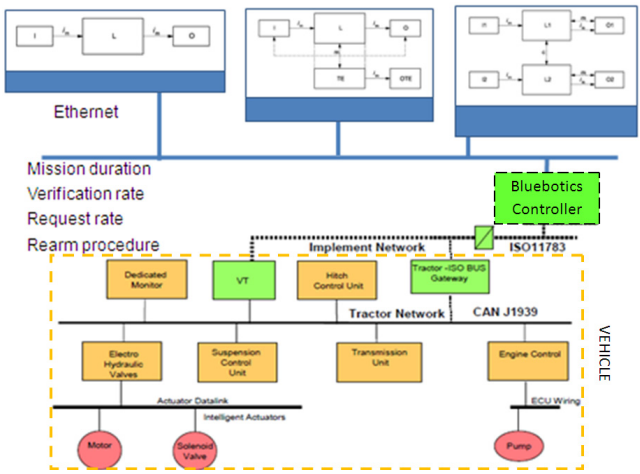

Fig.7. Predefined hardware configurations in the ISO 13849 and ISO 25119 standards. (Elaborated from Lenz et al. 2007)

Figure 7 shows a first approach towards the integration of several SRP/CS of varying hardware configurations that communicate with Bluebotics controller via Ethernet, while the latter interact with internal bus of the tractor via ISO11783 (ISOBUS). It is important to state that any hardware configuration should follow ASABE recommendations regarding environmental conditions (ASABE, 2008).

3.5 Software Specifications

In this sense, Hoffman (2006) provides probably the most complete review of actual complexity of software in tractors, given the great number of factors that affect the integrity of software in machines equipped with electronic systems, it is not possible to define an algorithm that will ascertain which techniques and

measures are best suited to each application. On the other hand, when selecting methods and measures for defining software, it is important to bear in mind that as well as the manual code programming, model-based developments may employ automatic code generation tools. (Lutz, 1992)

The ISO 25119-3 standard (2009) devotes forty pages to the chapter on software in relation to the safety of agricultural machines and indicates that it is necessary to define the method to be employed in defining the safety requirements for the software: natural language, semi-formal methods (based on diagrams and figures, or animation-based analyses), formal methods (based on mathematical procedures), or methods that employ computer-assisted tools (in the form of databases that can be automatically inspected and examined to assess consistency and completeness).

In general, the standard provides that the software architecture should not be commenced until a sufficient degree of maturity has been attained in defining the safety requirements, employing top-down methods to evaluate the combination of events that may give rise to hazardous situations, and bottom-up methods to decide which components in the system would be damaged.

In developing the software, the first step will be to define the modules that will be related to safety and then define the rest of the functions. The programming language should be such as to enable easy code verification, validation and maintenance. In this regard, it is desirable to use automatic code translation tools, pre-existing libraries that have been extensively verified, code debugging systems and software version control tools. It is not clear if object-oriented languages are preferable to procedure-based languages.

The use of defensive programming methods is recommended, capable of producing programmes that can detect control flows or erroneous data, so that the system may react in a predetermined and acceptable manner. Some defensive programming techniques include: changing that variables are in range and analysing the credibility of their values, a priori checks on parameters and procedures before running them, and separating parameters according to whether they are read-only or read-write.

In general, the following criteria should be followed: the programme should be divided into small software modules, the modules should be composed using sequences and iterations, a limited number of paths should be maintained in the software, complex ramifications and unconditional leaps should be avoided, loops should be linked to input parameter values, and complex calculations should be avoided when making decisions on forks and loops. Lastly, they recommend that dynamic variables be limited so that the memory requirements and a priori directions are known a priori. The use of interruptions should also be limited, especially when using critical software, so that the maximum time for inhibiting safety functions is controlled at all times. The use of check-lists is recommended in

order that the set of relevant issues are verified in each stage of the life cycle of the software.

3.6 Eliminating systematic faults and safety functions

There are a number of typical faults for which the ISO 25 119-2 (2009) standard provides certain recommendations: preventing the loss of electricity supply in electronic boxes, selecting manufacturing materials that are suitable for the setting in which they are to be used, correct component installation, compatibility, modularity of design, restricted use of common elements such as memories or electronic cards, separating safety-related and non-safety-related components in the control system, and checking design by employing assisted design systems for simulation and simulation programmes.

A number of typical safety functions are also defined by the ISO 25119-2 standard for consideration in design, i.e. 1) a lock to prevent switching on the system by accident, 2) the immediate halt function, 3) manual resetting, 4) automatic switching on and resetting after a fault, 5) response time (divided into detecting the fault, starting to take measures and managing to attain a safe operating mode), 6) safety-related parameters (position, speed, temperature, pressure), 7) external control functions (how to select external control, verify that switching the external control does not cause hazardous situations, and how to act in the event of loss of external control), 8) manual inhibition of safety functions (for example, for diagnostic purposes), and 9) the availability of alarms for the user.

3.7 Fault detection and diagnosis to improve safety

Once the safety functions have been defined, it is important to foresee available algorithms and procedures that are used in other fields of work such as spacecraft. In this sense NASA has show to be far ahead and the definitions provided are considered of major interest:

- Fault detection: addressing the occurrence of a miss function of any kind in a system, realizing that something is going wrong.
- Fault diagnosis: fault isolation, determining the cause of failure or what is particularly wrong in many cases as a source of common cause fault (CCF).
- Fault prognosis: detection the precursors of failure and predicting the remaining time before failure occurrence.

The procedures that can be used for any of the three tasks can be classified into model-based or data –driven (model-free) (Donca and Mihaila, 2010).

- Model-based fault diagnosis and prognosis: consisting either on qualitative or quantitative models that take advantage of fundamental knowledge of the problem.

- Data-driven fault diagnosis and prognosis: it is also referred as history-based knowledge. Methods available for Data-driven Fault Diagnosis and Prognosis combine: Data mining (also known as Knowledge Discovery in Databases KDD), Artificial Intelligence, Machine Learning and Statistics.

According to the nature of the information available we may define numerical and text data, and for the latter, further classification into structured (fit into narrow fields in databases) and unstructured text (nearer to natural language) is a relevant issue. In this context Text Mining refers to the tools that allow extracting knowledge from databases typical from customer (after-sales) services where unrestricted textual format for fault description is used (Harding et al., 2006; Hui and Jha, 2000).

There are several review papers and dedicated researches that make use of the three types of information for fault detection and diagnosis: Vibration signatures, CAN data and Warranty data.

For vibration signatures the following methods have been described and reviewed in the literature (2005 to 2010) (Schwabacher, 2005):

- Data-Driven Fault Detection: unsupervised anomalies detection algorithms (Orca, Grobot, DIAD), inversion induction monitoring System (data cluster into system modes), Neural Networks (NN) and envelope detection by means of hidden Markov models.
- Data-Driven Diagnosis: Feature extraction on data (Fast Fourier Transform in frequency domain, while signal energy and kurtosis in time domain), Support Vector Machines (SVM), wavelet transform and wavelet packet transform combined with SVM.
- Data-Driven Prognosis: NN, rule extractors, similarity based methods, autoregressive methods, fuzzy logic algorithms and Bayesian Belief NN.
- Model-based Diagnosis: hierarchical models with finite state machine.
- Model-based Prognosis: Kalman filters and stochastic differential equations.

For CAN data a very recent publication (Suwatthikula et al., 2011) proposes the use of Adaptive Neural Fuzzy Inference Systems (ANFIS) for the prediction of Network Health and fault diagnosis in CAN networks based on total differential resistance on the bus and the amount of error frames per second. It also enables to distinguish between internal (typically digital) and peripheral (mainly analogue) faults.

The characteristics of the ideal fault diagnosis system, as referred in 2010 by the only paper on FD in agricultural machinery (Craessaerts et al., 2010), include: 1)quick detection and isolation of faults, 2) robustness against noise and uncertainties, 3) novelty identification for unseen cases, 4) classification error

estimate, 5) adaptability to time varying processes, 6) low modelling and low computational requirements, and 7) multiple fault identification (several at a time).

The incorporation of fault detection and diagnosis tools for autonomous machinery is to play an important role for safety purposes.

3.8 Safety verification level when designing an agricultural machine

In accordance with the ISO 25119-1 standard, one very important aspect when designing an agricultural machine is deciding on the safety verification level that may require the participation of persons not linked to design, teams of staff other than designers, or even different departments or consultancy firms, for the agricultural performance (AgPL) levels, which go from "a" to "e" in ascending order (see Table 1).

Table 1. Degree of verification (Source: ISO 25119-1)

Degree of verification	AgPL = a	AgPL = b	AgPL = c	AgPL = d	AgPL = e
Review of hazard analysis and risk assessment	U2[a]	U2	U2	U3	U3
Review of safety plan Independent from author of the plan	–	–	U1	U2	U3
Review of safety requirements Independent from author and implementer of safety requirements	–	U1	U1	U1	U1
Review of V&V-plan					
- independent from plan author	–	-	U1	U2	U2
Review of the safety analysis (FMEA, FTA) Independent from author of the analysis Independent from developer of unit of observation	– –	 U1	 U1	U1 U2	U1 U3
Review of safety tests and trials Independent from planning and conducting the tests	–	–	U1	U1	U1
Review of safety documentation Independent from author of safety plan	–	–	U1	U2	U3
Safety audit Independent from those, who work in association with the processes required for functional safety	–	–	-	U2	U3
Assessment of the safety plan	–	–	-	U2	U3

[a] Independent review is required especially in situations assessed as C0 or S0

– No requirement for verification. The verification measures that will have to be carried out are governed in clause 6.4.2.

U1 Another person

U2 Another team (not the same direct supervisor)

U3 Another department or third party

(independent from the developing department, e.g.: independent management, independent resources, independent from release responsibilities, independent organization)

3.9 Building blocks for Intelligent Mobile Equipment (robots)

Some authors (Reid, 2004b) have defined unmanned vehicle not exactly in terms of safety requirements but as related to building blocks.

In this case the blocks are agents than can provide important complementary information to the safety function through the main controlled designed by Bluebotics.

The building blocks of intelligent mobile equipment proposed by Reid (2004b) are shown in Fig. 8. The elements are defined in terms of Machine Control (X-by-Wire and Navigation), Machine Awareness (Localization and Perception), and Intelligence (Mission Planning and Intelligent Systems). Hereafter, it is useful to further define the blocks:

X-by-Wire: These are basic control of the actuation surfaces of a machine that include the steering, brakes, throttle and other functions. It also relates to the basic machine health and the interaction of these controlled components.

Navigation: Elements of Navigation relate to how the various control systems lead to machine mobility. Navigation is concerned with issues of path tracking accuracy and how machine functions respond in a mission.

Localization: Localization is the awareness of the posture of the intelligent vehicle relating to position and orientation in the open environment.

Perception: Perception is the awareness of the features of the local surroundings that can include obstacles and other environmental features. Perception is a key element of vehicle safeguarding in the sense that obstacle features are detected with perception sensors.

Mission Planning: Mission Planning systems allow the determination of the tasks and behaviors of an intelligent machine system in the operating environment. All of these functions are connected by an intelligent control system that can arbitrate what needs to happen under dynamically changing situation. Path planning is one of the key tasks that are controlled in mission planning. Mission planning tools like simulation are a key part of advanced system development.

Intelligent Systems: The semi-autonomous or autonomous vehicle is an intelligent system. It has an architecture that is both modular and scalable to allow it to be deployed for application.

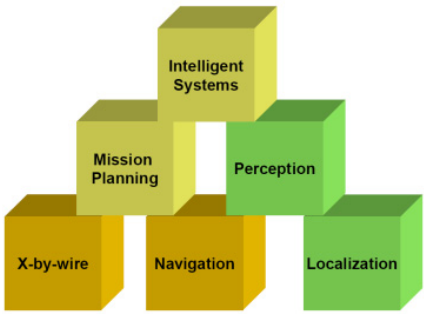

Fig.8. Building blocks for Intelligent Mobile Equipment (Source: Reid, 2004b)

4. Steps to be accomplished for "RHEA" robots

RHEA proposes the use of three robot fleets. The 3 ground mobile units will be based on small autonomous vehicles similar to New Holland tractor "Boomer 3050 CVT"– (4×4 wheel drive) powered by an engine (51 Hp) with a unit weight estimated in about 1.2 ton. The units will follow the rows at a speed of about 6km/h – with onboard equipment for navigation and application of treatments. The electronic equipment on-board the ground mobile units will be powered by a system based on solar panels and fuel cells.

Below are summarized the principal details of each ground mobile unit:

- **Sprayer Boom Vehicle in wheat:**

  This vehicle will be equipped with a spray boom (Fig.9) that will apply herbicide on wheat crops based on the information from the perception system on board the aerial units. The goal is to apply herbicide to at least 90% of the detected patches.

- **Physical weed control vehicle in maize:**

  This ground mobile unit will be equipped with end-effectors or tools, developed to destroy weeds in maize, which will be based on both thermal and mechanical devices (Fig.9). The goal is to destruct at least 90% of the detected weeds.

  The main idea is to equip the ground mobile unit with a 4.5 m hoe equipped with rigid or rotating tools for interrow cultivation and selective tools for in-row weed control. However, the best solution in this case could be the use of flaming, according to the high selectivity and the very low cost (in this respect, very simple, cheap, and easy to use and to adjust burners that are connected to very low LPG consumption will be developed).

- **Insecticide Application Vehicle in Olive:**

  The third vehicle will be equipped with a spray system to apply pesticide in olive trees (Fig.9). The goal is to apply the pesticide at least on 90% of the tree canopy.

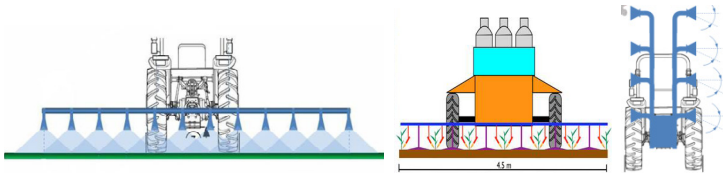

Fig.9. View of the different robot units (Sprayer boom, Physical control, and Insecticide unit).

According to the definitions and specifications provided in previous paragraphs, Fig. 10 provides a first approach toward the safety control loop of the vehicle. It is important to indicate that since around 10 safety functions have been identified and more than 20 sensors will most probably be providing information, and therefore a safety logic unit should be used for the safety loop.

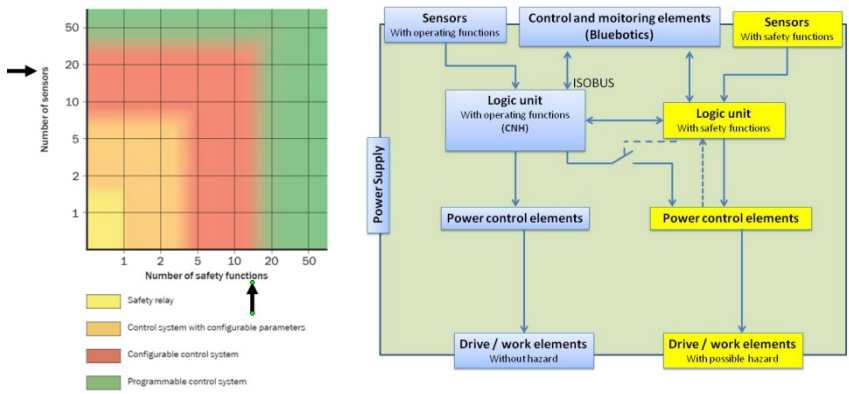

Fig. 10. Basic safety (Elaborated form: SICK Optic-Electronic, S.A.)

At this stage it is very important to clarify the tasks that should be considered in the particular case of RHEA for the risk assessment and therefore to define the performance level required for every SRP/CS.

Table 2 provides an example of tasks that take place during 3 diffrenets operating modes: labor, maintenance and transport, as defined by one of the end users in the RHEA project. This table should be considered by other partners in order to provide a similar approach for every of the three units. All partners should provide safety information concerning the most similar machine on equipment as stated at the beginning of the paper. Generally speaking, such manuals address the three operation modes and thus will be of highest relevance.

Table 2. Spraying tasks RHEA robot unit

Labor	**Maintenance**	**Transport**
Before	Mechanical	•Attachment
• Attachment (3 Points; PTO; Electric; Oil Hydraulic Jacks) • Filling With Water • Opening Bar and System Testing (Check Filters And Nozzles) • Addition Agrochemicals	• Cleaning, Check and Lubrication Of Moving Parts (Bar; Suspension System; Pump And PTO; Hydraulic Actuators)	•Checking Lighting System •Checking Elements That Could Shed Or Hang From The Machine
During	Hydraulic	
• Bars Opening and Closing • PTO Manipulation • Fill Water And Agrochemicals • Navigation	• Cleaning and Replacement (Filters, Nozzles, Pipes, Manometers)	
After	Electric	
• Cleaning (Clean Water Spray; Clean Filters) • Release (3 Points; PTO; Electic; Oil Hydraulic Jacks)	• Checking, Cleaning (Valves, Connection Boxes, Wiring, Other Sensors And Actuators)	

5. Conclusions

A dedicated review of safety standards and scientific state on this subject has been carried out in this work.

This paper aims at acting as the corner stone in the process of definition of safety specifications, functions and verification levels.

When all partners in the project agree and follow the recommendations described in the papers, the consortium should be confident in meeting a safety design at the end of the project.

A commission constituted by the authors of the paper together with the coordinator will be in charge of verifying the progress throughout the project stages.

Acknowledgement

The research leading to these results has received funding from the European Union's Seventh Framework Programme [FP7/2007-2013] under Grant Agreement nº 245986.

References

ASABE. 2008. Environmental considerations in development of mobile agricultural electrical/electronic components. ANSI/ASAE DEC 1990 (R2008)

Benneweis, R.K. (2006). Facilitating agriculture automation using standards. Club of Bologna. Proceedings, Volume nº17 – Bonn 3 sept. 2006.

Bunn, T.L., Slavova, S., Hall, L. (2008). Narrative text analysis of Kentucky tractor fatality reports. Accident Analysis and Prevention 40 (2008) 419-425.

Colémont, A., Van den Broucke, S. (2008). Measuring determinants of occupational health related behavior in flemish farmers: An application of the theory of planned behavior. Journal of Safety Research 39 (2008) 55-64.

Craessaerts, G., De Baerdemaeker, J. Saeys, W. (2010). Fault diagnostic systems for agricultural machinery. Biosystems Engineering 106 (1):26-36.

Donca, G., Mihaila., V.I. (2010). Aspects regarding data mining applied to fault detection. Annals of the Oradea University. Fascicle of Management and Technological Engineering, Volume IX (XIX), 2010.

Gerberich, S.G., Gibson, R.W., French, L.R., Lee, T-Y., Carr, W.P., Kochevar, L., Renier, C.M., Shutske, J. (1998). Machinery-related injuries: Regional rural injury study-I (RRIS-I). Accident Analysis and Prevention 30, No. 6 (1998) 793-804.

Harding, J.A., Shahbaz, M., Srinivas, S., Kusiak, A. (2006). Data Mining in Manufacturing: A Review. Journal of Manufacturing Science and Engineering 128, 969-976.

Hofmann, R. (2006). Software in Tractors: Aspects of Development, Maintenance and Support, Club of Bologna Proceedings, Volume nº17 – Bonn 3 sept. 2006.

Hui, S.C., Jha, G. (2000). Data mining for customer service support. Information & Management 38, 1-13.

ISO 11783: Tractors and machinery for agriculture and forestry -- Serial control and communications data network. Part 1: General specifications.

ISO 12100-1: Safety of machinery. Basic concepts, general principles for design. Part 1: Basic terminology, methodology.

ISO 13849-1: Safety of machinery. Safety-related parts of control systems. Part 1: General principles for design.

ISO 14121-1: Safety of machinery. Risk assessment. Part 1: Principles.

ISO 25119-1: Tractors and machinery for agriculture — Safety related parts of control systems — Part 1: General principles for design and development.

ISO 25119-2: Tractors and machinery for agriculture — Safety related parts of control systems — Part 2: Concept Phase.

ISO 25119-3: Tractors and machinery for agriculture and forestry — Safety related parts of control systems — Part 3: Series Development, Hardware, and Software.

ISO 26322-1: Tractors for agriculture and forestry — Safety — Part 1: Standard tractors.

ISO 4254-1: Agricultural machinery. Safety. Part 1: General requirements.

Lenz, J., Landman, R., Mishra, A. (2007). Customized Software in Distributed Embedded Systems: ISOBUS and the Coming Revolution in Agriculture. Agricultural Engineering International: the CIGR Ejournal. Manuscript ATOE 07 007. Vol. IX. July, 2007.

Lutz, R.R. (1992). Analyzing software requirements errors in safety-critical, embedded systems. Iowa State University of Science and Technology. Departament of Computer Science. Tech Report: TR 92-27. Submission date: August 27, 1992.

Reid, J. F. (2004b). Mobile intelligent equipment for off-road environments. Written for presentation at the Automation Tehcnologiy for Off-Road Equipment at 7-8 October 2004 Conference (Kyoto, Japan). ASAE Publication Number: 701P1004.

Reid, W.S. (2004a). Safety in perspective, for autonomous off road equipment (AORE). Written for presentation at the 2004 ASAE/CSAE Annual International Meeting. Paper number: 041151.

Schwabacher, M.A. (2005). A Survey of Data-Driven Prognostics. Infotech@Aerospace. AIAA 2005-7002. 26 - 29 September 2005, Arlington, Virginia.

Suwatthikula, J., McMurranb, R., Jonesa, R.P. (2011). In-vehicle network level fault diagnostics using fuzzy inference systems. Applied Soft Computing 11 (2011) 3709–3719.

Thelin, A. (1998). Rollover Fatalities-Nordic Perspectives. Journal of Agricultural Safety and Health 4(3): 157-160.

Application of mechanical and thermal weed control in maize as part of the RHEA project

A. Peruzzi, M. Raffaelli, M. Fontanelli, C. Frasconi and L. Martelloni

Centro Interdipartimentale di Ricerche Agro-Ambientali "Enrico Avanzi", via Vecchia di Marina 6, 56122, San Piero a Grado (PI), Italy

(e-mail: aperuzzi@agr.unipi.it)

Abstract: The European Project RHEA (Robot fleets for Highly Effective Agriculture and forestry management) aims to create a fleet of autonomous aerial and ground mobile units for general crop protection and the application of physical weed control in particular in maize. This paper describes the characteristics of the automated systems, that are currently being designed and developed for physical weed control in maize in the RHEA Project.

The first machine that was designed to apply PWC to maize as part of the RHEA Project (PWC-1) was able to perform mechanical and thermal treatments at the same time so as to remove weeds mechanically from the inter-row space and perform in-row selective and precision flaming. The machine can be modified for broadcast flaming (PWC-2) by replacing the mechanical tools for between-row weed control with burners working at different degrees of intensity, depending on the weed cover. LPG is the fuel source for the burners.

This very innovative application of PWC in maize represents a good opportunity for farmers in terms of reducing the use of herbicides and ensuring that their crops are of a superior quality.

1. Introduction

Weed management is a major issue in agriculture. Effective weed control is vital in order to achieve satisfactory yields and appropriate gains. Herbaceous and vegetable crops are two of the most susceptible sectors in terms of weed control (Bàrberi, 2002).

The European Union is promoting a limited and sustainable use of agrochemicals, including herbicides (Directive 2009/128/EC). For this reason, over the last few years, studies concerning with physical weed control (PWC) applications have increased and currently represent important research areas both in Europe

(Cloutier et al., 2007; Melander et al., 2005; van der Weide et al., 2008), and North America (Ulloa et al., 2011).

There are many effective solutions which perform physical weed controls both in-row and between-row, using both cheap "low-tech" mechanical and thermal tools and machines (Peruzzi et al, 2007; Raffaelli et al., 2010 and 2011) and expensive "high-tech" innovative systems. The study of these advanced technologies, which use very complex electronic systems that acquire and process all the data needed to distinguish between weed and crop plants ("intelligent weeding") have rapidly increased over the last ten years. They are mainly aimed at reducing the large degree of human labour still needed particularly in many low competitive vegetable crops, though low-tech machines are also used (Cloutier et al., 2007; van der Weide et al., 2008).

Several types of mechanical tools have therefore been designed and developed for use with these electronic management systems, for example, a blade that moves within and outside crop rows or a concave disc that tills the soil all around the cultivated plants (O'Dogherty et al., 2007).

Clearly, until now these sophisticated solutions have only been used in very widely spaced crops, such as lettuce and cabbage. These machines are also very expensive and very low, needing further development and test periods. Thus their use in weeding practices is still not economically viable for farmers (van der Weide et al., 2008).

However, besides mechanical tools, physical weed control (PWC) includes the use of thermal treatments. The most commonly used thermal treatment is flaming, which can be applied both before crop planting (both in sown and transplanted crops) and emergence (only in sown crops). It can also be used selectively in post emergence in tolerant crops such as maize, garlic, onion and many other cultivated vegetables and herbaceous species (Ascard et al., 2007, Ulloa et al., 2010 and 2011). The non selective use of flaming is always performed on all the cultivated surface and is included within the false seed-bed technique (or rather "stale seed-bed technique"). The selective use of flaming on the other hand is often reserved for narrows strips including the middle of the crop rows. However in some cases it is performed on all the cultivated surface (broadcast flaming) following a concept similar to that used in the post-emergence application of herbicides (Ascard et al., 2007, Ulloa et al., 2010 and 2011).

An "intelligent" and automated use of selective flaming treatments has never been tested until now. However it could represent a valid solution in physical weed control systems, including precision farming. In this regard, several "smart weeders" were recently tested on some of the most diffusely cultivated herbaceous crops, such as winter wheat and maize (Rueda-Ayala et al., 2010).

The next step for European farmers may be to use automated systems to perform PWC, which is one of the goals of the RHEA Project.

An automated machine that performs weed control should consist of four fundamental components: a crop and weed discrimination and detection system (presence, stage of development, soil cover, etc.); a decision making system that processes all the detected information and applies a series of different interventions in order to perform the most effective selective weed control; and an effective weed control system using both chemical (localized distribution of herbicides) and physical (mechanical and thermal) means; and finally an automatic guidance system based on the application of the "Real-time Kinematic Global Positioning System" and/or artificial vision systems that perform crop row detection and detect weed patches (Slaughter et al., 2008).

An automatic guidance system for selective weed control should also be able to work where there is a high density of weeds (up to 200 plants m^{-2}) and detect the crop rows efficiently with a negligible deviation in both transplanted and sown crops (Åstrand & Baerveldt, 2005). It is more difficult to perform row detection in sown crops, because of the non simultaneous emergence and the consequent different sizes of the cultivated plants (Slaughter et al., 2008). Moreover, in conventional cultivation the sown crops are often very similar in size to the weeds, making it essential to use another system for the identification (analysis of the shapes, etc.) (Åstrand & Baerveldt, 2005). However, this can be minimized with a well-prepared false or stale seed-bed, thus enabling the different stages of development to be differentiated as well as the size of the crop compared to the weeds (Cloutier et al, 2007, Peruzzi et al., 2007; Raffaelli et al., 2010 and 2011).

The European Project RHEA (Robot fleets for Highly Effective Agriculture and forestry management) falls within this context and aims to create a fleet of autonomous aerial and ground mobile units for general crop protection and the application of physical weed control in particular in maize.

This paper describes the characteristics of the automated systems, that are currently being designed and developed for physical weed control in maize in the RHEA Project . Maize was chosen as a wide row crop because of the agronomical and economical importance of this major crop both in Europe and internationally. In the European Union the harvested area estimated by FAOSTAT for grain maize in 2009 was about 13,850,000 ha with a total production of a little less than 8,4000,000 Mg. In recent years there have been ongoing initiatives supported by the European Union aimed at reducing the use of chemical inputs (e.g. herbicides) on this crop, encouraging more environmental friendly management such as integrated and organic farming systems.

2. RHEA Project: an overview

The RHEA Project is an EU-funded research project within the 7th FP. The leader of the project is Prof. Pablo Gonzalez-de-Santos of CSIC (Spain). The project started in 2010 and involves 15 European partners (universities, research centres, spin-off companies, private enterprises) with support from several technical, engineering, agronomic fields such as robotics, informatics, farm machinery, weed science, and telecommunications. The aim is to design and develop an autonomous robotic system for both chemical and non chemical weed control in herbaceous and vegetable crops, and pesticide application on fruit and forestry tree canopy. This can be achieved by means of a robot fleet, including ground and aerial units, working closely together. Each unit will be equipped with a detection and actuation system, and will work in three different scenarios: precise application of herbicides in wheat, physical weed control in maize, and pesticide application on olive tree canopies.

The aerial mobile units will be based on quadrotors (Drones), which will acquire relevant data (images and videos from the field) and send important information to a base station and the ground mobile units, such as the localization of weed patches. The ground mobile unit, which is the same for all the operative machines, will be based on an ordinary tractor, powered by a 37.5 kW engine. It will be equipped with specific sensors for automatic guidance, weed-crop discrimination, weed density assessments, etc.

This work describes the machines, which have already been designed and which are going to be built at the University of Pisa, for the application of PWC to maize..

3. Application of physical weed control in maize

The first machine that was designed to apply PWC to maize as part of the RHEA Project (PWC-1) was able to perform mechanical and thermal treatments at the same time so as to remove weeds mechanically from the inter-row space and perform in-row selective and precision flaming. The machine can be modified for broadcast flaming i.e. thermal treatment (PWC-2).

Fig. 1. Position of the pair of burners in the maize rows

For broadcast flaming, the mechanical tools for between-row weed control will be replaced by burners working at three different degrees of intensity, (which means three LPG pressures corresponding to three LPG doses and finally three levels of heat transfer), depending on the weed cover. LPG is the fuel source for the burners.

For PWC-1, mechanical treatment will be provided whether or not there are weeds, as it is very important from an agronomical point of view. Burners will be switched on only if weeds have been detected in the rows, while no between-row weed detection is required for the mechanical tools. Thermal treatment will be provided by a pair of burners per row (Fig. 1). The distance between the burners and the crop row will be 0.125 m. Weed detection should be provided on a 0.25 m wide cell, including the maize row in the middle. The two burners will work together and not independently, depending on the width of the cell. The pressure of the LPG, will be adjusted according to the weed cover. However it would be more effective to also take distinguish between weeds on the basis of their typology – at least monocots and dicots - and their stage of development. There will be three pressure levels: 0 Mpa when no weed is detected, 0.3 MPa and 0.4 MPa, according to a threshold of 25% weed cover.

The correct position of the tools (mechanical and thermal) will be guaranteed by a precision guidance system connected to a row detection system. Two steering wheels will maintain the correct position of the tools following the real alignment of the row (Fig. 2).

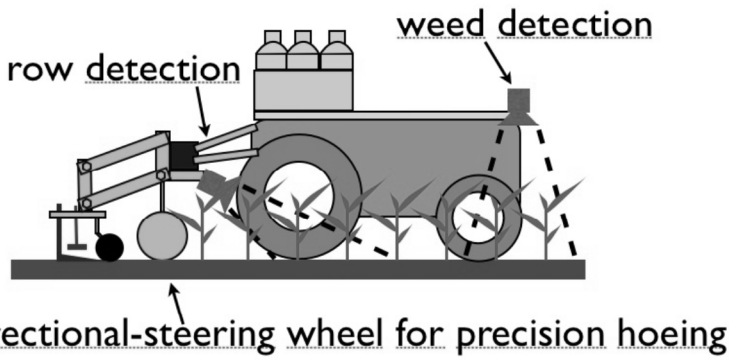

Fig. 2. The ”detection and positioning system” of the PWC-1 coupled to the Ground Mobile Unit

The machine for broadcast flaming (PWC-2) will provide flaming between the rows instead of the mechanical treatment. The system will be the same as described for PWC-1, however in this case a further weed detection system is required on five 0.5 m wide cells and in two 0.25 m wide cells. This treatment, which is more similar

to a chemical spraying application, could be performed only in cases where weed patches have been detected by Aerial Mobile Units.

4. Machines and tools for physical weed control in maize

The working width of the machine for mechanical and thermal treatments (PWC-1) is 4.5 m. This covers five entire inter-row spaces of 0.75 m each and 2 half inter-row spaces of 0.375 m each, corresponding to six entire units. Each unit tills the soil between the rows using one goose-foot rigid central tine and two “L” shaped adjustable rigid side sweeps. Two burners per element are placed in order to hit one side of each crop row (Fig. 3). The flame just hits the weeds growing in the “in-row” space and the lower, heat-tolerant part of the crop plant.

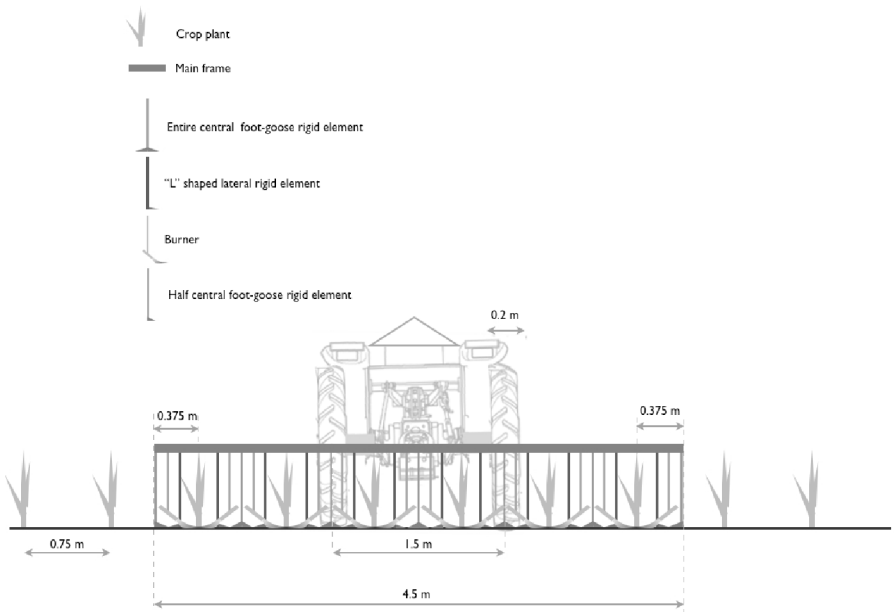

Fig. 3. The PWC-1 designed for the actuation of mechanical-thermal weed control in maize

The structure of the machine should be modular and divided into three frames. Each side frame has by a folding system driven by a hydraulic cylinder (Fig. 4). The central section will be 2.25 m long and the two side sections will be 1.125 m long.

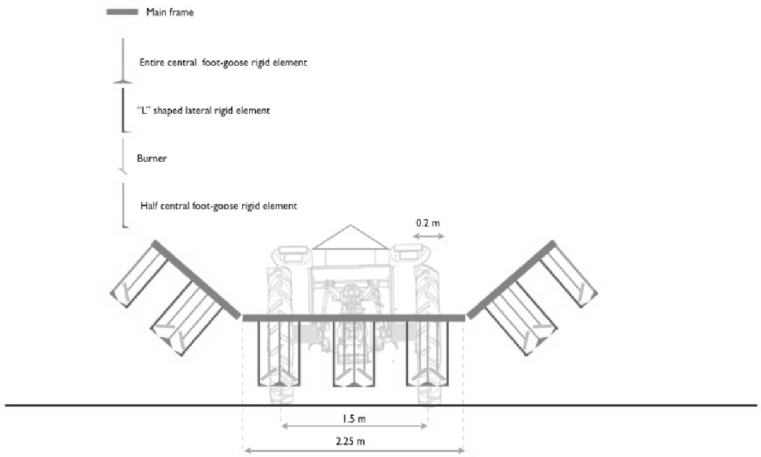

Fig. 4. The folding system of the PWC-1

In order to follow the row without damaging the crop, an automatic steering system will be provided that will be managed by a crop row perception system and driven by a central double rod hydraulic cylinder enabling small lateral movements, guided by two directional metal wheels. The inter-row mechanical treatment (hoeing) will be provided continuously and irrespectively of whether there are any weeds. This is very important from an agronomical point of view, as hoeing not only provides weed control but the shallow tillage improves soil conditions in terms of the roots of the crop and increases water availability.

The machines for thermal and mechanical treatment are equipped with five complete units of hoeing tools (each unit consists of three rigid elements, one central foot-goose and two lateral “L” shaped blades) ensuring an inter-row working width of 50 cm and two side half units (consisting of a half central foot-goose and one “L” shaped blade) working two 25 cm wide strips of the two side inter-row spaces. The working depth of each hoeing unit is about 3-5 cm. The uniformity of the working depth is guaranteed by a wheeled articulated parallelogram connected to the frame and by mounting both mechanical and thermal weed control devices (Fig. 5). Weed detection is only needed in a small band per row (25 cm is enough, 12.5 cm per side) in order to adjust the in-row flaming treatment. Each pair of burners will be adjusted in order to cover a 25 cm

wide band. Each burner will be set at an angle of 45° (with respect to the soil surface) and a distance of 10 cm from the soil. Thus, the machines for mechanical and thermal treatments are equipped with six pairs of 25 cm rod burners working six entire rows of the maize.

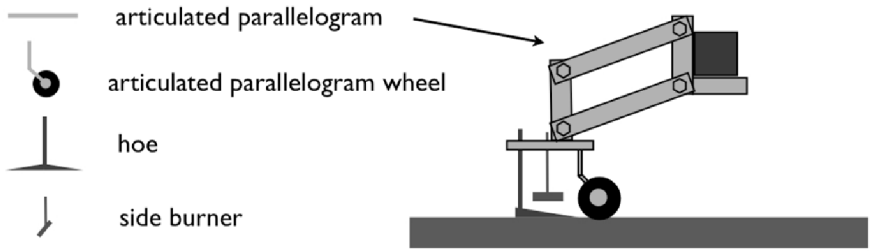

Fig. 5. The working tools and unit of PWC-1 that will be used in maize

The machine for broadcast flaming (PWC-2), will perform a fully flaming treatment along its working width (4.5 m). The design of these devices and the adjustments required are very similar to those described for PWC-1, however in this case five 50 cm wide (and two 25 cm wide rod burners will replace the hoeing units and will work on the entire inter-row space and on the two side half inter-row spaces, respectively (Fig. 6).

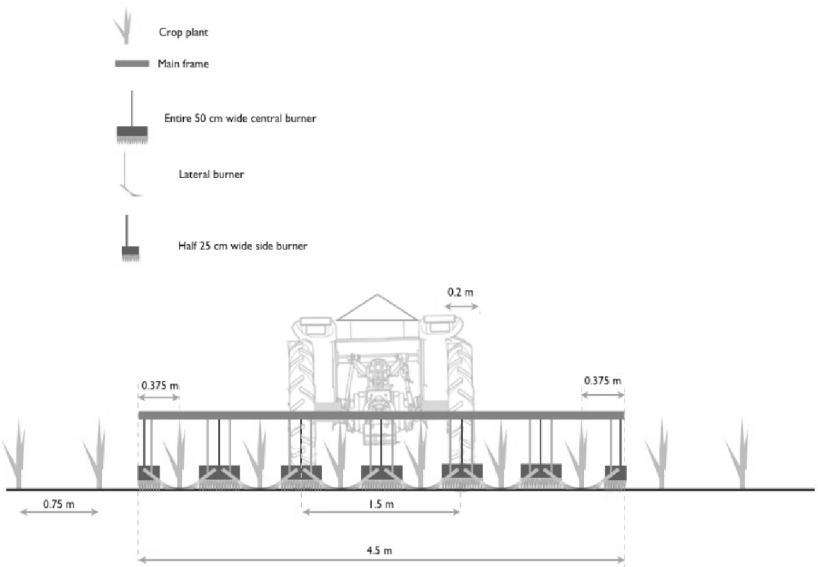

Fig. 6. The PWC-2 machine for broadcast flaming in maize

In this case a weed detection and weed/crop discrimination system is required along the full width of the machine.

Currently, research is ongoing at the University of Pisa to design more thermally efficient burners that will equip both the machines that will be used to perform PWC in maize. These new burners will be equipped not only with an external LPG/air mixer that allows primary air to be accessed, through specific holes, but also with a special inlet on the carter thus enabling the intake of secondary air. Both primary and secondary self-aspirating aerators are based on the Venturi effect. In the first case (external LPG/primary air mixer) depression is created by the flow of LPG at a high speed achieved by a passage through a narrow nozzle section. Secondary air is aspirated by the depression created by the flow of the flame (Fig. 7). Each burner will be provided by an electric automatic ignition system in order to ignite the pilot light at the beginning of the working phase.

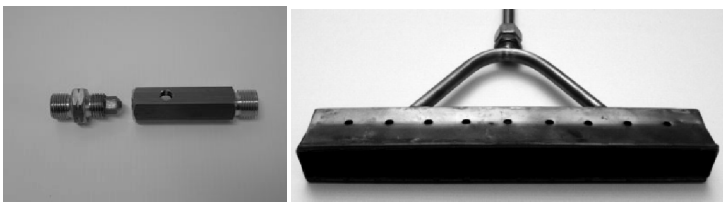

Fig. 7. External LPG primary air mixer (left), and burner using secondary air (right)

The LPG feeding system consists of some LPG tanks: six in PWC-1 feeding six pairs of side burners and 13 in PWC-2 feeding the same six pairs of side burners and seven central burners working in the inter-row spaces. A heat exchanger placed on the ground mobile unit and consisting in a hopper containing water that will be heated by the exhaust gases of the endothermic engine of the mobile unit will prevent the LPG tanks from cooling (Fig. 8).

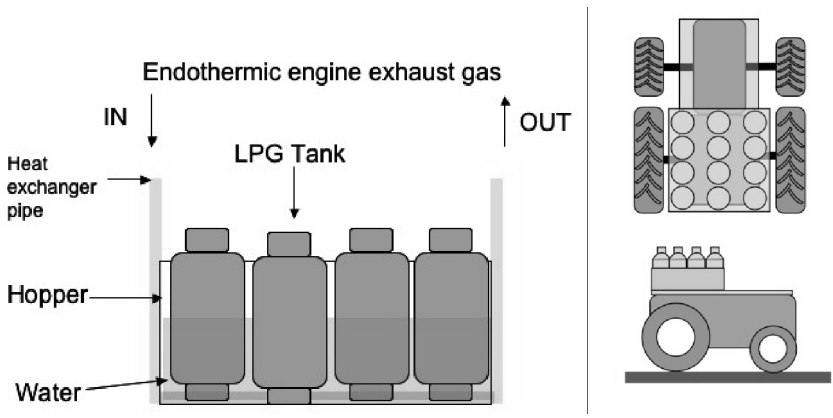

Fig. 8. The heat exchanger and its placement on the ground mobile unit

In order to reduce the mass and size of the heat exchanger, the LPG bottle should be arranged as a rectangular model in the case of mechanical-thermal application, and an hexagonal model for broadcast flaming (Fig. 9).

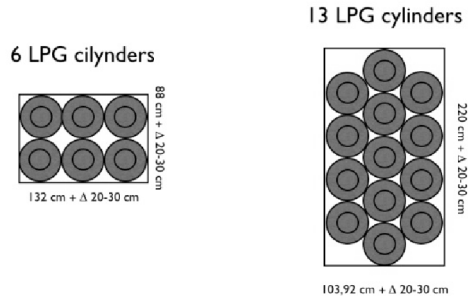

Fig. 9. The arrangement of the LPG tanks inside the hopper

The total estimated mass (water, LPG tanks, hopper etc.) will be about 600-700 kg. An automatic system will open each valve of the LPG tanks before the beginning of the working phase. For each tank, three automatic pressure gauges with a pressure regulator, controlling three different pipe LPG feeding systems: the first set on a very low pressure for the pilot flame of the burner, the second set on a value of 0.3 MPa for a low weed cover treatment (<25%), the third set on a value of 0.4 MPa for a high weed cover treatment (>25%), in accordance with the information provided by the perception system.

Table 1 shows data on the intensity of flaming (LPG doses) for the treated surfaces and the real consumption of LPG per surface unit in the case of PWC-1, on the basis of in-row thermal applications on 50% and 100% of the cultivated area.

Table 1 – Different flaming intensities and LPG consumption used for different weed cover ranges

Weed cover range (%)	Pressure (MPa)	Working Speed (km/h)	Effective LPG dose (kg/ha)	LPG consumption (kg/ha)	
				Treated surface 100%	Treated surface 50%
WC ≤ 25	0.3	6	46.33	15.44	7.72
WC > 25	0.4	6	54.36	18.12	9.06

The values of LPG consumption are really low particularly in the case of lower pressure on 50% of the total surface. However, if flaming at the higher dose on the total surface was required, the fuel consumption would be quite low.

5. Estimated effects of flaming on weeds and maize

Using the results of previous long-term research studies carried out at the University of Pisa on the effect of flaming at different doses on the main types of

grass (e.g. Echinocloa crus galli) and large leaves (e.g. Amaranthus spp, Abutilon theofrasti), which are the main weeds involved in maize cultivation (Peruzzi et al., 1998 and 2000), it was possible to predict some weed reduction levels determined by the two intensities of thermal treatment that will be used by both PWC-1 and PWC-2 in the RHEA Project (Table 2).

The data in Table 2 highlight that it is easier to control dicots in the first stage of development and obviously using the higher LPG dose. On the other hand, major problems could arise with monocots with the lower LPG dose at the 2-4 and 4-6 of true leaf stages.

Note that the data in Table 2 refer to dead plants (complete control), whereas the flaming with both the doses that will be used in the RHEA Project totally destroy the epigeal part of the weed plants, which will recover after an average period of 10-15 days. This will give the maize plants a good advantage, thus allowing their growth with very low or ideally no competition.

Table 2 – Estimated average levels of weed control (divided into monocots and dicots) for flaming with the doses that will be used in the RHEA Project (reworked data from Peruzzi et al., 1998 and 2000)

Weed type/ stage	Weed control (%)	
	LPG doses (kg ha^{-1})	
	46,33	54,36
Monocots		
emergence	68	73
2-4 leaves	59	71
4-6 leaves	52	79
Dicots		
cot	85	92
2-4 leaves	76	82
4-6 leaves	77	93

The good tolerance of maize to flaming with the two doses that will be used in the RHEA Project is confirmed by the data reported in Table 3. In all three stages of development considered in the experiments carried out in Italy and in the US, investigating the tolerance of maize to thermal intervention, the yield losses determined by flaming (with respect to untreated controls) were not significant and were very low (on average about 3% with the lower LPG dose and 11% with the higher) (Peruzzi et al., 1998 and 2000).

The maize stage characterized by the lower sensitivity to flaming was five true leaves, however the data reported in Table 3 confirmed that, if needed (e.g. as a consequence of early or late high weed presence), flaming can be done at maize emergence or at the 7-true leaf stage without significantly reducing the yield.

This is very important for farmers because it makes flaming on maize very versatile and thus it can be used in relation to the presence of weeds and their level of aggression . This is especially true in the case of the fleet of small robots that should be available at the end of the RHEA Project.

In order to perform a mechanical and thermal or a broadcast flaming treatment on maize at the 6 or 7 true leaf stage, machines with a sufficiently high ground clearance need to be used, as the height of the plants may be more or less than 45-50 cm (Leroux et al., 2001).

In this respect, using a ground mobile unit with a maximum ground clearance of 40 cm in the RHEA Project is a drawback, as it reduces the versatility of the use of PWC (flaming and hoeing), enabling it to be performed only until the height of the plants is lower than 40 cm (maybe at the 4 or 5 true leaf stage…).

Table 3. Estimated average level of yield loss (with respect to untreated control) in maize flamed (in-row and broadcast) at the doses that will be used in the RHEA Project (reworked data from Peruzzi et al. 2000, Ulloa et al, 2011).

Stage / **Dose (kg ha^{-1})**	**46 kg ha^{-1}**	**54 kg ha^{-1}**
	Yield loss (%)	Yield loss (%)
2 leaves	6	16
5 leaves	2	5
7 leaves	5	13

6. Final remarks

Physical weed control in maize in the RHEA Project has the following strengths:

- it will be very effective,
- it will be agronomically, environmentally and economically sound,
- in the case of PWC-1 there is a synergic and optimized use of mechanical (non selective) and thermal (selective) means
- in the case of PWC-2 the broadcast flaming is very precise because of the combined actions of the aerial and ground mobile units.

Nevertheless, there are some weaknesses :

- false seed-bed techniques are essential in order to increase PWC effectiveness in post-emergence selective treatments;
- there is a need for a low-medium degree of "total control" (dead plants) of monocots by flaming, using the defined driving speed of the ground mobile units (6 km/h),
- a low ground clearance of the ground mobile units will not enable late PWC-1 and PWC-2 interventions in maize.

This project will last until 2014 and the final versions of the robots will need to be ready by the end of 2013.

This very innovative application of PWC in maize represents a good opportunity for farmers in terms of reducing the use of herbicides and ensuring that their crops are of a superior quality.

Acknowledgement

The research leading to these results has received funding from the European Union's Seventh Framework Programme [FP7/2007-2013] under Grant Agreement nº 245986.

References

Ascard, J., Hatcher, P.E., Melander, B., Upadhyaya, M.K. Thermal weed control, In: Upadhyaya, M.K., Blackshaw, R.E. (Eds.), Non-chemical weed management, Cabi, Oxon, UK, 2007, pp. 155-175.

Bàrberi, P. Weed management in organic agriculture: are we addressing the right issues?, Weed Research, 2002, 42, 176-193.

Cloutier, D.C., van der Weide, R.Y., Peruzzi, A. & Leblanc, M.L. Mechanical weed management, In: Upadhyaya, M.K., Blackshaw, R.E. (Eds.), Non-chemical weed management, Cabi Oxon, UK, 2007, pp. 111-134.

Leroux, G. D., J. Douheret and M. Lanouette (2001). Flame weeding in corn. Physical Control Methods in Plant Protection, 47-60.

Peruzzi A., Di Ciolo S., Raffaelli M. (1998) - Effects of flaming on velvetleaf (Abutilon theophrasti L.) common amaranth (Amaranthus retroflexus) and cockspur grass (Echinocloa crus-galli L.). Proceedings AgEng '98 International Conference on Agricultural Engineering, Oslo 24/28 August, 1998, 603-604.

Peruzzi, A., M. Ginanni, M. Fontanelli, M. Raffaelli and P. Bàrberi (2007). Innovative strategies for on-farm weed management in organic carrot. Renewable Agriculture and Food Systems, 22, 246-259.

Raffaelli, M., M. Fontanelli, C. Frasconi, M. Ginanni and A. Peruzzi (2010). Physical weed control in protected leaf-beet in central Italy. Renewable Agriculture and Food Systems, 25, 8-15.

Raffaelli, M., M. Fontanelli, C. Frasconi, F. Sorelli, M. Ginanni and A. Peruzzi (2011). Physical weed control in processing tomatoes in Central Italy. Renewable Agriculture and Food Systems, 1-9.

Rueda-Ayala, V., Rasmussen, J. & Gerhards R. Mechanical Weed Control, In: Oerke, E.C., Gerhards, R., Menz, G., Sikora, R.A. (Eds.), Precision Crop Protection – the Challenge and Use of Heterogeneity, Springer Dordrecht Heidelberg London New York, 2010, pp. 279-294.

van der Weide, R. Y., P. O. Bleeker, V. T. J. M. Achten, L. A. P. Lotz, F. Fogelberg and B. Melander (2008). Innovation in mechanical weed control in crop rows. Weed Research, 48, 215-224.

Ulloa, S. M., A. Datta and S. Z. Knezevic (2010). Growth stage impacts tolerance of winter wheat (Triticum aestivum L.) to broadcast flaming. Crop Protection, 29, 1130-1135.

Ulloa, S. M., A. Datta, C. Bruening, B. Neilson, J. Miller, G. Gogos and S. Z. Knezevic (2011). Maize response to broadcast flaming at different growth stages: Effects on growth, yield and yield components. European Journal of Agronomy, 34, 10-19.

Wireless QoS-enabled Multi-Technology Communication for the RHEA Robotic Fleet

Thomas Hinterhofer and Slobodanka Tomic

FTW Telecommunications Research Center Vienna

Donau-City Straße 1/3, A-1220 Vienna, Austria

(e-mail: {hinterhofer,tomic}@ftw.at)

Abstract: The use of multiple communication interfaces based on heterogeneous wireless communication technologies can significantly improve network robustness and performance. The resulting communication systems are suitable for industrial and robotic control scenarios with special requirements on Quality of Service (QoS) and reliability. In this paper we present the communication system of the RHEA European project, which simultaneously uses 802.11a, 802.11g, ZigBee PRO and GPRS interfaces for communication within a mobile robotic fleet and with a static centralized mission planning and supervision entity. Furthermore, the approach for real-time monitoring and prediction of the multi-technology network health is described. This approach enables RHEA application developers to create applications that use information about current and predicted network health in order to react to or proactively adapt to potential communication issues like network partitioning or drops of communication performance.

1. Introduction

In the last decade, wireless communication has shown its capability to substitute wired communication and to support mobility scenarios. Its enormous success is caused by simplicity, flexibility and fast installation at a low price. A multiplicity of wireless standards emerged targeted for different application fields and end users. Especially technologies working in the Industrial, Scientific and Medical (ISM) radio band are of interest as they can be used without licensing. The performance of such technologies is impaired by devices not part of the communication system which provoke congestion and interferences. Industrial or robotic control applications usually have tight requirements regarding communication performance in terms of latency, throughput and connectivity (Willig et al., 2005) which are hard to guarantee if a non-privileged usage of the ISM radio band is assumed.

As a result, the communication system for the Robot Fleets for Highly Effective Agriculture and Forestry Management (RHEA) European project is based on the simultaneous usage of multiple communication technologies (802.11a, 802.11g, ZigBee PRO, GPRS), with the goal to improve the level of network robustness and performance that may be achieved with a single wireless technology. This lowers the risk that the unpredictability of the wireless communication channel will disrupt the overlay communication service. Timely delivery is one of the most important QoS requirements for industrial and robotic control applications. If redundancy of communication interfaces is not applied, wireless transmission characteristics like fast fading or interference can result in a message delivery deadline violation. The simultaneous usage of multiple communication technologies working in different frequency bands can significantly reduce the risk of a service disruption as it is unlikely that transmissions over both technologies are affected at the same time. Also deadline violations caused by congestion of the wireless channel can be reduced if the selection of communication technologies is coordinated among neighbouring devices.

The paper is organized as follows. Section 2 presents related work in the context of reliable wireless industrial communication, network topology control and prediction of network partitioning and mobility. The RHEA robotic fleet and corresponding high-level communication requirements are introduced in Section 3. Section 4 continues with the description of the communication infrastructure, its configuration and an analysis of the expected application traffic. Section 5 presents our multi-technology management approach for providing QoS-enabled communication within the robotic fleet. Finally, Section 6 concludes with the benefits and applicability of our approach and presents our planned future work.

2. Related Work

Wireless industrial communication has become an important research field. Willig (2008) investigates a selection of recent and emerging topics in wireless industrial communications taking different wireless communication technologies into account. In order to improve wireless network performance and QoS, the use of multiple transmission and receiving interfaces for communication between two nodes has been studied extensively and has resulted in different approaches. A tutorial paper about Multiple-Input-Multiple-Output (MIMO) is presented by Gesbert et al. (2003). MIMO approaches are based on spatial diversity without the need for extra frequency bandwidth. By contrast, Kyasanur and Vaidya (2005) discuss routing and interface assignment in multi-channel wireless networks and propose an interface assignment strategy for 802.11 multi-hop wireless networks.

A different approach to improve QoS in wireless communication networks is topology adaptation/control and prediction. Topology prediction based on mobility prediction is presented in Wang and Li (2002) and in Al-Hattab and Agbinnya (2008) and is also used for our approach. Furthermore, we adopt and extend the notion of

failure margin introduced by Avresky and Natchev (2003) to multi-technology link failures. The resulting multi-technology network monitoring and prediction approach is based on connectivity and k-connectivity in wireless ad-hoc networks as discussed by Santi and Blough (2003), Wan and Yi (2004) and Jia et al. (2005).

3. RHEA Robotic Fleet

The RHEA robotic fleet consists of three independent autonomous Ground Mobile Units (GMU) and a stationary base station. GMUs operate in the mission field and are under the control of the base station, which executes mission planning and supervision functionalities. Application information exchange takes place only between the base station and the GMUs as depicted in Fig. 1.

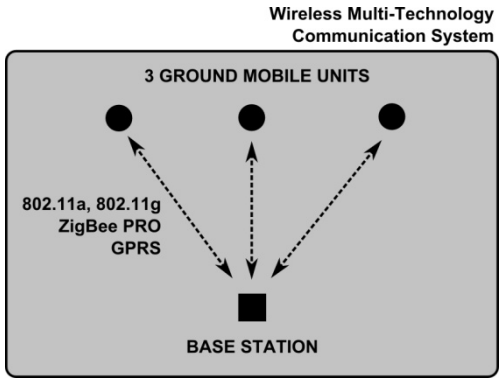

Fig. 1. High-Level Overview of RHEA Wireless Communication

The communication has to be tolerant to the underlying unpredictability of the wireless channel. Especially randomly occurring fast fading due to multipath propagation (multipath induced fading) and interferences caused by contesting devices have to be handled without disruption of the communication services used by the application layer. Also mobility of GMUs can lead to some communication problems, for example a GMU can move out of the transmission range and become disconnected. This has to be detected in advance through communication monitoring and prediction, which is used by the application to prevent approaching communication problems.

4. Multi-Technology Communication

4.1 Transmission Range

The RHEA robotic fleet will operate in a field of size 250 m x 100 m (Fig. 2). We assume that the base station is located 15 m apart from the field borders. As a consequence of this position and taking the turn radius of the GMUs into account, the operational area is defined to be of size 300 m x 150 m. Within this area, communication between the GMUs and the base station has to be maintained.

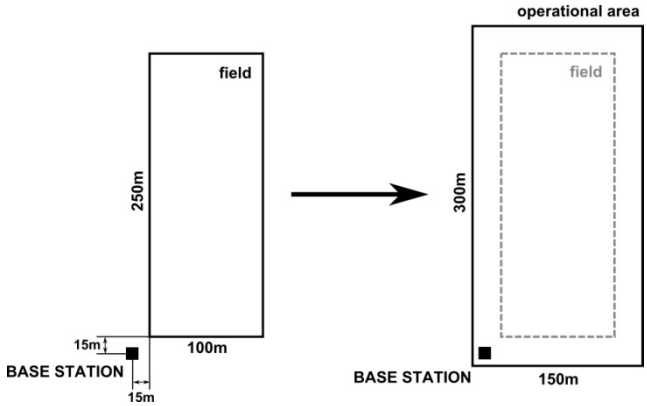

Fig. 2. RHEA Field Size and Resulting Operational Area

4.2 Infrastructure and Network Topology

The RHEA base station and the GMUs are equipped with four previously mentioned communication technologies. In addition, four solar powered embedded systems (ZB1-ZB4) are located at the border of the operational area (Fig. 3). These systems are equipped with ZigBee radios, which increase the range and redundancy of the ZigBee mesh network.

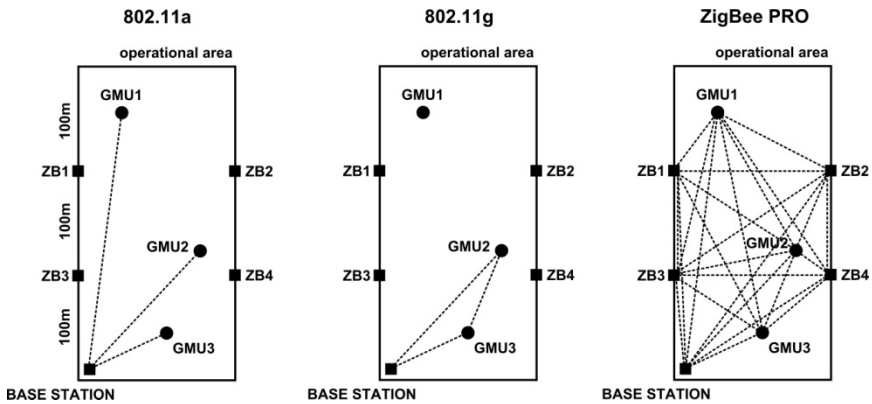

Fig. 3. Network Topologies of 802.11a, 802.11g and ZigBee PRO

The 802.11a network is configured in infrastructure mode and supports Dynamic Frequency Selection (DFS). Thus, it can be used in Europe in the 5GHzine o ISM band outdoor with a transmit power of up to 27dBm (500mW) EIRP. Assuming free line-of-sight and no interfering devices, every GMU is able to connect to the base station regardless of its location within the operational area (Fig. 3).

The 802.11g network is configured in ad-hoc mode. In Europe, the maximum transmit power is limited to 20dBm (100mW) EIRP. As we can assume free line-of-

sight between our communication units, we expect a transmission range of 100 to 150 m. As illustrated in Fig. 3, a GMU, here GMU1, is disconnected if there is no multi-hop path to the base station. Simulation has shown that 51% of all possible GMU locations result in the availability of multi-hop paths to the base station if a transmission range of 140m and a field size of 300 m x 150 m are assumed.

In the ZigBee network, the base station is configured as the coordinator. All other devices are configured as routers as power consumption is not an issue. The ZigBee devices are operating in non-beaconed mode at a fixed transmit power of 17dBm (50mW). Given free line of sight, our ZigBee modules (Digi International XBee PRO S2 with 5dBi omnidirectional antenna) provide a transmission range of 7km, which easily connects any two devices and results in a highly meshed network (Fig. 3).

4.3 RHEA Application Traffic

To adapt the wireless multi-technology management to the requirements of RHEA applications, the occurring types of traffic were analyzed (Fig. 4). We divided the application traffic into control, data and logging traffic. Control traffic is characterized by a very small or even no payload. Some control traffic messages have the highest requirements, e.g. those carrying informing about safety critical stop of the mission operation or the occurrence of GMU errors.

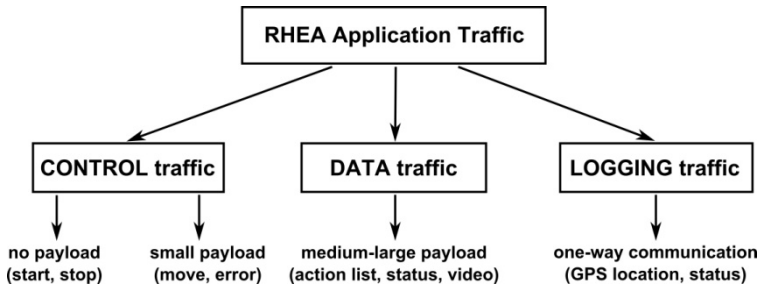

Fig. 4. RHEA Application Traffic Classification

As important as the requirement for reliable transmission of application traffic is the requirement that the application layer is aware of the multi-technology network health at any time. Disconnections between the base station and GMUs and communication performance bottlenecks should be reliably detected. We propose a multi-technology management approach designed to monitor and predict upcoming communication issues, as presented in Section 5. With this approach, the system continuously in real time calculates the number of links that can fail without causing communication problems among communicating units. To characterize this number we adopted a notion of failure margin as presented by Avresky and Natchev (2003) to link failures. The system further creates alarms if the link failure margin for communication between two communication units drops below a configurable threshold. In this way by real time monitoring the system predicts and avoids approaching communication problems.

5. Multi-Technology Management

5.1 Topology Discovery and Distribution

In the proposed approach, the monitoring and prediction of the multi-technology network health is based on the knowledge of four matrices/vectors representing the current status of all communication technologies. The `3x2` 802.11a matrix (`11A`) in (1) has an entry for every directed link (downlink `DL`, uplink `UL`) between the corresponding GMU operating in managed mode and the base station configured in master mode. The base station broadcasts information from matrix `11A` over 802.11a at a configurable rate. In (2), every entry in the `4x4` 802.11g matrix (`11G`) corresponds to one directed link of the 802.11g network topology. For example, g_{12} represents the link from the base station to GMU1. Here the Optimized Link State Routing (OLSR) protocol is used, which proactively and periodically distributes network information. As a consequence, the network topology is always known by every device.

$$11A = \begin{array}{c} \\ GMU1 \\ GMU2 \\ GMU3 \end{array} \begin{array}{c} \begin{array}{cc} DL & UL \end{array} \\ \begin{pmatrix} a_{11} & a_{12} \\ a_{21} & a_{22} \\ a_{31} & a_{32} \end{pmatrix} \end{array} \tag{1}$$

$$11G = \begin{array}{c} \\ BS \\ GMU1 \\ GMU2 \\ GMU3 \end{array} \begin{array}{c} \begin{array}{cccc} BS & GMU1 & GMU2 & GMU3 \end{array} \\ \begin{pmatrix} - & g_{12} & g_{13} & g_{14} \\ g_{21} & - & g_{23} & g_{24} \\ g_{31} & g_{32} & - & g_{34} \\ g_{41} & g_{42} & g_{43} & - \end{pmatrix} \end{array} \tag{2}$$

The matrix of the ZigBee PRO network (`ZBP`) in (3) is of size `8x8`. It is similar to the 802.11g matrix. Every entry represents one directed link of the network topology. In contrast to the 802.11g network, the topology of the ZigBee network has to be actively requested. The ZigBee standard offers a method for requesting the neighbor table of a specific network node (cf. Mgmt_Lqi_req and Mgmt_Lqi_rsp commands in the ZigBee-2007 specification). By using this functionality the knowledge about the whole ZigBee network topology can be re-constructed at each node. Finally, the `GPRS` matrix in (4) has one entry for the base station and every GMU. As GPRS is not being used for communication between the base station and the GMUs, the matrix entries will only be retrieved from an online source using GPRS.

$$ZBP = \begin{array}{c} \\ BS \\ GMU1 \\ GMU2 \\ GMU3 \\ ZB1 \\ ZB2 \\ ZB3 \\ ZB4 \end{array} \begin{array}{c} \begin{array}{cccccccc} BS & GMU1 & GMU2 & GMU3 & ZB1 & ZB2 & ZB3 & ZB4 \end{array} \\ \begin{pmatrix} - & z_{12} & z_{13} & z_{14} & z_{15} & z_{16} & z_{17} & z_{18} \\ z_{21} & - & z_{23} & z_{24} & z_{25} & z_{26} & z_{27} & z_{28} \\ z_{31} & z_{32} & - & z_{34} & z_{35} & z_{36} & z_{37} & z_{38} \\ z_{41} & z_{42} & z_{43} & - & z_{45} & z_{46} & z_{47} & z_{48} \\ z_{51} & z_{52} & z_{53} & z_{54} & - & z_{56} & z_{57} & z_{58} \\ z_{61} & z_{62} & z_{63} & z_{64} & z_{65} & - & z_{67} & z_{68} \\ z_{71} & z_{72} & z_{73} & z_{74} & z_{75} & z_{76} & - & z_{78} \\ z_{81} & z_{82} & z_{83} & z_{84} & z_{85} & z_{86} & z_{87} & - \end{pmatrix} \end{array} \tag{3}$$

$$GPRS = \begin{pmatrix} BS \\ GMU1 \\ GMU2 \\ GMU3 \end{pmatrix} \tag{4}$$

In our starting approach, every entry of `11A`, `11G`, and `ZBP` consists of two bytes representing the Link Quality (LQ) and the Link Utilization (LU). LQ depends on the link signal strength and the link error rate and LU represents the recent utilization percentage of a configurable time interval.

During operation, some communication units may become separated from others. Figure 5 illustrates a scenario where GMU1 is disconnected from the 802.11g network due to its limited transmission range. As a consequence, GMU1 cannot discover the topology of the remaining connected part via OLSR. Thus, we introduce the possibility to provide this information using an alternative communication technology. For example, in the previous case, the base station forwards the 802.11g knowledge (`11G` matrix) to GMU1 using 802.11a.

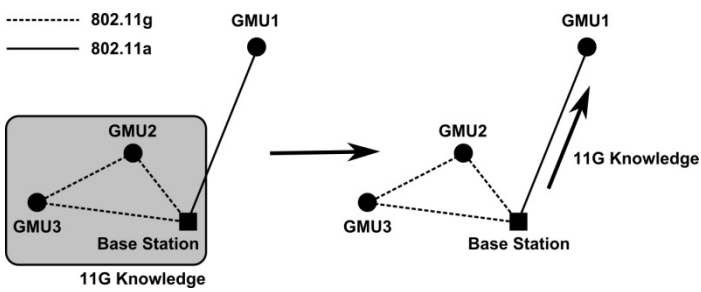

Fig. 5. Topology Distribution

In order to control the amount of traffic caused by network knowledge distribution, we further introduce the distribution radius. It defines the number of hops in a multi-technology topology that a technology matrix shall be forwarded. As illustrated in Fig. 6, without topology distribution node E is only aware of the links (1), (4), (6), (7), (8) and (9). If the distribution radius is configured to 1, node D distributes its knowledge of links (3) and (5) to node E. Link (2) is distributed from D to E if the distribution radius is 2.

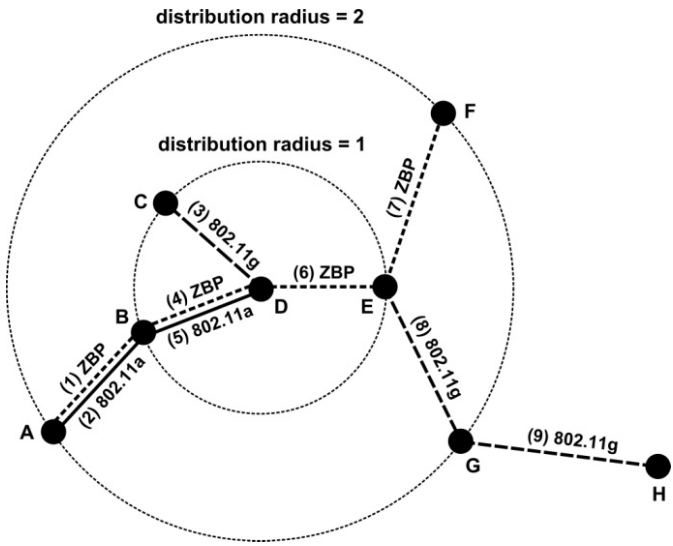

Fig. 6. Topology Distribution Radius

If the distribution radius is set to zero, a communication unit (GMU or base station) will have only local knowledge, which is limited to topology knowledge that it can acquire over single technology networks to which it connects. In the RHEA topology, a distribution radius of 2 will always result in full multi-technology topology knowledge at every communication unit.

In addition to the link state information, we propose that the communication system also uses mission information. This is provided by the base station, which knows the actual position and the mission plan of all GMUs at any time. The relevant information, which may be maintained in a database, includes the positions of the base station and the stationary ZigBee systems, as well as continuously updated information about the position and movement for each GMU. Every row of matrix `MU` in (5) refers to information about specific mobile units and is updated at some time T1, with the direction and the speed that will be maintained until the time T2. With this information, the location of the GMU can be predicted at any time between T1 and T2. This prediction approach works well for the RHEA robotic fleet as the GMU movements will feature long straight lines.

$$MU = \begin{matrix} \\ GMU1 \\ GMU2 \\ GMU3 \end{matrix} \begin{matrix} \begin{matrix} GPS & Direction & Speed & Time1 & Time2 \end{matrix} \\ \begin{pmatrix} m_{11} & m_{12} & m_{13} & m_{14} & m_{15} \\ m_{21} & m_{22} & m_{23} & m_{24} & m_{25} \\ m_{31} & m_{32} & m_{33} & m_{34} & m_{35} \end{pmatrix} \end{matrix} \tag{5}$$

The matrix SU in (6) contains static GPS localization data of all stationary units, which is provided at system start-up.

$$SU = \begin{pmatrix} GPS_{BS} \\ GPS_{ZB1} \\ GPS_{ZB2} \\ GPS_{ZB3} \\ GPS_{ZB4} \end{pmatrix} \tag{6}$$

MU and SU can be retrieved by the GMUs using GPRS.

5.2 Congestion and Interference Avoidance

The dynamic technology selection to transmit application traffic is based on two objectives. Firstly, the requested QoS has to be achieved. Secondly, technology selection is also based on the neighborhood of the transmitting communication unit. This cooperative technology selection will result in lower channel congestion and interferences, which enhances the overall multi-technology communication performance.

5.3 Failure Margin and k-Connectivity

The term failure margin is related to the property of k-connectivity in graph theory. Calculating the failure margin is an effective way of estimating the reliability (in terms of connectivity) of an overlay end-to-end connection. Figure 7 depicts the case in which a failure of a single link (link 6) in the underlying physical topology will lead to a disconnection of communication unit B from the network and from the communication unit A. In such a case we say that for the communication between A and B the corresponding failure margin is 0.

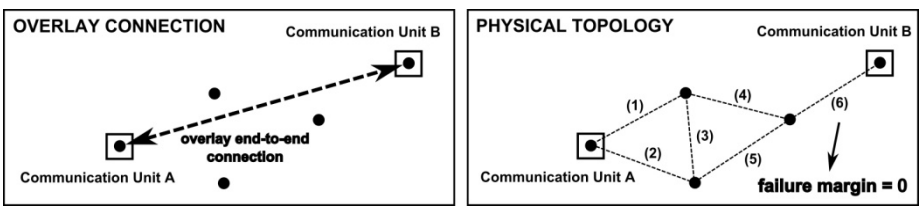

Fig. 7. Partitioning Failure Margin (Case 1)

In the second case (Fig. 8), because of the additional link (link 7) in the physical topology the failure margin for the communication between A and B will be 1. The

higher the failure margin, the lower is the probability that wireless channel problems such as fast fading or interference will lead to the loss of connectivity.

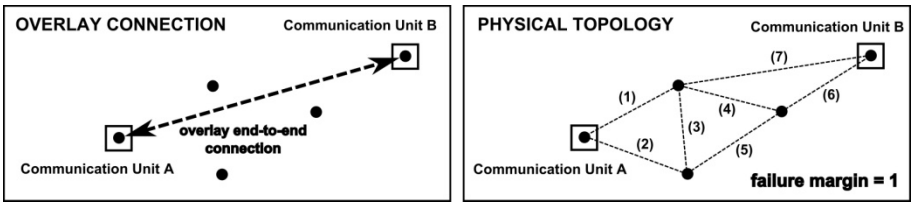

Fig. 8. Partitioning Failure Margin (Case 2)

The notion of failure margin is relevant only for mesh networks. This means that in the RHEA multi-technology communication system, the calculation of the failure margin is performed for the 802.11g and the ZigBee networks based on the technology state information `11G` and `ZBP` introduced in Section 5.1.

Example calculations for 802.11g and ZigBee networks are depicted in Fig. 9.

Due to the fact that additional ZigBee embedded systems are deployed at the border of the operational area, the ZigBee network features a high link redundancy. At any time, assuming ideal conditions, up to 6 links can fail without partitioning the network. Hence the failure margin for communication among any two nodes is 6, and it is unlikely that fast fading leads to partitioning of the network. If we assume that there are no external jamming sources, which can block the whole ZigBee network, only a GMU out of transmission range will lead to a drastic drop of the failure margin.

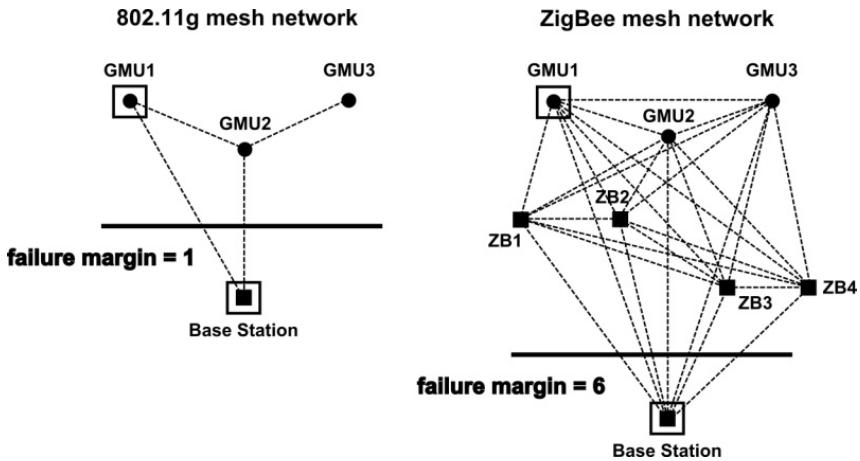

Fig. 9. Partitioning Failure Margin between GMU1 and Base Station

The calculation of the failure margin is a minimum cut problem of graph theory. There exist efficient algorithms that solve the problem in polynomial time given the

adjacency matrix of the graph as input. A comparison of known algorithms is presented by Chekuri et al. (1997). The adjacency matrices of the 802.11g and the ZigBee networks can be based on the matrices `11G` and `ZBP` introduced in Section 5.1.

5.4 Multi-Technology Extension

One important novel aspect of the RHEA communication system is that the calculation of the failure margin is extended to multi-technology level. An abstract example for multi-technology failure margin is depicted in Fig. 10. Considering only technology 1 a single link failure can cause disconnection of communication units (CU) A and B. Also communication units A and B are not connected to C. Taking technology 2 into account results in a failure margin of 1 between communication unit A and B. Furthermore, sub-network 1 and sub-network 2 are now connected resulting in positive failure margins between communication unit A and C and between communication unit B and C.

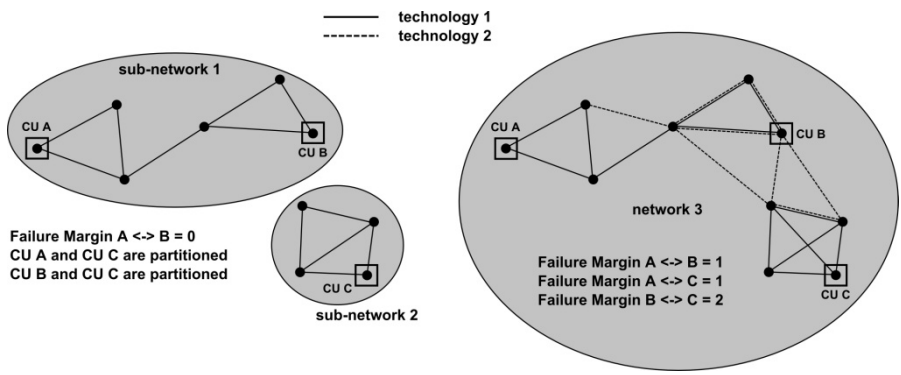

Fig. 10. Multi-Technology Failure Margin

For RHEA applications, not only prediction and prevention of partitioning is of interest. Also the detection of upcoming bottlenecks for throughput or latency is relevant in order to proactively adapt application level behaviour. A multi-technology example for a critical point for communication performance is given in Fig. 11. As a consequence of the mesh network, the failure margin between communication unit A and B is 3. Also throughput is high, as technology 1 connects communication unit A and B. Nevertheless, a single link failure can cause a throughput drop from 6Mbit/s to 250kbit/s. Therefore, the margin to the critical drop of communication performance is 0.

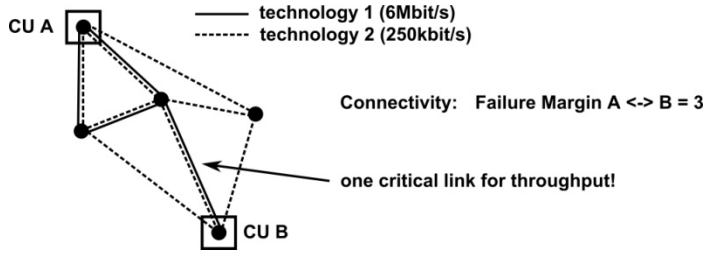

Fig. 11. Margin to Critical Drop of Communication Performance (e.g. Throughput)

We use the term degradation margin to refer to the link failure margin to the mentioned critical drop of communication performance. Awareness of the degradation margin enables the application to dynamically scale its throughput requirements in order to avoid disruptions of the most important control traffic in case of communication issues.

5.5 Connection Monitoring

As already mentioned, the failure (or degradation) margin is calculated for communication between two communication units (GMU or base station). To monitor a connection, this has to be registered by the application at a special connection monitoring function, the so-called Wireless Link QoS (WLQ) manager. The failure or degradation margin calculations are performed by the WLQ manager for all such registered connections. In Fig. 12, an application running at communication unit A requests monitoring of the connection between communication unit A and B. This connection is registered at the WLQ manager executed at communication unit A. The WLQ manager then calculates the expected multi-technology connection performance (expected latency, throughput) as well as failure margins and creates alarms that notify about approaching communication issues. In order to determine actual throughput and latency, the WLQ managers analyze the RHEA application traffic on the related interfaces and create additional testing traffic if needed.

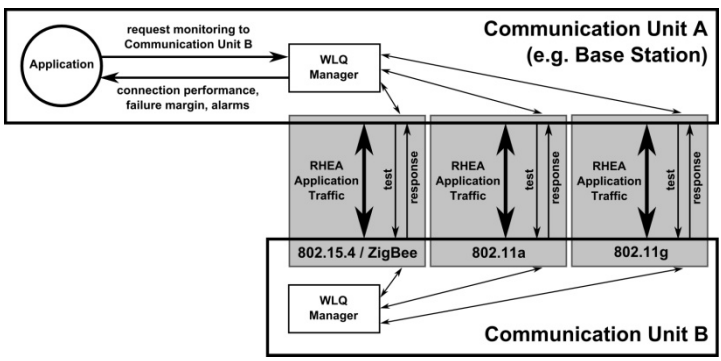

Fig. 12. Connection Monitoring at Wireless Link QoS (WLQ) Manager

6. Conclusions and Future Work

The introduced multi-technology communication approach shall significantly increase the reliability of connectivity and communication performance within the RHEA robotic fleet. Firstly, wireless effects like fast fading caused by multipath propagation and interference can be minimized as the concurrently used technologies are working at different frequency bands. Secondly, approaching communication problems such as loss of connectivity or drop of communication performance (latency, throughput) can be predicted using discovery/distribution of multi-technology topology information and information about the robotic mission plan.

This paper describes the details of multi-technology network learning and prediction. We proposed an approach to proactively acquire network topology and link state knowledge, which is distributed over multiple technologies. The distribution behavior can be controlled by the introduced distribution radius. Furthermore, we presented an extension of failure margin calculation to multi-technology level. The failure margin defines the number of links, which can fail without network partitioning. In addition, we proposed the calculation of the degradation margin, which represents the maximum number of link failures a connection can tolerate without a possible drop of communication performance (latency, throughput). Based on the gathered knowledge, failure (and degradation) margins can be calculated in real time. The application can actively request the information about the multi-technology network health or it can define alarming thresholds. If the observed network performance parameter drops below this threshold, a notification alarm is sent to the application, which can react to the changed network status.

Apart from multi-technology network and link state knowledge, we propose to use fleet localization and prediction of locations to be able to correlate the network knowledge with the movements of the robotic fleet. This will further improve network learning and prediction. The real-time monitoring and alarming functionalities of the communication layer enable the verification of the network health at any time, which is the basis for a safe mission operation of the RHEA robotic fleet.

Acknowledgement

The research leading to these results has received funding from the European Union's Seventh Framework Programme [FP7/2007-2013] under Grant Agreement nº 245986.

References

M. Al-Hattab and J. I Agbinnya (2008). Topology Prediction and Convergence for Networks on Mobile Vehicles. *Proceedings of the International Conference on Computer and Communication Engineering (ICCCE 2008)*, pp. 266-269.

D. Avresky and N. Natchev (2003). Failure Margin and Performance Degradation in "F-Cycle Ring" Networks. *Proceedings of the International Parallel and Distributed Processing Symposium (IPDPS'03)*, 6 pp.

C. S. Chekuri et al. (1997). Experimental Study of minimum cut algorithms. *Proceedings of the eighth annual ACM-SIAM symposium on Discrete algorithms (SODA '97)*, pp. 324-333.

D. Gesbert, M. Shafi, D. Shiu, P. J. Smith and A. Naguib (2003). From Theory to Practive: An Overview of MIMO Space-Time Coded Wireless Systems. *IEEE Journal on Selected Areas in Communications*, Vol. 21, No. 3, pp. 281-302.

X. Jia, D. Kim, S. Makki, P. Wan and C. Yi (2005). Power Assignment for k-Connectivity in Wireless Ad Hoc Networks. *Proceedings of the 24th Annual Joint Conference of the IEEE Computer and Communication Societies (INFOCOM 2005)*, pp. 2206-2211.

P. Kyasanur and N. H. Vaidya (2005). Routing and Interface Assignment in Multi-Channel Multi-Interface Wireless Networks. *IEEE Wireless Communications and Networking Conference (WCNC 05)*, pp. 2051-2056.

P. Santi and D. M. Blough (2003). The Critical Transmitting Range for Connectivity in Sparse Wireless Ad Hoc Networks. *IEEE Transactions on Mobile Computing*, Vol. 2, No. 1, pp. 25-39.

P. Wan and C. Yi (2004). Asymptotic Critical Transmission Radius and Critical Neighbor Number for k-Connectivity in Wireless Ad Hoc Networks. *Proceedings of the 5th ACM international symposium on Mobile ad hoc networking and computing (MobiHoc 04)*, pp. 1-8.

K. H. Wang and B. Li (2002). Group Mobility and Partition Prediction in Wireless Ad-Hoc Networks. *IEEE International Conference on Communications (ICC 2022)*, pp. 1017-1021.

A. Willig (2008). Recent and Emerging Topics in Wireless Industrial Communications: A Selection. *IEEE Transactions on Industrial Informatics*, Vol. 4, No. 2, pp. 102-124.

A. Willig (2005). Wireless Technology in Industrial Networks. *Proceedings of the IEEE*, Vol. 93, No. 6, pp. 1130-1151.

Vehicle Guidance Implemented on a Single-Board Computer

Michael Hödlmoser [1,2], Christoph Bober [3], Martin Kampel [1,2] and Michael Brandstötter [2]

[1] CogVis Ltd, Wiedner Hauptstrasse 17/3a, 1040 Vienna, Austria

(e-mail: [hoedlmoser, kampel, brandstoetter]@cogvis.at).

[2]Computer Vision Lab, Institute of Computer Aided Automation, Vienna University of Technology, Favortitenstrasse 9/183, 1040 Vienna, Austria

(e-mail: [hoedl,kampel]@caa.tuwien.ac.at)

[3]University of Applied Sciences Technikum Vienna, Höchstädtplatz 5, 1200 Vienna, Austria

(e-mail: se10m017@technikum-wien.at)

Abstract: Introducing 3D visual computing to the field of agriculture allows automatic crop detection, diagnosis and management using autonomous ground mobile vehicles. Structure from motion is an algorithm which describes the determination of the 3D structure as well as the positions of a moving camera over time. Having this 3D information allows autonomous vehicle guidance and obstacle detection. As crops are planted in rows, we provide information on where the vehicle is located between two crop rows. Due to spatial limitations on the vehicle the algorithm is implemented on a single-board computer. This demonstration paper describes principles and limitations of the implementation and shows preliminary results.

1. Introduction

Neuroscience studies have pointed out that a human's brain works with a 3D representation of objects and somehow (unclear how) stores the 3D information to achieve object detection and recognition at the level humans have been experiencing.

A 3D scene reconstruction can on the one hand be applied to non-rigid objects, where the object is moving and the camera is static, as in (Buch, 2009) and (Toshev,

2009). On the other hand, it is also possible to reconstruct rigid objects or a whole 3D scene, where the camera is moving through 3D space, as described in (Leibe, 2007). A prerequisite for 3D reconstruction is to find corresponding points between frames from different viewpoints or from temporal subsequent ones. Structure from motion (SfM) describes the methodology to extract 3D information from a camera in motion. By triangulating corresponding points between subsequent frames both the camera positions and the 3D points are obtained. The trajectory of the camera's movement is determined by combining the camera's positions over time.

In the last two decades, a precise management of agricultural land has been made possible due to the availability of new technologies (global positioning system, geographic information service). The introduction of 3D visual computing algorithms to the area of agriculture provides the availability of tackling guidance or obstacle detection tasks for autonomous vehicles, which are used for crop detection, diagnosis and management. As crops are always planted in rows, we determine the vehicle's location between two crop rows based on the calculated 3D information.

In this paper we present a real-time implementation of the SfM algorithm on a single-board computer (SBC), which has been developed under the RHEA project. Based on the implementation called Bundler and presented in (Snavely2008), we determine the trajectory of the moving vehicle the SBC is mounted on. After having the current structure of the vehicle's environment we determine the position of the vehicle between two crop rows. The principles and limitations of running SfM on a SBC as well as the calculation of the vehicle's position are described in Section 2. Functional and non-functional requirements for the system are provided in Section 3. To show the practicability and the accuracy of the system, some preliminary results are shown in Section 4.

2. Implementation

The SBC used in this demonstration paper is a Pandaboard featuring an OMAP4430 processor (Dual-Core ARM Cortex-A9) running at 1GHz and providing 1GB DDR2 RAM. The USB connector of the SBC is used to plug in a Logitech USB camera. We use Ubuntu 10.10 as operating system which is available for the ARM platform and has been adapted to the OMAP4 processor family. Figure 1 shows the setup used for this implementation.

SfM describes the method to determine both a moving camera's position over time and 3D points. This information is needed to get the vehicle’s trajectory by connecting all camera locations over time and to get the vehicle’s position relatively to the crop row, which are the 3D points in the 3D space environment. This is accomplished in three major steps. First, a feature detector is used to localize features in the images. Afterwards, corresponding features are detected

and finally the scene is reconstructed using a bundle adjustment algorithm, as described in (Snavely, 2008).

Fig. 1. SBC test setup. A Logitech USB camera is attached to the Board.

We are using an adapted version of Bundler, which is a collection of tools intended to recover 3D information from unordered images. To make Bundler running in real-time on our embedded hardware, the system considers only five images at a time for the SfM algorithm and deletes older ones. We additionally removed parts of Bundler, which are not needed for our implementation and combined the bundle of algorithms into one single framework.

2.1 Feature Detection, Feature Matching and Triangulation

To get corresponding features in two consecutive frames of a scene, it is important to detect features which are invariant to scale, rotation, affine transformations and different lighting conditions. These conditions are fulfilled by the so called scale invariant feature transform (SIFT) features, which are described in (Lowe2004). The principal goal of the detection algorithm is the transformation of image data into a scale invariant coordinate system relatively to local features. In a first step, all potential feature points are detected by a Difference-of-Gaussian function. Next, the location is estimated and points having a low contrast are discarded. After that the gradient and the orientation of all feature points are calculated. Figure 2 shows detected features in a random frame of our test sequence. For matching the features in two consecutive frames, the location, gradient and orientation are taken for comparing two features. To get a matching pair, the nearest neighbouring algorithm is used. The minimal Euclidean distance indicates a pair of features.

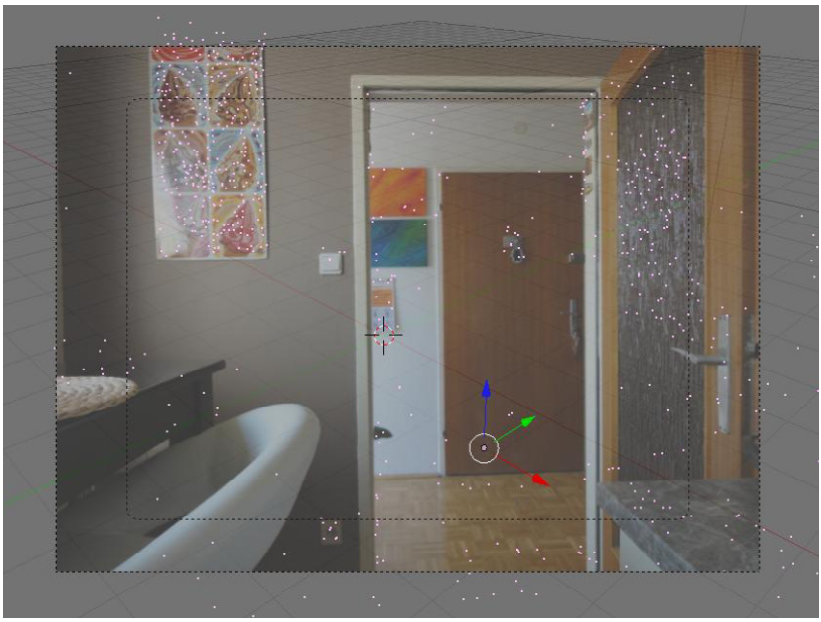

Fig. 2. Detected SIFT Features

After establishing point correspondences, these features can be used to reconstruct the environment as well as the current camera position. By introducing triangulation, a 3D point P can be determined from two or more corresponding points x_0 and x_1. When two cameras are perfectly aligned, the 3D point P is given by the intersection of the rays going through the points x_0, x_1 and the camera centres C_0 and C_1, as shown in the left image of Fig. 3. When the two cameras are not perfectly aligned or the feature points provide small errors due to noise in the image, a mean position must be found for the 3D point, which is demonstrated in the right image of Fig. 3.

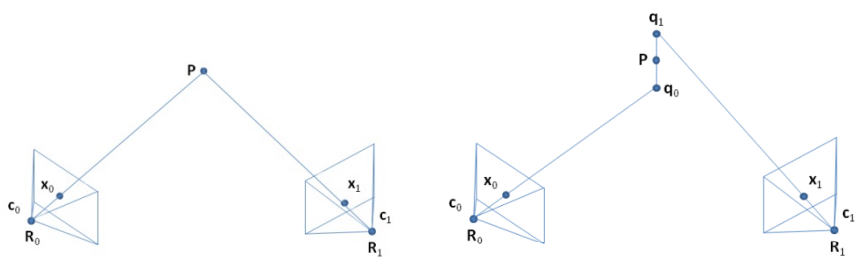

Fig. 3. Determination of 3D point by using triangulation of corresponding 2D points (left) and corresponding but noisy points (right).

2.2 Two-Frame Structure from Motion and Global Alignment

A calibrated camera is described by its internal parameters focal length and principal point, which is expressed by the camera matrix. Besides, the location of the camera in 3D world space is described by a translation and an orientation. These three features are known as the camera's pose. When having internally calibrated cameras, the rotation and translation as well as the 3D point can be determined from corresponding points. When having two cameras and positioning one camera in the origin of a common coordinate system, the so called essential matrix can be calculated which then describes rotation and translation of the second camera.

After doing pairwise calibration between consecutive frames i and i-1, a global alignment must be established to get all camera positions for every time instance. Figure 4 shows the application flow.

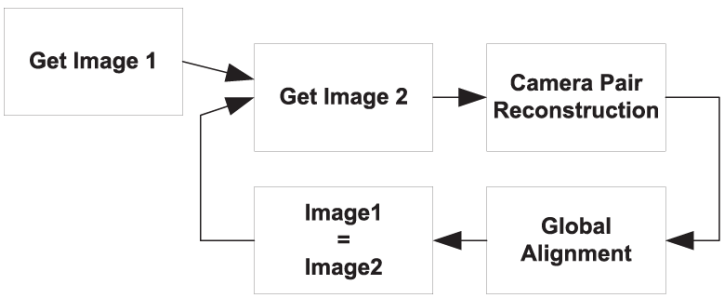

Fig. 4. Application flow of the SfM algorithm

When we then connect all the camera positions, we get the trajectory of the vehicle in 3D space. The rotation and translation for the camera at time instance i is calculated by $R_i = R_{i-1} * R_i$ and $t_i = t_{i-1} + R_{i-1} * t_i$.

The output of SfM is used to check the position of the vehicle between the crop rows and find divergences of the moving direction. We determine the current camera location and search for 3D points, which are within a certain distance along the moving direction. We then divide those points in two clusters, regarding the perpendicular distance to the moving camera and take the mean distance between each cluster and the camera location, perpendicular to the moving direction. Figure 5 shows the determination of the distances between the current camera centre and the two 3D point clusters, where each cluster represents a crop row.

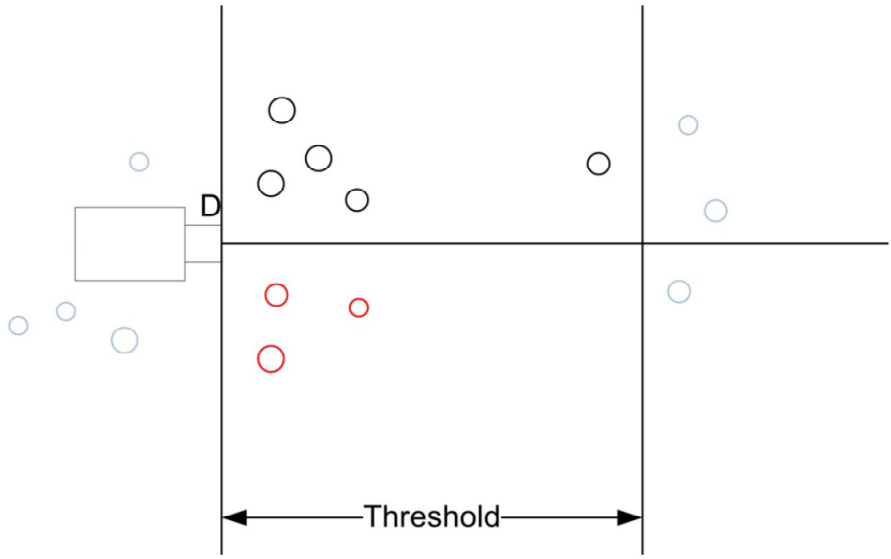

Fig. 5. Determination of the distance between the current camera centre and the two 3D point clusters, which represent the crop rows.

3. Non-Functional Requirements

The quality of the reconstruction depends from the number of feature points detected in the 2D images. It is important to find as many feature points on the crop row as possible to detect possible obstacles on the path. The faster the vehicle moves between two crop rows, the larger the distance between reconstructed points and the vehicle must be. We assume that braking takes longer than changing the moving direction. Exploiting the equation of motion, the minimum distance between reconstructed points and the moving vehicle is given by

$$A_{\min} = \left(vApplicationCycle + \frac{v^2}{2a_b} \right),$$

where v is the current velocity in m/s, a_b is the braking deceleration and vApplicationCycle is the time it takes to process one frame in cycles per seconds. The top image of Fig. 6 shows the minimum distance between reconstructed points and the vehicle under varying cycle times when the braking deceleration is set to 5 m/s^2. The maximum velocity can then be calculated by

$$v^2 + CyclesPerSecond \cdot v - 2a \cdot A_{\min} = 0 .$$

The bottom image of Fig. 6 shows the maximum velocity under varying cycle times.

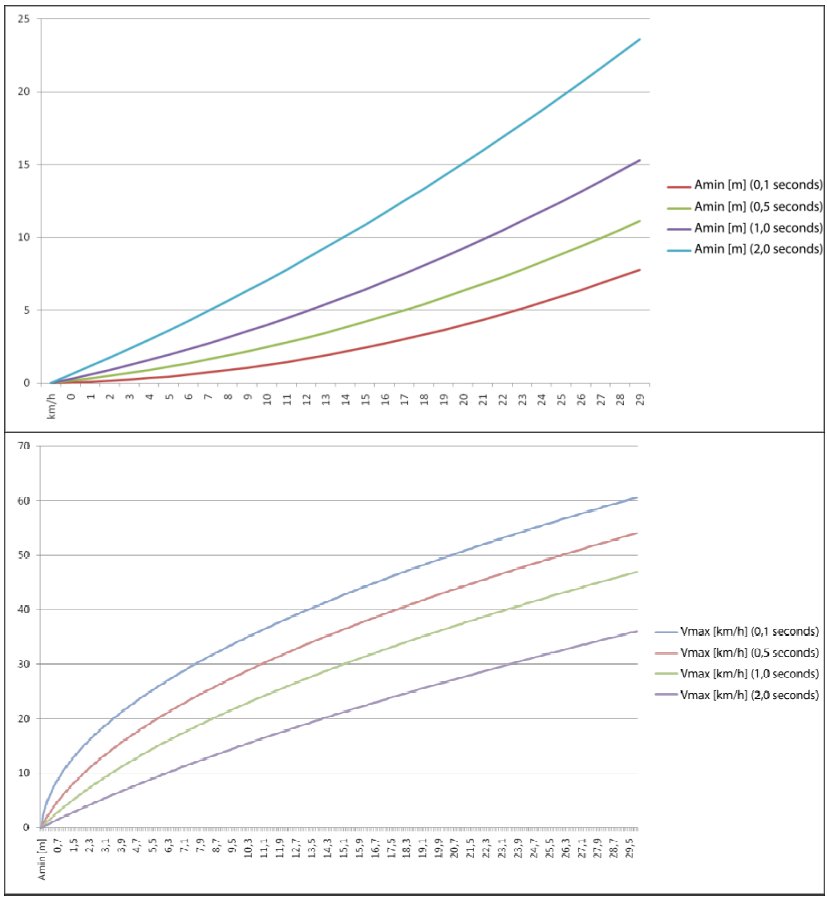

Fig. 6. Top: Minimum distance between reconstructed points and moving vehicle under varying cycle times. Bottom: Maximum possible velocity under varying cycle times.

4. Experiments

To show the practicability of our implementation, we do some real world experiments.

In a first setup, we move our SBC by hand through a scene where boundaries are present to the left and to the right of the camera, which should simulate crop rows. We therefore use ten images, where the setup is moved through a kitchen. A curve fitting algorithm is used to interpolate the camera positions between these images for better demonstration results. We connected a Logitech USB Webcam Pro 9000, operating at a resolution of 640x480 to the SBC, as can be seen in Fig. 6. The reconstruction of the 3D scene is depicted in Fig. 7. The leftmost column shows input images, the column in the middle shows the 3D points projected onto the

image plane. The rightmost column shows the reconstructed point cloud of the scene and the camera positions. Red and green coloured points show the ones which are used and detected as simulated crop rows and for calculating the distance between the rows and the camera position.

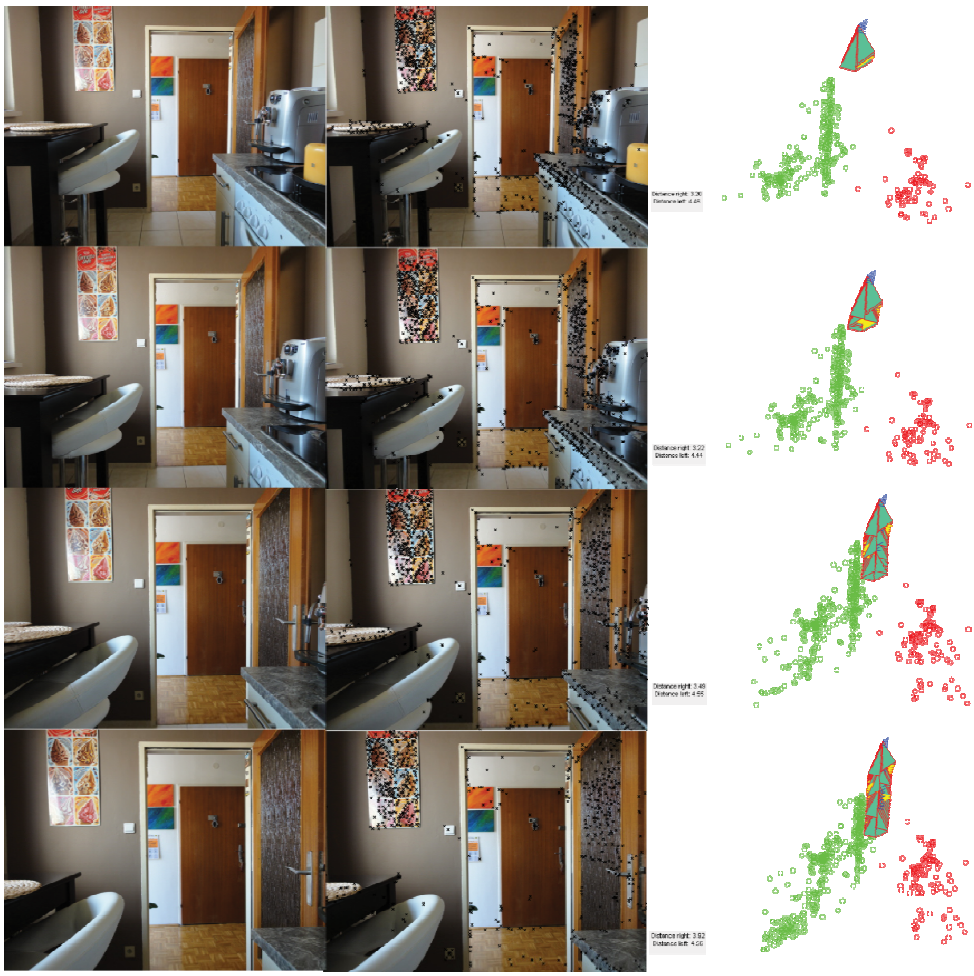

Fig. 7. From left to right: input images, reprojected 3D points, reconstructed 3D points and camera positions. This figure is best viewed in colour.

In a second experiment, we want to determine the minimal resolution necessary to reconstruct an environment based on 2D images. A video having a resolution (downloaded from www.rainsoft.de) of 1344x372 pixels is used in this setup. We are not using any potential crop row points but only reconstruct the trajectory and compare it to GPS reference data. In the video, a vehicle is driving straight and then turning right at an intersection. Figure 8 shows a sample frame from the sequence,

Fig. 9 shows the reconstructed path using different resolutions. As can be seen, a minimal resolution of 168x47 pixels must be used to get reasonable results.

Fig. 8. Sample frame from the sequence used for the second experiment.

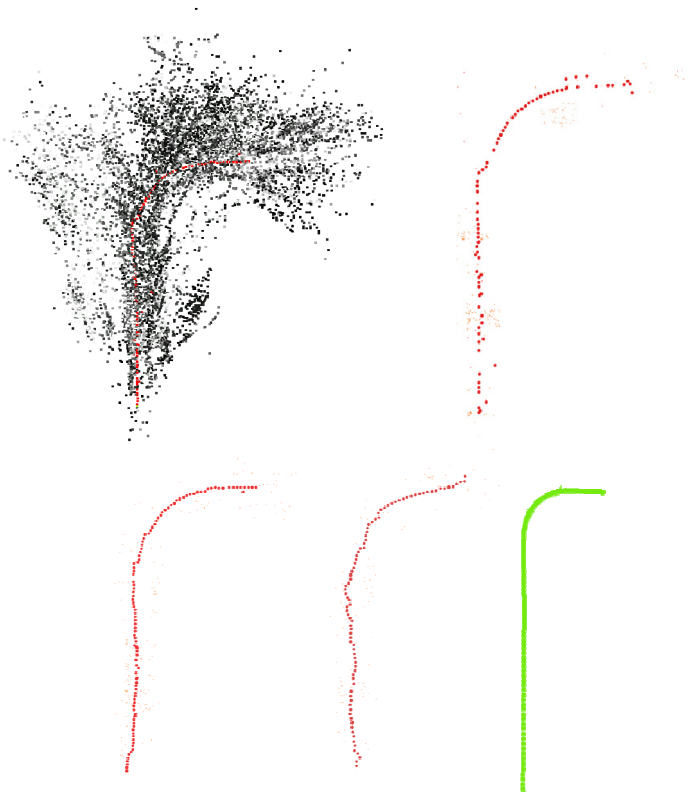

Fig. 9. From left to right, top to bottom: Reconstructed path and environment. Reconstructed path using a resolution of 1344x372 pixels / 168x47 pixels / 127x35 pixels and the GPS reference data.

6. Conclusions

In this paper we presented a SfM algorithm running on a SBC, which is used in the research field of agriculture for finding the path between two crop rows. This task is necessary to develop a new generation of automatic and robotic systems for chemical and physical - mechanical and thermal - effective weed management focused on both agriculture and forestry. We also showed some non-functional requirements which need to be met when using the system in real world environments and showed some preliminary results of the reconstruction.

Acknowledgement

The research leading to these results has received funding from the European Union's Seventh Framework Programme [FP7/2007-2013] under Grant Agreement nº 245986.

References

N. Buch, J. Orwell, and S. Velastin (2009). 3d extended histogram of oriented gradients (3dhog) for classification of road users in urban scenes. In Proc. of BMVC.

B. Leibe, N. Cornelis, K. Cornelis, and L. Van Gool (2007). Dynamic 3d scene analysis from a moving vehicle. In Proc. of CVPR.

N. Snavely, S. M. Seitz, and R. Szeliski (2008). Modeling the world from internet photo collections. IJCV, 80(2):189–210.

A. Toshev, A. Makadia, and K. Daniilidis (2009). Shape-based object recognition in videos using 3d synthetic object models. In Proc. of CVPR, pages 288–295.

D. Lowe (2004). Distinctive image features from scale-invariant keypoints. *International Journal of Computer Vision,* 60, 2 (2004), pp. 91-110.

ISBN 978-84-615-6184-1

RHEA: Robot Fleets for Highly Effective Agriculture and Forestry Management
NMP2-LA-2010-245986